附件 13

中国地质大学（武汉）

本科毕业论文（设计）论文翻译

毕业论文题目：基于煤岩强度感知的煤矿井下钻进过程操作参数优化

翻译论文题目：基于 PI 控制器的摩擦下钻杆的实用稳定性分析

Practical Stability Analysis of a Drilling Pipe Under Friction With a PI-Controller

学　　院：未来技术学院　　专业：自动化

学生姓名：曾康慧　　学号：20211003337

指导教师：吴　敏　　职称：教　授

指导教师：陆承达　　职称：教　授

基于 PI 控制器的摩擦下钻杆的实用稳定性分析

Matthieu Barreau, Frédéric Gouaisbaut 和 Alexandre Seuret

摘要—本文主要研究基于 PI 控制器控制的钻杆稳定性分析。该模型是由常微分方程与偏微分方程耦合而成，因而呈现无限维的特性。基于时滞系统的最新研究成果，我们通过黎曼坐标投影构造状态扩展，并在此基础上提出新的李雅普诺夫泛函。首先，我们利用线性矩阵不等式框架，给出扭转动力学线性模型的指数稳定性结果。随后，又通过一项新的稳定性定理，详细分析可能导致著名“粘滑”现象的非线性摩擦力。我们通过数值模拟验证该方法的有效性，同时也显示出仅使用 PI 控制器并不能有效减弱粘滑振荡。

关键词—摩擦，线性矩阵不等式，李雅普诺夫方法，石油钻井，偏微分方程，比例积分控制，稳定性分析.

I. 引言

研究复杂机械的行为是一项巨大挑战，因为它们通常表现出非线性和耦合的特性 [49]。钻井机构正是一个典型示例：在钻杆上可能出现钻头跳动、粘滑或旋转等多种非线性现象 [14]。这些现象通常会引起振动，从而增加钻杆的疲劳并降低油井的使用寿命。因此，首要挑战在于提供一个能反映这些效应的动态模型。

文献中已有多种模型，从最简单的有限维模型 [13], [41] 到更复杂但更接近实际的无限维系统。有限维系统是迈出研究井中振动的重要第一步，因为它们能指出导致振动的关键因素。然而，有限维模型难以精确体现基于偏微分方程 (Partial Differential Equation, PDE) 的物理定律。因此，在钻杆背景下，一个耦合的有限/无限维模型更为自然，并已在 [14], [20], [38] 等文献中提出。

第二个挑战在于如何设计控制器来消除或至少减弱这些不良影响。已有许多控制技术应用于有限维模型，包括 [13], [15] 中探讨的简单比例积分 (Proportional-Integral, PI) 控制器，以及滑模控制 [30] 或 H_∞ [41] 等更高阶方法。然而，要将这些控制器扩展到耦合的有限/无限维系统上并不容易。

过去十年间，对无限维系统的分析取得了显著进展。例如，半群理论 [48] 极大地简化了这类问题中解的存在性和唯一性证明，并因此推动了李雅普诺夫 (Lyapunov) 理论向某些 PDE 范畴的扩展 [9], [16], [33]。基于这些成果，人们对带 PI 控制器的线性化无限维钻杆系统进行了稳定性分析 [44], [45]。鉴于 PI 控制器只有两个可调自由度，为了提高性能，一些改进控制器随之提出，例如 [47] 中的改进 PI 控制器以及 [38] 中的延迟 PI 和基于平坦性的控制。更复杂的控制器则来自 PDE 的 backstepping 技术，该方法最初在 [25] 中提出，并在 [10], [12], [35] 等文献中得到应用。

然而，这些技术几乎都基于 Lyapunov 方法，因而在耦合系统中常面临缺乏高效 Lyapunov 泛函的问题。时滞系统的最新进展 [42] 提出了层次化的 Lyapunov 泛函，可有效用于耦合的常微分方程 (Ordinary Differential Equation, ODE)/弦方程 [8]。由于这一方法依赖状态扩展，难以手动分析稳定性，但可将其转化为使用线性矩阵不等式 (Linear Matrix Inequality, LMI) 描述的优化问题，故而能够便捷地求解。

本文利用这一丰富的 Lyapunov 泛函，对仅包含扭转效应的无限维钻杆模型在 PI 控制器下的稳定性研究进行了重新审视。本文的首个贡献体现在定理 1 中：它给出了一个确保线性闭环系统渐近稳定性的 LMI。随后，第二个定理讨论了受控非线性系统的实用稳定性。例如，它表明若线性系统稳定，则对应的非线性系统同样可保持稳定；此外，还给出了黏滑过程中振荡幅度的精确上界。

本文结构如下：第 2 节讨论了文献中的各种模型，强调了处理无限维问题的必要性；第 3 节给出了问题的形式化描述；第 4 节则专门研究线性系统，为后续在第 5 节中处理非线性系统做准备；最终，第 6 节给出了数值模拟示例，以说明该方法的有效性，并对 PI 控制器的设计做出总结。

符号说明：对于多变量函数 $(x,t)\mapsto u(x,t)$，符号 u_t

稿件于 2019 年 4 月 3 日收到；2019 年 7 月 31 日修订；2019 年 9 月 16 日接受。出版日期为 2019 年 12 月 20 日；当前版本的日期为 2021 年 2 月 9 日。最终稿于 2019 年 9 月 19 日收到。这项工作由 ANR 项目 SCIDiS 合同号 15-CE23-0014 支持。由副编辑 Y. Orlov 推荐。（通讯作者：Matthieu Barreau）

作者隶属于系统分析与建筑实验室，国家科学研究中心，法国图卢兹 31062（电子邮件：mbarreau@laas.fr；aseuret@laas.fr；fgouaisb@laas.fr）。

本文中一个或多个图片的彩色版本可以在 https://ieeexplore.ieee.org 网站上找到。

数字对象标识符 10.1109/TCST.2019.2943458

表示 $\frac{\partial u}{\partial t}$，$u_x = \frac{\partial u}{\partial x}$。我们还使用符号 $L^2 = L^2((0,1);\mathbb{R})$ 和 Sobolev 空间：$H^n = \{z \in L^2; \forall m \leqslant n, \frac{\partial^m z}{\partial x^m} \in L^2\}$。$L^2$ 中的范数是 $\|z\|^2 = \int_\Omega |z(x)|^2 dx = \langle z, z\rangle$。对于任何方阵 A 和 B，定义以下操作：$\mathrm{He}(A) = A + A^\top$ 和 $\mathrm{diag}(A,B) = \left[\begin{smallmatrix} A & 0 \\ 0 & B \end{smallmatrix}\right]$。正定矩阵集的大小为 n，表示为 $\mathbb{S}^n_+$，为了简化，如果矩阵 P 属于该集合，则 $P \succ 0$。

II. 模型描述

钻杆是一种用于将石油从地表深处抽取上来的机制，如图 1 所示。在整个论文中，$\Phi(\cdot,t)$ 是沿着钻杆的扭转角度，$\Phi(0,t)$ 和 $\Phi(L,t)$ 分别是井顶部和底部的角度。这口井是一根大约一公里长的金属杆，因此在顶部施加的扭矩 $u_1(t)$ 所产生的旋转速度与底部的不同。此外，钻头与底部岩石的相互作用由扭矩 T 建模，该扭矩取决于 $\Phi_t(L,t)$。

当钻头钻入岩石时，会产生轴向压缩，记为 Ψ。这种压缩是由于在顶部施加的垂直力 u_2 沿着杆传播而产生的，该力用于上下推动井。

这种描述自然地引出了两个控制目标，以防止机制破裂。第一个是保持管道末端的旋转速度 $\Phi(L,t)$ 在一个恒定值 Ω_0，防止管道扭曲。另一个是保持钻速恒定，以确保沿杆没有压缩。

文献中提出了几种模型来实现这些控制目标。它们的性质非常不同，导致了各种分析和控制技术。书籍 [38]（第 2 章）和综述 [40] 提供了这些技术的概述，基本上分为四类。为了更好地激励后续使用的模型，提出了现有建模工具的简要概述，但读者可以参考 [40] 和原始论文，以更好地理解模型的构建方式。

A. 集总参数模型

这些模型是文献中最早获得的模型 [13], [27], [41]，整个机制由一系列谐振子描述。它们可以分为两大类：

1) 第一类假设扭转角度 $\Phi(0,t) = \Phi_r(t)$（顶部）和 $\Phi(L,t) = \Phi_b(t)$（底部）的动态由两个耦合的谐振子描述。驱动系统的扭矩 u_1 作用于 Φ_r 的动态，受控角度是 Φ_b。该模型中没有考虑轴向动态。此模型可以在 [13], [32], [41] 中找到。
2) 另一种两自由度模型在 [27], [34] 中描述。这里也有两个耦合的谐振子，分别表示 $\Psi(L,t)$ 和 $\Phi(L,t)$ 的轴向和扭转动态。该模型仅考虑管道末端的运动，而忽略了沿杆发生的物理现象。

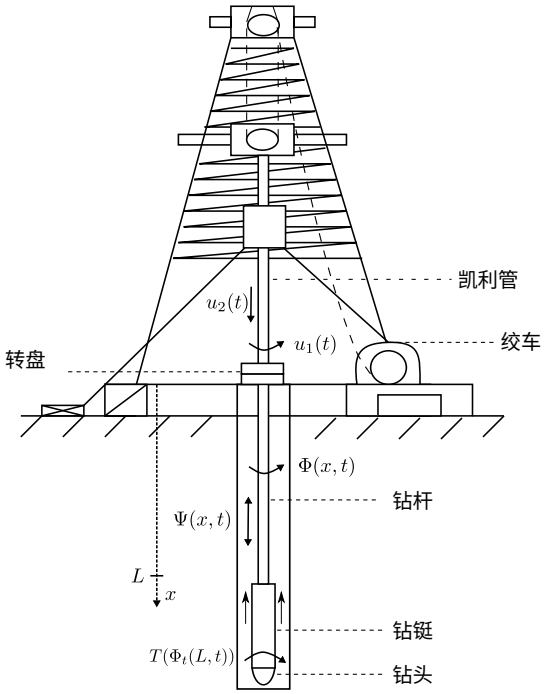

图 1: 钻井机构示意图，最初取自 [39]。物理值对应的数据见表 II

第一类模型可以通过以下方程组描述：

$$\begin{cases} I_r\ddot{\Phi}_r + \lambda_r(\dot{\Phi}_r - \dot{\Phi}_b) + k(\Phi_r - \Phi_b) + d_r\dot{\Phi}_r = u_1, \\ I_b\ddot{\Phi}_b + \lambda_b(\dot{\Phi}_b - \dot{\Phi}_r) + k(\Phi_b - \Phi_r) + d_b\dot{\Phi}_b = -T(\dot{\Phi}_b), \end{cases} \tag{1}$$

其中参数见表 I。T 是一个由 $\dot{\Phi}_b$ 的非线性函数建模的扭矩，它描述了钻头与岩石的相互作用[1]。通过仅考虑前述模型的两个主导极点，可以导出一个二阶集总参数模型 (Lumped Parameter Models, LPM)。

图 2 所示的现场测量示例显示了这种扭矩 T 对角速度的影响。出现的周期性方案称为粘滑。它由于静摩擦系数和库仑摩擦系数之间的差异而产生，使得扭矩函数 T 上出现反阻尼效应。尽管表面角速度似乎变化不大，但井下的角速度存在一个周期，并且角速度周期性地接近于零，这意味着钻头卡在岩石上。

粘滑效应主要出现在控制钻井机构上期望的角速度 Ω_0 较低时。确实，如果角速度 $\Phi_t(L,t)$ 较小，旋转台在 $x = 0$ 处提供的扭矩会增加管道的扭转。这种增加导致 $\Phi_t(L,t)$ 更高，但扭矩函数上的负阻尼意味着 T 更小。因此，$\Phi_t(L,t)$ 增加，这种现象称为滑动阶段。然后，控制律减少扭矩以使 $\Phi_t(L,t)$ 匹配 Ω_0。由于扭矩也增加，这导致了粘滞阶段，其中 $\Phi(L,t)$ 保持接近于

[1]关于 T 的各种模型的详细描述，请参见 [38]（第 3 章）。

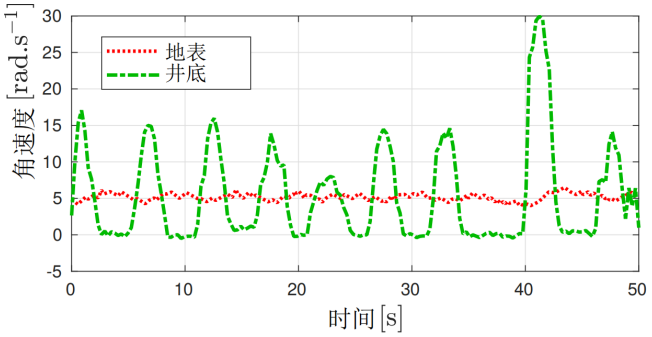

图 2: 由于井底的摩擦扭矩对钻井机构产生的非线性效应这些测量在现场进行 [41]

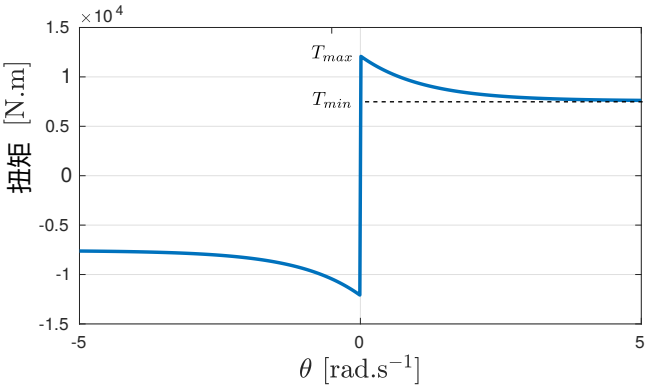

图 3: 扭矩的非线性部分 T_{nl} 是来自 Karnopp 工作的真实摩擦扭矩的近似 [23]

0。于是，粘滑循环出现。注意，对于较高的 Ω_0 值，这种情况不会发生，因为扭矩 T 随 $\Phi_t(L,t)$ 的变化不大，使得系统更容易控制。在图 2 中，可以看到振荡的频率为 0.17Hz，幅度在每秒 10 到 25 弧度之间。

建模这种现象非常重要，因为在研究机械设备时，摩擦效应是相当常见的。在 [40] 中，作者比较了一些 T 的模型，并得出它们产生非常相似的结果。主要特征是随着 $\Phi_t(L,t)$ 的增加，T 减小。一个标准模型参考了 Karnopp [23] 和 Armstrong-Helouvry [3], [4] 的初步工作，其中摩擦项呈指数衰减，如 [31] 中所述。此定律如下所示，其中 $\theta = \Phi_t(L,\cdot)$ 以弧度每秒表示：

$$\begin{aligned} T(\theta) &= T_l(\theta) + T_{nl}(\theta), \\ T_l(\theta) &= c_b\theta, \\ T_{nl}(\theta) &= T_{sb}\left(\mu_{cb} + (\mu_{sb} - \mu_{cb})\, e^{-\gamma_b|\theta|}\right) \operatorname{sign}(\theta). \end{aligned} \tag{2}$$

该模型已在 [32], [38] 中使用。

请注意，在 [2] 中提供了这种机制在钻井系统特定背景下的现场描述，并得出结论，这些模型是类似结构中可见非线性现象的合理近似。

在这个阶段，集总参数模型因其简单性而有趣，但没有考虑问题的无限维性质，因此仅在小振动情况下是一个很好的近似 [39]。考虑连续介质力学并导致分布参数系统，可以进行更深入的建模。

B. 分布参数模型

为了处理前述模型的有限维近似，另一种从机械方程推导出的模型导致了一组 PDE，如 [14], [49] 的工作中所描述的那样。在 [1], [2] 中对该模型进行了丰富的描述，其中从控制的角度介绍了系统，并与现场测量进行了比较。在最初的论文中，该模型仅关注沿管道传播

表 I: 集总参数模型的参数值及其含义，取自 [13], [32], [41]

参数含义		值
I_r	转盘和驱动惯量	2122 kg.m^2
I_b	钻头和钻柱惯量	374 kg.m^2
k	钻柱刚度	1111 N.m.rad^{-1}
λ_r	顶部耦合阻尼	425 N.m.s.rad^{-1}
λ_b	底部耦合阻尼	23.2 N.m.s.rad^{-1}
d_r	转盘阻尼	425 N.m.s.rad^{-1}
d_b	钻头阻尼	50 N.m.s.rad^{-1}
γ_b	速度衰减率	0.9 s.rad^{-1}
μ_{cb}	库仑摩擦系数	0.5
μ_{sb}	静摩擦系数	0.8
c_b	底部阻尼常数	0.03 N.m.s.rad^{-1}
T_{sb}	静摩擦扭矩	15 145 N.m

的扭转。轴向传播在 [1], [40] 的模型中引入。新模型由两个一维波动方程组成，分别表示 $x \in (0,L)$ 和 $t > 0$ 的每个变形：

$$\Phi_{tt}(x,t) = c_t^2\Phi_{xx}(x,t) - \gamma_t\Phi_t(x,t), \tag{3a}$$
$$\Psi_{tt}(x,t) = c_a^2\Psi_{xx}(x,t) - \gamma_a\Psi_t(x,t), \tag{3b}$$

其中 Φ 是扭转角度，Ψ 是轴向运动，$c_t = \sqrt{G/\rho}$ 是角度的传播速度，γ_t 是内部阻尼，$c_a = \sqrt{E/\rho}$ 是轴向速度，γ_a 是轴向分布阻尼。物理参数及其值的列表见表 II，图 1 有助于更好地理解物理系统。换句话说，如果 $\Psi(\cdot,t) = 0$，则管道中没有压缩，意味着钻头没有跳动；如果 $\Phi_{tt}(\cdot,t) = 0$，则沿管道的角速度相同，意味着

表 II: 物理参数、含义及其值 [1], [40]

参数含义		值
L	管道长度	2000m
G	剪切模量	79.3×10^9 N.m^{-2}
E	杨氏模量	200×10^9 N.m^{-2}
Γ	钻柱的横截面	35×10^{-4} m^4
J	惯性矩	1.19×10^{-5} m^4
I_B	底部集总惯量	89 kg.m^2
M_B	底部质量	40 000 kg
ρ	密度	8000 kg.m^{-3}
g	角动量	2000 N.m.s.rad^{-1}
h	粘性摩擦系数	200 kg.s^{-1}
γ_a	分布轴向阻尼	0.69 s^{-1}
γ_t	分布角度阻尼	0.27 s^{-1}
δ	钻头重量系数	1 m^{-1}

没有扭转的增加或减少。

为了使前述模型良好定义，必须在 (3) 中加入顶部和底部的边界条件（在 $x = 0$ 和 $x = L$ 处）。在这一部分中，仅推导了顶部的边界条件。在 $x = 0$ 处存在粘性阻尼，因此顶部施加的扭矩与角速度之间存在不匹配。轴向部分的顶部边界条件基于相同的方案，得到以下条件，对于 $t > 0$：

$$GJ\Phi_x(0,t) = g\Phi_t(0,t) - u_1(t), \tag{4a}$$
$$E\Gamma\Psi_x(0,t) = h\Psi_t(0,t) - u_2(t). \tag{4b}$$

底部边界条件（$x = L$）更难以理解，因此在处理更复杂的模型时再推导。

C. 中立型时滞模型

研究以 PDE 形式表示的无限维问题是一个相关的挑战。前面得到的方程是阻尼波动方程，但在 $\gamma_a = \gamma_t = 0$ 的特殊情况下，系统可以转换为中立型时滞系统，如 [38] 中所做的那样。这种新形式使得可以使用其他工具来分析其稳定性，例如 Lyapunov-Krasovskii 定理或频域方法，从而使其稳定性分析稍微容易一些。

然而，这种形式的主要缺点是假设阻尼发生在边界而不是沿着管道。这种有用的简化，即使在许多文章中遇到 [12], [38], [39]，也已知会显著改变系统的行为 [1]。确实，似乎没有内部阻尼的情况下，波动方程很容易重新表述为一个传输方程系统。因此，可以直接在管道顶部以延迟 c^{-1} 观察到管道底部发生的情况。这使得控制变得更容易。

D. 耦合的 ODE/PDE 模型

为了克服前面提到的问题，[39] 中提出了一个比 (3) 推导出的模型更简单的模型，其中使用谐振子来描述轴向振动，模型结果是一个耦合的 ODE/PDE。
另一种可能性，例如在 [14], [38] 中报告的是提出一个二阶 ODE 作为底部边界条件（$x = L$）对于 $t > 0$：

$$GJ\Phi_x(L,t) = -I_B\Phi_{tt}(L,t) - T\left(\Phi_t(L,t)\right), \tag{5a}$$
$$E\Gamma\Psi_x(L,t) = -M_B\Psi_{tt}(L,t) - \delta T\left(\Phi_t(L,t)\right), \tag{5b}$$

其中 T 表示由岩石施加在钻头上的扭矩，如方程 (2) 中所述。注意，方程 (5a) 来自角动量守恒，其中 $GJ\Phi_x(L,t)$ 是来自管道顶部的扭矩。方程 (5b) 是牛顿第二运动定律的直接应用，其中 $E\Gamma\Psi_x(L,t)$ 是从顶部传递到钻头的力，而 $\delta T\left(\Phi_t(L,t)\right)$ 是由于岩石相互作用产生的钻头重量。由于 (5) 是一个二阶时间微分方程，注意到 (3) 与 (5) 确实导致了一个耦合的 ODE/PDE。

存在其他底部边界条件，导致轴向和扭转动力学之间更复杂的耦合。然而，它们引入了延迟，需要对钻头有更好的了解。为了保持内容的通用性，本文中使用的边界条件 (5) 是根据 [14], [39], [45] 提出的。

最后一点，通过基于(3a)，(4a) 和 (5a) 的一些变换，可以推导出一个系统，可以使用 backstepping 控制器 [12], [37]。这就是为什么今天广泛使用这个模型的主要原因。

E. 模型比较

在本小节中，我们提议比较耦合的 ODE/PDE 模型和仅考虑扭转的集总参数模型。我们在此考虑系统的大 Ω_0 线性化，因此通过设置 $T = 0$ 忽略粘滑效应。

首先，记 $\mathcal{H}_{DPM}$ 为分布参数模型（Distributed Parameter Model, DPM）中从 u_1 到 $\Phi(L,\cdot)$ 的传递函数，$\mathcal{H}_{LPM}$ 为 LPM 中从 u_1 到 Φ_b 的传递函数。我们还定义 $\mathcal{H}_{LPM2}$ 为 $\mathcal{H}_{LPM}$ 的截断，仅考虑两个主导极点。图 4 绘制了 $\mathcal{H}_{DPM}$、$\mathcal{H}_{LPM}$ 和 $\mathcal{H}_{LPM2}$ 的波特图。

显然，LPM 在稳态和低频率下捕捉到了 DPM 的行为，直到共振发生在大约 $\sqrt{k/I_b}$ rad.s^{-1}。从控制的

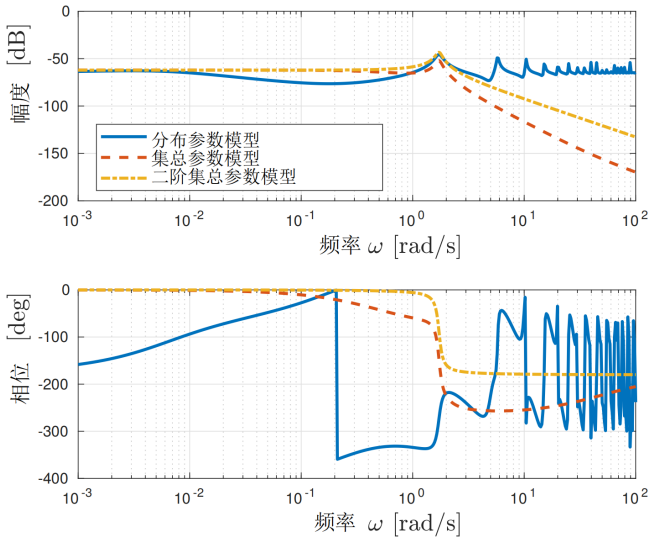

图 4: $\mathcal{H}_{DPM}$、$\mathcal{H}_{LPM}$ 和 $\mathcal{H}_{LPM2}$ 的波特图

角度来看，DPM 具有无限多的谐波，如图所示，但随着频率增加（每十倍频程约为-10 dB），其幅度较低且被阻尼。幅度图不足以在三个模型之间做出巨大差异。然而，考虑到相位，我们看到明显的差异。DPM 在多个频率上穿过-180 度，使得控制裕度相当难以评估。此外，这表明 DPM 在共振后的行为差异巨大，因此更难控制。因此，当受控时，它们可能表现出非常不同的行为。这就是为什么我们在本研究中专注于 DPM，即使它比 LPM 更难控制。

III. 问题陈述

前一小节中推导出的耦合非线性 ODE/PDE 模型可以写成如下形式，对于 $t>0$ 和 $x\in[0,1]$：

$$\begin{cases} \phi_{tt}(x,t)=\tilde{c}_t^2\phi_{xx}(x,t)-\gamma_t\phi_t(x,t),\\ \phi_x(0,t)=\tilde{g}\phi_t(0,t)-\tilde{u}_1(t),\\ \phi_t(1,t)=z_1(t),\\ \dot{z}_1(t)=-\alpha_1\phi_x(1,t)-\alpha_2 T(z_1(t)), \end{cases} \tag{6}$$

$$\begin{cases} \psi_{tt}(x,t)=\tilde{c}_a^2\psi_{xx}(x,t)-\gamma_a\psi_t(x,t),\\ \psi_x(0,t)=\tilde{h}\psi_t(0,t)-\tilde{u}_2(t),\\ \psi_t(1,t)=y_1(t),\\ \dot{y}_1(t)=-\beta_1\psi_x(1,t)-\beta_2 T(z_1(t)), \end{cases} \tag{7}$$

其中归一化参数见表 III。注意，现在空间变量的范围是 $x\in[0,1]$ 以简化计算。初始条件如下：

$$\begin{cases} \phi(x,0)=\phi^0(x), \quad \phi_t(x,0)=\phi^1(x),\\ \psi(x,0)=\psi^0(x), \quad \psi_t(x,0)=\psi^1(x),\\ z_1(0)=\phi^1(1), \qquad y_1(0)=\psi^1(1). \end{cases}$$

由于前述问题的解的存在性和唯一性不是本文的主要贡献，因此在后续内容中假设其存在性和唯一性。这个问题已经被广泛研究（见 [10], [12], [37], [39], [44] 等），并且如果初始条件 $(\phi^0,\phi^1,\psi^0,\psi^1)$ 满足边界条件，解属于以下空间（更多细节见 [9]）：

$$\mathbb{X}=H^1\times L^2,\ \mathbb{X}_1=H^2\times H^1,$$

$$(\phi,\phi_t,\psi,\psi_t,z_1,y_1)\in C^0(\mathbb{X}_1^2\times\mathbb{R}^2).$$

表 III: 归一化参数

参数	表达式	值
$\phi(x,t)$	$\Phi(xL,t)$	-
$\psi(x,t)$	$\Psi(xL,t)$	-
$\tilde{c}_t$	c_tL^{-1}	1.57
$\tilde{c}_a$	c_aL^{-1}	2.5
α_1	$\frac{GJ}{LI_B}$	5.3
β_1	$\frac{E\Gamma}{LM_B}$	8.75
α_2	I_B^{-1}	$1.12\cdot10^{-2}$
β_2	$\frac{\delta}{M_B}$	$2.5\cdot10^{-5}$
$\tilde{g}$	$\frac{g}{GJ}$	$2.1\cdot10^{-3}$
$\tilde{h}$	$\frac{h}{E\Gamma}$	$2.86\cdot10^{-7}$
$\tilde{u}_1(t)$	$\frac{1}{GJ}u_1(t)$	-
$\tilde{u}_2(t)$	$\frac{1}{E\Gamma}u_2(t)$	-

由于前述问题的解的存在性和唯一性不是本文的主要贡献，因此在后续内容中假设其存在性和唯一性。这个问题已经被广泛研究（见 [10], [12], [37], [39], [44] 等），并且如果初始条件 $(\phi^0,\phi^1,\psi^0,\psi^1)$ 满足边界条件，解属于以下空间（更多细节见 [9]）：

$$\mathbb{X} = H^1 \times L^2,\ \mathbb{X}_1 = H^2 \times H^1,$$
$$(\phi, \phi_t, \psi, \psi_t, z_1, y_1) \in C^0(\mathbb{X}_1^2 \times \mathbb{R}^2).$$

备注 *1:* 需要注意的是，由于符号函数的存在，$\theta \mapsto T_{nl}(\theta)$ 在 $\theta = 0$ 时未定义。然而，由于非线性直接作用于变量 z，因此根据 Filipov 的意义，ODE 系统存在唯一解 [19]。关于这一点的更详细讨论见 [11]。 □

系统 (6)-(7) 是两个子系统的级联：

1) 系统 (6) 是描述扭转角度 ϕ 的耦合非线性 ODE/弦方程。
2) 系统 (7) 是受外部扰动 $T(z_1)$ 影响的 Ψ 的耦合线性 ODE/弦方程。

显然，第二个子系统的扰动取决于第一个子系统中的 ϕ。由于它们非常相似，本文中进行的分析同样适用于第二个子问题。这就是为什么我们只研究扭转的演变。

IV. 线性系统的指数稳定性

系统 (6) 是一个非线性系统，因为在 (2) 中引入了摩擦项 T_{nl}。然而，对于较高的期望角速度 Ω_0，T_{nl} 可以假设为常数，如图 3 所示。此外，研究这个线性系统可以看作是研究非线性系统的第一步，主要依赖于本节推导的稳定性定理。

在 $\Omega_0 \gg 1$ 附近，T 的线性模型为：

$$T(\theta) = c_b\theta + T_{nl}(\Omega_0) = c_b\theta + T_0 \tag{8}$$

对于较高的 Ω_0 值，$T_0 = T_{nl}(\Omega_0)$ 接近于 $T_{smooth}(\Omega_0)$，在 Ω_0 趋于无穷大时，它们是相等的。因此，对于相对较大的角速度，非线性摩擦项对系统的影响不大。

在我们的案例中，针对这个问题提出的控制器在 [13], [15], [45] 中以不同的设置进行了研究，是一个基于钻头顶部角速度单一测量的简单比例/积分控制器（即 $\phi_t(0,t)$）。因此引入了以下变量：

$$\begin{aligned} \tilde{u}_1(t) &= -k_p\left(\phi_t(0,t) - \Omega_0\right) - k_i z_2(t), \\ \dot{z}_2(t) &= \phi_t(0,t) - \Omega_0, \end{aligned} \tag{9}$$

其中 k_p 和 k_i 是 PI 控制器的增益。结合方程 (6)、(8) 和 (9) 得到：

$$\begin{cases} \phi_{tt}(x,t) = c^2\phi_{xx}(x,t) - \gamma_t\phi_t(x,t), \\ \phi_x(0,t) = (\tilde{g} + k_p)\phi_t(0,t) - k_p\Omega_0 + k_i C_2 Z(t), \\ \phi_t(1,t) = C_1 Z(t), \\ \dot{Z}(t) = AZ(t) + B\begin{bmatrix}\phi_t(0,t)\\ \phi_x(1,t)\end{bmatrix} + B_2\begin{bmatrix}\Omega_0\\ T_0\end{bmatrix}, \end{cases} \tag{10}$$

其中

$$A = \begin{bmatrix} -\frac{c_b}{I_B} & 0 \\ 0 & 0 \end{bmatrix},\quad B = \begin{bmatrix} 0 & -\alpha_1 \\ 1 & 0 \end{bmatrix},\quad B_2 = \begin{bmatrix} 0 & -\alpha_2 \\ -1 & 0 \end{bmatrix},$$
$$Z = \begin{bmatrix} z_1 & z_2 \end{bmatrix}^\top,\quad C_1 = \begin{bmatrix} 1 & 0 \end{bmatrix},\quad C_2 = \begin{bmatrix} 0 & 1 \end{bmatrix}.$$

为了简化符号，$c = \tilde{c}_t$。我们记

$$X = (\phi_x, \phi_t, z_1, z_2) \in C^1([0,\infty), \mathcal{H})$$

其中 $\mathcal{H} = L^2 \times L^2 \times \mathbb{R}^2$ 是系统 (10) 的无限维状态。线性情况下的控制目标是实现 (10) 的平衡点的指数稳定性，即 $\phi_t(1)$ 指数趋向于给定的常数参考值 Ω_0。为此，引入了以下在 $\mathcal{H}$ 上的范数：

$$\|X\|_{\mathcal{H}}^2 = z_1^2 + z_2^2 + c^2\|\phi_x(\cdot)\|^2 + \|\phi_t(\cdot)\|^2$$

(10) 的平衡点的定义及其指数稳定性如下定义所示。

定义 *1:* $X_\infty \in \mathcal{H}$ 是 (10) 的一个**平衡点**，如果对于初始条件为 X_∞ 的 (10) 的轨迹 $X \in C^1([0,\infty), \mathcal{H})$，满足：

$$\forall t > 0, \quad \|\dot{X}(t)\|_{\mathcal{H}} = 0$$

定义 *2:* 设 X_∞ 是 (10) 的一个平衡点。如果

$$\forall t > 0, \quad \|X(t) - X_\infty\|_{\mathcal{H}} \le \gamma\, \|X_0 - X_\infty\|_{\mathcal{H}}\, e^{-\mu t}$$

对于 $\gamma \geqslant 1$，$\mu > 0$ 和任何满足边界条件的初始条件 $X_0 \in \mathcal{H}$ 成立，则称 X_∞ 是 μ-**指数稳定**的。这里，X 是初始条件为 X_0 的 (10) 的轨迹。

因此，如果存在 $\mu > 0$ 使得 X_∞ 是 μ-指数稳定的，则称 X_∞ 是**指数稳定**的。

在陈述本部分的主要结果之前，提出一个关于平衡点的引理。

引理 *1:* 假设 $k_i \neq 0$，则 (10) 存在唯一的平衡点

$X_\infty = (\phi_x^\infty, \phi_t^\infty, z_1^\infty, z_2^\infty) \in \mathcal{H}$，并且它满足 $\phi_t^\infty = \Omega_0$。

证明. (10) 的平衡点 X_∞ 满足：$(\phi_{xt}^\infty, \phi_{tt}^\infty, \frac{d}{dt}z_1^\infty, \frac{d}{dt}z_2^\infty) = 0$。

由于 $\frac{d}{dt}z_2^\infty = \phi_t^\infty(0,t) - \Omega_0 = 0$ 并且 $\partial_x\phi_t^\infty = 0$ 和 $\partial_t\phi_t^\infty = 0$，$\phi_t^\infty = \Omega_0$ 成立。

我们还从 $\phi_{xx}^\infty = 0$ 和 $\partial_t\phi_x^\infty = 0$ 得到 ϕ_x^∞ 是 x 的一阶多项式。结合边界条件，如果 $k_i \neq 0$，该系统有唯一解：

$$X_\infty = \left(\phi_x^\infty, \Omega_0, \Omega_0, \frac{\phi_x^\infty(0) - \tilde{g}\Omega_0}{k_i}\right),$$

其中 $\phi_x^\infty(x) = \frac{\gamma_t\Omega_0}{c^2}(x-1) - \frac{c_b}{\alpha_1 I_B}\Omega_0 - \frac{\alpha_2}{\alpha_1}T_0$ 对于 $x \in [0,1]$。 ∎

A. 闭环系统 (10)的指数稳定性

本部分的主要结果如下所述。

定理 1: 设 $N \in \mathbb{N}$。假设存在 $P_N \in \mathbb{S}^{2+2(N+1)}$，$R = \mathrm{diag}(R_1, R_2) \succeq 0, S = \mathrm{diag}(S_1, S_2) \succ 0$，$Q \in \mathbb{S}_+^2$ 使得以下 LMI 成立：

$$\begin{aligned} &\Theta_N = c\,\Theta_{1,N} + \Theta_{2,N} - Q_N \prec 0, \\ &P_N + S_N \succ 0, \end{aligned} \tag{11}$$

以及

$$\begin{aligned} &\Gamma_0 = cR + \tfrac{\gamma_t}{2}U_0 - Q \succeq 0, \\ &\Gamma_1 = cR + \tfrac{\gamma_t}{2}U_1 - Q \succeq 0, \end{aligned} \tag{12}$$

其中

$$\Theta_{1,N} = H_N^\top \left[\begin{smallmatrix} S_1+R_1 & 0 \\ 0 & -S_2 \end{smallmatrix}\right] H_N - G_N^\top \left[\begin{smallmatrix} S_1 & 0 \\ 0 & -S_2-R_2 \end{smallmatrix}\right] G_N,$$

$$\Theta_{2,N} = \mathrm{He}\left(D_N^\top P_N F_N\right),$$

$$\begin{aligned} F_N &= \begin{bmatrix} I_{2+2(N+1)} & 0_{2+2(N+1),2} \end{bmatrix}, \\ D_N &= \begin{bmatrix} J_N^\top & cM_N^\top \end{bmatrix}^\top, \quad J_N = \begin{bmatrix} A & 0_{2,2(N+1)} & B \end{bmatrix}, \\ M_N &= \mathbb{1}_N H_N - \bar{\mathbb{1}}_N G_N - \begin{bmatrix} 0_{2(N+1),2} & L_N & 0_{2(N+1),2} \end{bmatrix}, \\ U_0 &= \left[\begin{smallmatrix} 2S_1 & S_1+S_2+R_2 \\ S_1+S_2+R_2 & 2(S_2+R_2) \end{smallmatrix}\right], \; U_1 = \left[\begin{smallmatrix} 2(S_1+R_1) & S_1+S_2+R_1 \\ S_1+S_2+R_1 & 2S_2 \end{smallmatrix}\right], \\ G_N &= \begin{bmatrix} ck_iC_2 & 0_{2,2(N+1)} & G \\ -ck_iC_2 & & \end{bmatrix}, \quad G = \left[\begin{smallmatrix} 1+c(\tilde{g}+k_p) & 0 \\ 1-c(\tilde{g}+k_p) & 0 \end{smallmatrix}\right], \\ H_N &= \begin{bmatrix} C_1 & 0_{2,2(N+1)} & H \\ C_1 & & \end{bmatrix}, \qquad H = \left[\begin{smallmatrix} 0 & c \\ 0 & -c \end{smallmatrix}\right], \end{aligned} \tag{13}$$

$$\begin{aligned} Q_N &= \mathrm{diag}(0_2, Q, 3Q, \cdots, (2N+1)Q, 0_2), \\ S_N &= \mathrm{diag}\left(0_2, S, 3S, \cdots, (2N+1)S\right), \\ L_N &= \left[\ell_{j,k}\Lambda\right]_{j,k\in[0,N]} - \frac{\gamma_t}{2}\mathrm{diag}\left(\left[\begin{smallmatrix} 1 & 1 \\ 1 & 1 \end{smallmatrix}\right], \ldots, \left[\begin{smallmatrix} 1 & 1 \\ 1 & 1 \end{smallmatrix}\right]\right), \\ \mathbb{1}_N &= \begin{bmatrix} \Lambda \\ \vdots \\ \Lambda \end{bmatrix}, \quad \bar{\mathbb{1}}_N = \begin{bmatrix} \Lambda \\ \vdots \\ (-1)^N\Lambda \end{bmatrix}, \quad \Lambda = \begin{bmatrix} c & 0 \\ 0 & -c \end{bmatrix}, \end{aligned}$$

and

$$\ell_{k,j} = \begin{cases} (2j+1)(1-(-1)^{j+k}), & \text{if } j \leqslant k, \\ 0 & \text{其它}, \end{cases}$$

则系统 (10) 的平衡点是指数稳定的。因此，$\lim_{t\to+\infty}|\phi_t(1,t) - \Omega_0| = 0$。

证明将在后面给出，但首先推导一些实际后果和初步结果。

备注 2: 用于推导前述结果的方法首先在 [42] 中引入以处理时滞系统。前文证明了该定理提供了一系列 LMI 条件。这意味着如果定理 1 的条件对于 $N = N_1 \geqslant 0$ 成立，那么对于所有 $N > N_1$ 这些条件也成立。因此，随着定理阶数 N 的增加，LMI 提供了更精确的分析。

然而，更精确的分析代价是决策变量数量的增加，从而导致更高的计算负担。在 [42] 中对于时滞系统以及在 [8] 中对于耦合的 ODE/弦方程系统，注意到即使对于低阶 N 也能获得非常精确的结果。 □

由于我们旨在证明系统 (10) 的平衡点 X_∞ 在定义 2 的意义上是指数稳定的，因此对于 $t \geq 0$ 定义以下变量：

$$\tilde{X}(t) = X(t) - X_\infty = \left(\tilde{\phi}_x(t), \tilde{\phi}_t(t), \tilde{z}_1(t), \tilde{z}_2(t)\right),$$

其中 X 是系统 (10) 的轨迹。

以下引理在 [7] 中给出，提供了一种方法来估计系统 (10) 的指数衰减率，只要已知 Lyapunov 泛函 V。

引理 2: 设 V 是系统 (10) 的 Lyapunov 泛函，$\mu \geq 0$。假设存在 $\varepsilon_1, \varepsilon_2, \varepsilon_3 > 0$ 使得以下条件成立：

$$\begin{cases} \varepsilon_1\|\tilde{X}\|_{\mathcal{H}}^2 \leqslant V(\tilde{X}) \leqslant \varepsilon_2\|\tilde{X}\|_{\mathcal{H}}^2, \\ \dot{V}(\tilde{X}) + 2\mu V(\tilde{X}) \leqslant -\varepsilon_3\|\tilde{X}\|_{\mathcal{H}}^2, \end{cases} \tag{14}$$

则系统 (10) 的平衡点是 μ-指数稳定的。如果 $\mu = 0$，则

它是指数稳定的。

定理 1 的证明. 为简化起见，本文中使用以下符号表示 $k \in \mathbb{N}$：

$$\tilde{\chi}(x) = \begin{bmatrix} \tilde{\phi}_t(x) + c\tilde{\phi}_x(x) \\ \tilde{\phi}_t(x) - c\tilde{\phi}_x(x) \end{bmatrix}, \quad \tilde{\mathfrak{X}}_k(t) = \int_0^1 \tilde{\chi}(x,t)\mathcal{L}_k(x)dx, \tag{15}$$

其中 $\{\mathcal{L}_k\}_{k\in\mathbb{N}}$ 是附录 A 中定义的勒让德多项式的正交族。$\tilde{\mathfrak{X}}_k$ 是 $\tilde{\chi}$ 沿勒让德多项式的 k 次投影系数。$\tilde{\chi}$ 指的是黎曼坐标，并且具有有用的性质，如 [8] 中所讨论的。

1) Lyapunov 泛函候选的选择: 所提出的 Lyapunov 泛函受 [7], [8], [36] 的启发，并分为两部分，如下所示：

$$V_N(\tilde{X}) = \tilde{Z}_N^\top P_N \tilde{Z}_N + \mathcal{V}(\tilde{\chi}) \tag{16}$$

其中 $\tilde{Z}_N = \begin{bmatrix} \tilde{z}_1 & \tilde{z}_2 & \tilde{\mathfrak{X}}_0^\top & \cdots & \tilde{\mathfrak{X}}_N^\top \end{bmatrix}^\top$ 和

$$\mathcal{V}(\tilde{\chi}) = \int_0^1 \tilde{\chi}^\top(x) \begin{bmatrix} S_1+xR_1 & 0 \\ 0 & S_2+(1-x)R_2 \end{bmatrix} \tilde{\chi}(x)dx.$$

$\mathcal{V}$ 是一个传统的 Lyapunov 泛函候选，用于传输系统，如 [16] 中所示。

2) 指数稳定性:

存在 ε_1: 这一部分受 [7] 的启发。不等式 $P_N + S_N \succ 0, R \succeq 0$ 意味着存在 $\varepsilon_1 > 0$ 使得：

$$\begin{aligned} P_N + S_N &\succeq \varepsilon_1 \mathrm{diag}\left(I_2, \tfrac{1}{2}\mathcal{I}_N\right), \\ S &\succeq \tfrac{\varepsilon_1}{2} I_2, \end{aligned} \tag{17}$$

其中 $\mathcal{I}_N = \mathrm{diag}\left\{(2k+1)I_2\right\}_{k\in[0,N]}$。这一陈述对 V_N 意味着：

$$\begin{aligned} V_N(\tilde{X}) &\geq \tilde{Z}_N^\top (P_N + S_N)\tilde{Z}_N - \sum_{k=0}^{N}(2k+1)\tilde{\mathfrak{X}}_k^\top S \tilde{\mathfrak{X}}_k \\ &\quad + \int_0^1 \tilde{\chi}(x)^\top \left(S - \frac{\varepsilon_1}{2} I_2\right)\tilde{\chi}(x)dx + \frac{\varepsilon_1}{2}\|\tilde{\chi}\|^2 \\ &\geq \varepsilon_1 \left(\tilde{z}_1^2 + \tilde{z}_2^2 + \tfrac{1}{2}\|\tilde{\chi}\|^2\right) \\ &\quad - \sum_{k=0}^{N}(2k+1)\tilde{\mathfrak{X}}_k^\top \tilde{S}\tilde{\mathfrak{X}}_k + \int_0^1 \tilde{\chi}^\top(x)\tilde{S}\tilde{\chi}(x)dx \\ &\geq \varepsilon_1 \|\tilde{X}\|_{\mathcal{H}}^2, \end{aligned}$$

其中 $\tilde{S} = S - \frac{\varepsilon_1}{2} I_2$，这结束了 ε_1 存在性的证明。

存在 ε_2: 与之前相同的思路，存在足够大的 $\varepsilon_2 > 0$ 使得：

$$\begin{aligned} P_N &\preceq \varepsilon_2 \mathrm{diag}\left(I_2, \tfrac{1}{4}\mathcal{I}_N\right), \\ \begin{bmatrix} S_1+xR_1 & 0 \\ 0 & S_2+(1-x)R_2 \end{bmatrix} &\preceq \tfrac{\varepsilon_2}{4} I_2. \end{aligned}$$

使用这些不等式在 (16) 中得到：

$$\begin{aligned} V_N(\tilde{X}) &\leq \varepsilon_2 \left(\tilde{z}_1^2 + \tilde{z}_2^2 + \sum_{k=0}^{N}\frac{2k+1}{4}\tilde{\mathfrak{X}}_k^\top \tilde{\mathfrak{X}}_k + \frac{1}{4}\|\tilde{\chi}\|^2\right) \\ &\leq \varepsilon_2 \left(\tilde{z}_1^2 + \tilde{z}_2^2 + \tfrac{1}{2}\|\tilde{\chi}\|^2\right) = \varepsilon_2 \|\tilde{X}\|_{\mathcal{H}}^2. \end{aligned}$$

最后一个不等式是引理 4 的直接应用。

存在 ε_3: $\tilde{\chi}$ 的时间导数为：

$$\tilde{\chi}_t(x) = \Lambda\tilde{\chi}_x(x) - \gamma_t \begin{bmatrix} 1 \\ 1 \end{bmatrix} \tilde{\phi}_t(x)$$

注意到 $\tilde{\phi}_t(x) = \frac{1}{2}\begin{bmatrix} 1 & 1 \end{bmatrix}\tilde{\chi}(x)$，我们得到：

$$\tilde{\chi}_t(x) = \Lambda\tilde{\chi}_x(x) - \frac{\gamma_t}{2}\begin{bmatrix} 1 & 1 \\ 1 & 1 \end{bmatrix}\tilde{\chi}(x) \tag{18}$$

沿着 (6) 轨迹的 $\mathcal{V}$ 的导数为：

$$\dot{\mathcal{V}}(\tilde{\chi}) = 2c\mathcal{V}_1(\tilde{\chi}) - \frac{\gamma_t}{2}\mathcal{V}_2(\tilde{\chi})$$

其中

$$\begin{aligned} \mathcal{V}_1(\tilde{\chi}) &= \int_0^1 \tilde{\chi}_x^\top(x) \begin{bmatrix} S_1+xR_1 & 0 \\ 0 & -S_2-(1-x)R_2 \end{bmatrix} \tilde{\chi}(x)dx, \\ \mathcal{V}_2(\tilde{\chi}) &= \int_0^1 \tilde{\chi}^\top(x)U(x)\tilde{\chi}(x)dx, \\ U(x) &= \begin{bmatrix} 2(S_1+xR_1) & S_1+S_2+xR_1+(1-x)R_2 \\ S_1+S_2+xR_1+(1-x)R_2 & 2(S_2+(1-x)R_2) \end{bmatrix}. \end{aligned}$$

对 $\mathcal{V}_1$ 进行分部积分得到：

$$\begin{aligned} 2\mathcal{V}_1(\tilde{\chi}) &= \tilde{\chi}^\top(1) \begin{bmatrix} S_1+R_1 & 0 \\ 0 & -S_2 \end{bmatrix} \tilde{\chi}(1) \\ &\quad - \tilde{\chi}^\top(0) \begin{bmatrix} S_1 & 0 \\ 0 & -S_2-R_2 \end{bmatrix} \tilde{\chi}(0) \\ &\quad - \int_0^1 \tilde{\chi}^\top(x) \begin{bmatrix} R_1 & 0 \\ 0 & R_2 \end{bmatrix} \tilde{\chi}(x)dx. \end{aligned}$$

之前的计算得到以下导数：

$$\begin{aligned} \dot{\mathcal{V}}(\tilde{\chi}) &= c\left(\tilde{\chi}^\top(1) \begin{bmatrix} S_1+R_1 & 0 \\ 0 & -S_2 \end{bmatrix} \tilde{\chi}(1) \right. \\ &\quad \left. - \tilde{\chi}^\top(0) \begin{bmatrix} S_1 & 0 \\ 0 & -S_2-R_2 \end{bmatrix} \tilde{\chi}(0)\right) \\ &\quad - \int_0^1 \tilde{\chi}\,(x)\left(cR + \frac{\gamma_t}{2}U(x)\right)\tilde{\chi}(x)dx. \end{aligned} \tag{19}$$

通过凸性论证，如果 (12) 得到验证，则 $cR+U(x)\succeq Q\succ 0$ 对于 $x\in[0,1]$ 成立。因此，注意到 $\tilde{\chi}(0)=G_N\tilde{\xi}_N$，$\tilde{\chi}(1)=H_N\tilde{\xi}_N$，我们得到：

$$\dot{\mathcal{V}}(\tilde{\chi})\leq c\tilde{\xi}_N^\top\Theta_{1,N}\tilde{\xi}_N-\int_0^1\tilde{\chi}^\top(x)Q\tilde{\chi}(x)dx,$$

其中

$$\tilde{\xi}_N=\begin{bmatrix}\tilde{Z}_N^\top & \tilde{\phi}_t(0) & \tilde{\phi}_x(1)\end{bmatrix}^\top.$$

使用引理 5 并且 $\dot{\tilde{Z}}_N=D_N\tilde{\xi}_N$ 和 $\tilde{Z}_N=F_N\tilde{\xi}_N$，我们得到以下结果：

$$\begin{aligned}\dot{V}_N(\tilde{X}) &= \mathrm{He}\left(\dot{\tilde{Z}}_N^\top P_N\tilde{Z}_N\right)+\dot{\mathcal{V}}(\tilde{\chi})\\ &\leq \tilde{\xi}_N^\top\Theta_N\tilde{\xi}_N+\sum_{k=0}^{N}(2k+1)\tilde{\mathfrak{x}}_kQ\tilde{\mathfrak{x}}_k\\ &\qquad -\int_0^1\tilde{\chi}^\top(x)Q\tilde{\chi}(x)dx,\end{aligned}\tag{20}$$

其中 Θ_N 定义在 (11) 中。由于 $\Theta_N\prec 0$ 和 $Q\succ 0$，我们得到：

$$\begin{aligned}\Theta_N &\preceq -\varepsilon_3\mathrm{diag}\left(I_2,\tfrac{1}{2}I_2,\tfrac{3}{2}I_2,\ldots,\tfrac{2N+1}{2}I_2,0_2\right),\\ Q &\succeq \tfrac{\varepsilon_3}{2}I_2.\end{aligned}$$

然后，$\dot{V}_N$ 的上界为：

$$\begin{aligned}\dot{V}_N(\tilde{X}) &\leq -\varepsilon_3\left(\tilde{z}_1^2+\tilde{z}_2^2+\tfrac{1}{2}\|\tilde{\chi}\|^2\right)\\ &\quad+\sum_{k=0}^{N}(2k+1)\tilde{\mathfrak{x}}_k^\top\left(Q-\frac{\varepsilon_3}{2}I_2\right)\tilde{\mathfrak{x}}_k\\ &\quad-\int_0^1\tilde{\chi}^\top(x)\left(Q-\frac{\varepsilon_3}{2}I_2\right)\tilde{\chi}(x)dx\\ &\leq -\varepsilon_3\|\tilde{X}\|_{\mathcal{H}}^2.\end{aligned}$$

最后一个不等式直接应用了贝塞尔不等式 (31)。

结论：使用引理 2，我们确实得到了所有轨迹 (10) 到期望平衡点的指数收敛。 ∎

B. 具有保证衰减率的指数稳定性

可以通过对 LMI 进行轻微修改来估计指数收敛的衰减率 μ，如下推论所示。

推论 1: 设 $N\in\mathbb{N}$，$\mu>0$ 和 $\gamma_t\geq 0$。如果存在 $P_N\in\mathbb{S}^{2+2(N+1)}$，$R=\mathrm{diag}(R_1,R_2)\succeq 0, S=\mathrm{diag}(S_1,S_2)\succ 0, Q\in\mathbb{S}_+^2$ 使得 (12) 和以下 LMI 成立：

$$\begin{aligned}&\Theta_{N,\mu}=\Theta_N+2\mu F_N^\top\left(P_N+S_N\right)F_N\prec 0,\\ &P_N+S_N\succ 0,\end{aligned}\tag{21}$$

参数定义如定理 1 中所述，则系统 (10) 的平衡点是 μ-指数稳定的。

证明. 为了证明具有至少 $\mu>0$ 的衰减率的指数稳定性，我们使用引理 2。与之前的证明类似，我们有 $\varepsilon_1,\varepsilon_2>0$ 的存在性。ε_3 的存在性略有不同。首先，注意到对于 Lyapunov 泛函候选 (16)，我们得到：

$$\begin{aligned}V_N(\tilde{X}_\phi) &\geq \tilde{Z}_N^\top P_N\tilde{Z}_N+\int_0^1\tilde{\chi}^\top(x)S\tilde{\chi}(x)dx\\ &\geq \tilde{Z}_N^\top P_N\tilde{Z}_N+\sum_{k=0}^{N}(2k+1)\tilde{\mathfrak{x}}_k^\top S\tilde{\mathfrak{x}}_k\end{aligned}$$

这个不等式是使用方程 (31) 得到的。使用前述定理的符号表示：

$$V_N(\tilde{X}_\phi)\geq\tilde{\xi}_N^\top F_N^\top\left(P_N+S_N\right)F_N\tilde{\xi}_N\tag{22}$$

回到 (20) 并使用 (21) 得到：

$$\begin{aligned}\dot{V}_N(\tilde{X}_\phi) &\leq \tilde{\xi}_N^\top\Theta_{N,\mu}\tilde{\xi}_N-2\mu\tilde{\xi}_N^\top\left(F_N^\top P_NF_N+S_N\right)\tilde{\xi}_N\\ &\quad+\sum_{k=0}^{N}(2k+1)\tilde{\mathfrak{x}}_k^\top Q\tilde{\mathfrak{x}}_k-\int_0^1\tilde{\chi}^\top(x)Q\tilde{\chi}(x)dx\end{aligned}$$

将不等式 (22) 代入前述不等式中得到：

$$\begin{aligned}\dot{V}_N(\tilde{X}_\phi)+2\mu V_N(\tilde{X}_\phi) &\leq \tilde{\xi}_N^\top\Theta_{N,\mu}\tilde{\xi}_N\\ &\quad+\sum_{k=0}^{N}(2k+1)\tilde{\mathfrak{x}}_k^\top Q\tilde{\mathfrak{x}}_k-\int_0^1\tilde{\chi}^\top(x)Q\tilde{\chi}(x)dx\end{aligned}$$

使用与之前证明相同的技术，得到 $\varepsilon_3>0$ 的存在性，使得：

$$\dot{V}_N(\tilde{X}_\phi)+2\mu V_N(\tilde{X}_\phi)\leq -\varepsilon_3\|\tilde{X}_\phi\|_{\mathcal{H}}^2$$

引理 2 然后得出 μ-指数稳定性。 ∎

备注 3: 波动方程有时可以建模为中立型时滞系统 [6], [38]。这种系统已知具有一些必要的稳定性条件，如 [6], [9] 中所述。在书中 [9] 推导了以下准则：

$$\mu\leq\frac{c}{2}\log\left|\frac{1+c(\tilde{g}+k_p)}{1-c(\tilde{g}+k_p)}\right|=\mu_{max}\tag{23}$$

这个结果表明存在一个最大衰减率，如果这个最大值为负，则系统是不稳定的。LMI $\Theta_N^\mu \prec 0$ 包含了相同的必要条件，这意味着系统的中立特性得到了很好的捕捉。□

C. 对控制中的小延迟具有强稳定性

系统 (10) 的中立特性带来的一个实际后果是它对控制中的延迟非常敏感 (9)。确实，如果控制稍有延迟，可以从频率分析中推导出一个新的必要稳定性条件（等同于 (23)）（见 [21] 的推论 3.3）：

$$\left|\frac{1-c\tilde{g}}{1+c\tilde{g}}\right| + 2\left|\frac{ck_p}{1+c\tilde{g}}\right| < 1$$

实际上，这个不等式更为严格，并且取 $k_p \neq 0$ 实际上会导致鲁棒性的降低（即使某些其他性能可能会提高）。这种现象在许多文章中进行了研究 [22], [29], [44]。因此，为了在环路中对延迟具有鲁棒性，需要确保以下条件：

$$0 \leq k_p \leq \frac{1}{2c}\left(|1+c\tilde{g}| - |1-c\tilde{g}|\right) = \tilde{g} = 2.1 \cdot 10^{-3}$$

这个关于 k_p 的不等式在考虑无限维问题时出现，而在处理任何有限维模型时不会出现。这一点表明考虑无限维问题更为现实。有关该点的更多信息，感兴趣的读者可以参考 [5]。

V. 系统 (6)-(9)的实际稳定性

之前进行的实验表明，对于较大的 Ω_0，非线性系统 (6)-(9) 的轨迹指数收敛到 X_∞，线性系统也是如此。换句话说，之前的结果是针对大期望角速度 Ω_0 的非线性系统的局部稳定性测试，并不能直接扩展到全局分析。

一般来说，对于非线性系统，确保平衡点的全局指数稳定性可能会很复杂。在许多工程情况下，全局指数稳定性并不是要求。实际上，考虑到系统中的不确定性或非线性，对于工程师来说，确保轨迹保持在平衡点附近是更为合理和可接受的。这种特性在 Levinson 的意义上称为耗散性 [26] 或实际稳定性（在 [24] 中也称为全局一致最终有界性）。

定义 *3:* 系统 (6) 是**实际稳定的**，如果存在 $X_{bound} \geq 0$，使得对于初始条件 $X_0 \in \mathcal{H}$ 的解 X：

$$\forall \eta > 0, \exists T_\eta > 0, \forall t \geq T_\eta, \quad \|X(t) - X_\infty\|_{\mathcal{H}} \leq X_{bound} + \eta \tag{24}$$

说系统 (6)-(9) 是实际稳定的，意味着存在 $T_\eta > 0$，使得对于任何 $x \in [0,1]$，$\phi_t(x,t)$ 在 $t \geq T_\eta$ 时保持接近 Ω_0。这种特性已经在 [39] 中应用于钻井系统。例如，在非线性情况下，目标是设计一种控制律，以减少发生粘滑现象时的振幅。

本节的目标是推导一个 LMI 测试，以确保非线性系统 (6) 及其控制器 (9) 的实际稳定性：

$$\begin{cases} \phi_{tt}(x,t) = c^2\phi_{xx}(x,t) - \gamma_t\phi_t(x,t), \\ \phi_x(0,t) = (\tilde{g}+k_p)\phi_t(0,t) - k_p\Omega_0 + k_iC_2Z(t), \\ \phi_t(1,t) = C_1Z(t), \\ \dot{Z}(t) = AZ(t) + B\begin{bmatrix}\phi_t(0,t)\\ \phi_x(1,t)\end{bmatrix} + B_2\begin{bmatrix}\Omega_0\\ T_{nl}(z_1(t))\end{bmatrix}, \end{cases} \tag{25}$$

备注 *4:* 为简化书写，ϕ 可以同时表示线性或非线性系统的解，具体取决于上下文。在本部分中，它指的是非线性系统 (25) 的解。□

A. 系统 (25)的实际稳定性

实际稳定性的思想是通过使用适当的扇区条件来嵌入静态非线性，就像对饱和现象所做的那样 [43]。然后，使用鲁棒工具将导致一些 LMI 测试，以确保实际稳定性。

引理 *3:* 对于几乎所有的 $\tilde{z}_1 \in \mathbb{R}$，以下条件成立：

$$\begin{aligned} &T_{nl}(\tilde{z}_1+\Omega_0)^2 \leq T_{max}^2, \qquad T_{min}^2 \leq T_{nl}(\tilde{z}_1+\Omega_0)^2, \\ &-2\left(\tilde{z}_1+\Omega_0\right)T_{nl}(\tilde{z}_1+\Omega_0) \leq 0. \end{aligned} \tag{26}$$

证明. 这些不等式可以通过使用 (2) 轻松验证。■

这些新信息是以下定理的基础。

定理 *2:* 设 $N \in \mathbb{N}$ 且 $V_{max} > 0$。如果存在 $P_N \in \mathbb{S}^{2+2(N+1)}$，$R = \mathrm{diag}(R_1, R_2) \succeq 0, S = \mathrm{diag}(S_1, S_2) \succ 0, Q \in \mathbb{S}_+^2, \tau_0, \tau_1, \tau_2, \tau_3 \geq 0$ 使得 (12) 成立，并且：

$$\begin{aligned} &\Xi_N = \bar{\Theta}_N - \tau_0\Pi_0 - \tau_1\Pi_1 - \tau_2\Pi_2 - \tau_3\Pi_3 \prec 0, \\ &P_N + S_N \succ 0, \end{aligned} \tag{27}$$

其中

$$\begin{aligned} \bar{\Theta}_N = &\,\mathrm{diag}(\Theta_N, 0_2) \\ &-\alpha_2\,\mathrm{He}\left((F_{m1}-T_0F_{m2})^\top e_1^\top P_N\tilde{F}_N\right), \end{aligned}$$

$$\tilde{F}_N = \begin{bmatrix} F_N & 0_{2(N+1)+2,2} \end{bmatrix}, \quad e_1 = \begin{bmatrix} 1 & 0_{1,2(N+1)+1} \end{bmatrix}^\top,$$

$$F_{m1} = \begin{bmatrix} 0_{1,2(N+1)+4} & 1 & 0 \end{bmatrix}, \quad F_{m2} = \begin{bmatrix} 0_{1,2(N+1)+4} & 0 & 1 \end{bmatrix},$$

$$\Pi_0 = V_{max} F_{m2}^\top F_{m2} - \tilde{F}_N^\top (P_N + S_N) \tilde{F}_N,$$

$$\Pi_1 = \pi_2^\top \pi_2 - T_{max}^2 \pi_3^\top \pi_3, \quad \Pi_2 = T_{min}^2 \pi_3^\top \pi_3 - \pi_2^\top \pi_2,$$

$$\Pi_3 = -\operatorname{He}((\pi_1 + \Omega_0 \pi_3)^\top \pi_2),$$

$$\pi_1 = \begin{bmatrix} 1, 0_{1,2(N+1)+3}, 0, 0 \end{bmatrix}, \quad \pi_2 = \begin{bmatrix} 0_{1,2(N+1)+4}, 1, 0 \end{bmatrix},$$

$$\pi_3 = \begin{bmatrix} 0_{1,2(N+1)+4}, 0, 1 \end{bmatrix},$$

并且所有参数定义如定理 1 中所述，则系统 (25) 的平衡点 X_∞ 是实际稳定的。更具体地说，方程 (24) 对于 $X_{bound} = \sqrt{V_{max} \varepsilon_1^{-1}}$ 成立，其中 ε_1 定义在 (17) 中。

证明. 首先，进行与之前相同的变量变换：

$$\tilde{X} = X - X_\infty.$$

由于非线性仅影响系统 (25) 的 ODE 部分，与之前部分的区别在于 $\tilde{Z}$ 的动态：

$$\begin{aligned} \dot{\tilde{Z}}(t) &= \tfrac{d}{dt} \left(Z(t) - \begin{bmatrix} z_1^\infty \\ z_2^\infty \end{bmatrix} \right) \\ &= A \tilde{Z}(t) + B \begin{bmatrix} \tilde{\phi}_t(0,t) \\ \tilde{\phi}_x(1,t) \end{bmatrix} + B_2 \begin{bmatrix} 0 \\ T_{nl}(\tilde{z}_1(t) + \Omega_0) - T_0 \end{bmatrix}. \end{aligned}$$

使用与 (16) 中相同的 Lyapunov 泛函，正定性以完全相同的方式得到保证。对于时间导数的界限，遵循与之前相同的策略，我们很容易得到：

$$\begin{aligned} \dot{V}_N(\tilde{X}) \leq \tilde{\xi}_N^\top \Theta_N \tilde{\xi}_N - 2\alpha_2 (T_{nl}(\tilde{z}_1 + \Omega_0) - T_0) e_1^\top P_N \tilde{Z}_N \\ + \sum_{k=0}^{N} (2k+1) \tilde{\mathfrak{X}}_k^\top Q \tilde{\mathfrak{X}}_k - \int_0^1 \tilde{\chi}^\top(x) Q \tilde{\chi}(x) dx. \end{aligned} \tag{28}$$

我们引入一个新的扩展状态变量 $\bar{\xi}_N = \begin{bmatrix} \tilde{\xi}_N^\top & T_{nl}(\tilde{z}_1 + \Omega_0) & 1 \end{bmatrix}^\top$。使用定理 2 的符号表示，方程 (28) 重写为：

$$\begin{aligned} \dot{V}_N(\tilde{X}) \leq \bar{\xi}_N^\top \bar{\Theta}_N \bar{\xi}_N^\top + \sum_{k=0}^{N} (2k+1) \tilde{\mathfrak{X}}_k^\top Q \tilde{\mathfrak{X}}_k \\ - \int_0^1 \tilde{\chi}^\top(x) Q \tilde{\chi}(x) dx. \end{aligned}$$

由于其最后的 2×2 对角块是 0_2，因此不可能确保 $\bar{\Theta}_N \prec 0$。

然后我们使用实际稳定性的定义。我们想要证明，如果存在 $\varepsilon_3 > 0$ 使得当 $V_N(\tilde{X}) \geq V_{max}$ 时 $\dot{V}_N(\tilde{X}) \leq -\varepsilon_3 \|\tilde{X}\|_{\mathcal{H}}^2$，则系统是实际稳定的。

设 $\mathcal{S} = \left\{ \tilde{X} \in \mathcal{H} \mid V_N(\tilde{X}) \leq V_{max} \right\}$，前述断言意味着该集合是一个不变且有吸引力的集合。使用 (17)，我们得到 $\left\{ \tilde{X} \in \mathcal{H} \mid \|\tilde{X}\|_{\mathcal{H}} \leq X_{bound} = V_{max}^{1/2} \varepsilon_1^{-1/2} \right\} \supseteq \mathcal{S}$，这意味着系统是实际稳定的。

一个实际稳定的充分条件是 V_N 在球的半径 V_{max} 之外严格递减。这个条件重写为 $V_N(\tilde{X}) \geq V_{max}$ 并且以下条件成立：

$$\begin{aligned} V_N(\tilde{X}) - V_{max} &\geq \tilde{Z}_N^\top P_N \tilde{Z}_N + \int_0^1 \tilde{\chi}^\top(x) S \tilde{\chi}(x) dx - V_{max} \\ &\geq -\bar{\xi}_N^\top \Pi_0 \bar{\xi}_N \geq 0. \end{aligned}$$

前述不等式是使用贝塞尔不等式 (31) 对 $\int_0^1 \tilde{\chi}^\top(x) S \tilde{\chi}(x) dx$ 得到的。因此，如果 $\bar{\xi}_N^\top \Pi_0 \bar{\xi}_N \leq 0$，则 $V_N(\tilde{X}) \geq V_{max}$。

注意到 $\tilde{z}_1 = \pi_1 \bar{\xi}_N, T_{nl}(\tilde{z}_1 + \Omega_0) = \pi_2 \bar{\xi}_N$ 和 $1 = \pi_3 \bar{\xi}_N$，引理 3 重写为：

$$\forall i \in \{1,2,3\}, \quad \bar{\xi}_N \ \Pi_i \ \bar{\xi}_N \leq 0.$$

因此，一个实际稳定的充分条件是：

$$\forall \bar{\xi}_N \neq 0 \text{ s. t. } \forall i \in [0,3], \bar{\xi}_N^\top \Pi_i \bar{\xi}_N \leq 0, \quad \bar{\xi}_N^\top \bar{\Theta}_N \bar{\xi}_N < 0. \tag{29}$$

一种称为 *S-variable* 的技术，如 [18] 中所述，将前述不等式转化为 LMI 条件。实际上，[18] 中的定理 1.1 表明，如果存在 $\tau_0, \tau_1, \tau_2, \tau_3 > 0$ 使得条件 (29) 得到验证，则

$$\bar{\Theta}_N - \sum_{k=0}^{3} \tau_i \Pi_i \prec 0$$

因此，与定理 1 类似，条件 (27) 意味着 $\mathcal{S}$ 是系统 (25) 的不变且有吸引力的集合。然后，系统 (25) 的平衡点 X_∞ 是实际稳定的，$X_{bound} = \sqrt{V_{max} \varepsilon_1^{-1}}$。 ■

注意，如果扭矩函数不是完全已知的，可以更改下限和上限 T_{min} 和 T_{max} 以获得更保守但对 T_{nl} 不确定性具有鲁棒性的结果。为了使 (27) 可行，必须满足约束 $\bar{\xi}_N^\top \Pi_1 \bar{\xi}_N \leq 0$，这意味着需要提出 T_{nl} 的上限。

B. 关于 X_{bound} 的优化

条件 (27) 是一个双线性矩阵不等式（BMI），因为 τ_0、τ_1、τ_2 和 τ_3 是决策变量，因此很难获得其全局最优

解。然而，以下引理给出了该问题存在解的充分条件。

推论 2: 存在 V_{max} 和 $\tau_0 > 0$ 使得定理 2 成立，当且仅当存在 $N > 0$ 使得 LMI (12) 和 (11) 得到满足。

换句话说，系统 (25) 的平衡点是实际稳定的，当且仅当线性系统 (10) 是指数稳定的。

证明. 首先注意到，当 $\tau_3 = 0$ 时，扩展 (27) 得到：

$$\Xi_N = \left[\begin{array}{c|cc} \Theta_{N,\tau_0/2} & \multicolumn{2}{c}{\kappa_{P_N}} \\ \hline & \tau_2-\tau_1 & 0 \\ \kappa_{P_N}^\top & \hline 0 & \tau_1 T_{max}^2 - \tau_2 T_{min}^2 \\ & & -\tau_0 V_{max} \end{array}\right], \quad (30)$$

其中 $\kappa_{P_N} \in \mathbb{R}^{(4+2(N+1))\times 2}$ 仅依赖于 P_N。

充分性证明: 假设存在 $N > 0$ 使得 LMI (12) 和 (11) 得到满足。考虑 $\tau_2 = 0$ 并使用 Schur 补对 Ξ_N 进行处理，$\Xi_N \prec 0$ 等价于：

$$\Theta_{N,\tau_0/2} - \kappa_{P_N} \begin{bmatrix} -\frac{1}{\tau_1} & 0 \\ 0 & \frac{1}{\tau_1 T_{max}^2 - \tau_0 V_{max}} \end{bmatrix} \kappa_{P_N}^\top \prec 0,$$

其中 $\tau_0 V_{max} > \tau_1 T_{max}^2$。由于 $\Theta_N \prec 0$，考虑 τ_0 足够小，τ_1 足够大且 $V_{max} > \tau_1 \tau_0^{-1} T_{max}^2$，前述条件总是满足的，因此定理 2 适用。

必要性证明: 假设 $\Xi_N \prec 0$ 并且 (12) 成立。那么其第一个对角块必须是负定的。因此 $\Theta_N \prec 0$，根据定理 1，系统 (10) 是指数稳定的。 ■

备注 5: 注意到 (30) 为定理 2 提供了一个必要条件，即 $\Theta_{N,\tau_0/2} \prec 0$。换句话说，$\tau_0$ 与线性系统的衰减率相关，我们得到以下条件：$\tau_0 < 2\mu_{max}$。 □

得益于推论 2，如果定理 1 得到验证，以下方法应有助于解决 BMI 问题。假设对于给定的 $N \in \mathbb{N}$，方程 (11) 和 (12) 得到验证。

1) 固定 $\tau_0 = 2\mu_{max}$，如 (23) 中定义。
2) 检查方程 (11)、(12) 和 (27) 是否对 V_{max} 为严格正的决策变量得到满足。如果不是这种情况，则减少 τ_0 并重新执行此步骤。
3) 得益于推论 2，存在一个足够小的 τ_0 使得方程 (11)、(12) 和 (27) 得到满足。冻结此值。
4) 由于问题是无界的，可以在不损失一般性的情况下固定一个变量，例如 $V_{max} = 10^4$，并解决以下优化问题：

$$\begin{aligned} \min_{P_N,S,R,Q,\tau_1,\tau_2,\tau_3,\varepsilon_P} \quad & -\varepsilon_P \\ & (11),(12) \text{ 和}(27), \\ \text{约束条件：} \quad & P_N + S_N - \mathrm{diag}(\varepsilon_P, 0_{2N+3}) \succ 0, \\ & R \succeq 0, S \succ 0, Q \succ 0. \end{aligned}$$

5) 然后计算 $X_{bound} = \sqrt{V_{max}\varepsilon_1^{-1}}$，其中 ε_1 定义在 (17) 中。

VI. 实例与仿真

本节致力于数值仿真[2] 并对 PI 调节得出一些结论。在第一小节中，我们关注线性系统，第二小节则专注于非线性情况。

A. 关于线性模型

本小节总结了关于线性模型的结果。

1) 衰减率的估计: 主要结果是直接应用推论 1 对于 $k_p = 10^{-3}$ 和 $k_i = 10$。实际上，使用一种二分法算法，得到了表 IV。它显示了在给定阶数 0 到 6 之间的估计衰减率 μ。

表 IV 中首先要注意的是层次属性，衰减率是阶数的递增函数，如备注 2 中所述。还要注意的是，阶数 0 和阶数 1 之间的差距显著，表明使用投影确实改善了结果。

对于高于 2 的阶数，估计的衰减率略有增加，并且在四位小数的精度下，它在 $N = 6$ 时达到最大值。由于这是使用方程 (23) 获得的最大允许衰减率，这表明本文使用的 Lyapunov 泛函和条件 (21) 是准确的，并提供了良好的分析。图 5 表示了线性系统的仿真，并确认了相同的观察结果。实际上，可以看到系统的能量被指数曲线很好地界定，并且随着 N 的增加，界限变得越来越准确。

2) 闭环系统的稳定性: 我们现在感兴趣的是估计耦合系统的衰减率 μ_{max} 为阶数 $N = 5$ 时的增益 k_p 和 k_i 的稳定区域。这导致了图 6，可以很容易地看到，增加增益 k_p 会减少可能的 k_i 范围，同时增加其速度（见方程 (23)）。很自然地注意到，k_i 越大，系统越慢，而增加比例增益会导致系统更快。总之，对于小值的 k_p

[2]数值仿真使用一阶近似，至少有 80 个空间离散点和 9949 个时间离散点。仿真使用 Yalmip [28] 结合 SDP 求解器 SDPT-3 [46] 进行。代码可在 *https://homepages.laas.fr/mbarreau* 获取。

阶数	$N=0$	$N=1$	$N=2$	$N=3$	$N=6$
μ $(\times 10^{-3})$	0.87	4.24	7.31	7.59	7.73

表 IV: 估计的衰减率作为使用阶数 N 的函数。注意 $\mu_{max} = 7.73 \cdot 10^{-3}$ 是使用 (23) 对于 $k_p = 10^{-3}$，$k_i = 10$ 计算的。

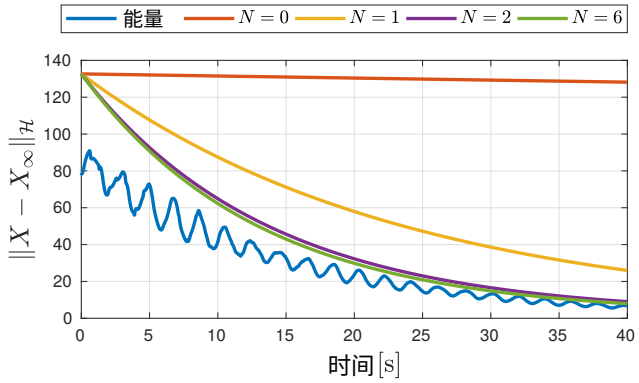

图 5: 线性系统的 X 能量，对于 $k_p = 10^{-3}$，$k_i = 10$ 和 $\Omega_0 = 5$ 初始条件是 $\phi^0(x) = 4\left(\int_0^x \phi_x^\infty(s)ds + 0.1\cos(2x)\right)$，$\phi^1 = 2\Omega_0$ 和 $Z(0) = 2\,[z_1^\infty \; z_2^\infty]^\top$

和 k_i，系统是稳定的，这是两篇论文 [44], [45] 使用不同的 Lyapunov 泛函得出的结论。注意，使用之前的论文，不可能量化“足够小的增益 k_p 和 k_i”的概念，而使用本文的方法可以给出估计。

B. 粘滑效应对非线性模型的影响

前一小节显示，对于某些增益 k_p 和 k_i，线性模型是全局渐近稳定的，因此非线性系统 (25) 对于较大的期望角速度 Ω_0 是局部渐近稳定的。这可以在图 7a 中验证，参数为 $k_p = 10^{-3}$，$k_i = 10$ 和 $\Omega_0 = 10$。可以看到，如果初始条件接近平衡点，线性和非线性系统的行为相似。

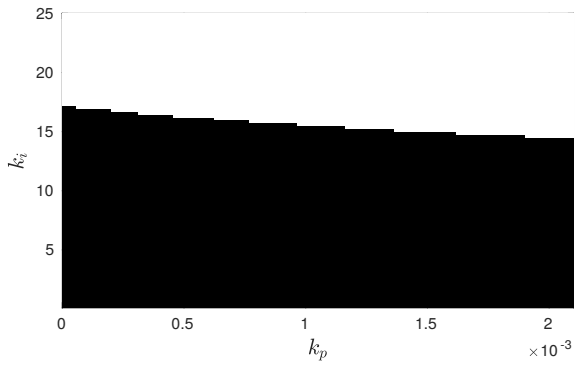

图 6: 使用定理 1，对于 $N = 5$，导致系统具有最大衰减率的增益 k_p 和 k_i 的值。黑色区域是稳定的，白色区域被认为是不稳定的，直到阶数 5

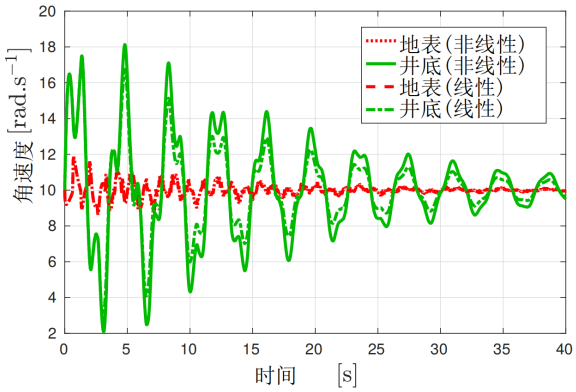

(a) 系统 (10) 和 (25)：$\Omega_0 = \phi^1 = 10$，$\phi^0(x) = (1 + 0.32\sin(x))\int_0^x \phi_x^\infty(s)ds$ 和 $Z(0) = (z_1^\infty \; z_2^\infty)^\top$

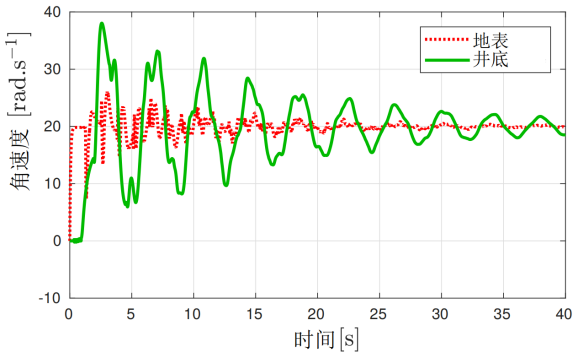

(b) 系统 (25)：$\Omega_0 = 20$，$\phi^0 = 0$，$\phi^1 = 0$ 和 $Z(0) = 0_{2,1}$

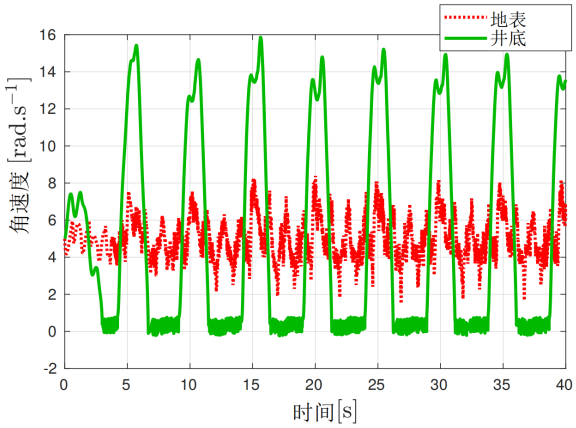

(c) 系统 (25)：$\Omega_0 = \phi^1 = 5$，$\phi^0(x) = (1 + 0.1\sin(x))\int_0^x \phi_x^\infty(s)ds$ 和 $Z(0) = (z_1^\infty \; z_2^\infty)^\top$

图 7: 系统 (10) 和 (25) 的数值仿真，参数为 $k_p = 10^{-3}$，$k_i = 10$

Ω_0 越高，吸引域越大。实际上，调节试图将系统带入 T_{nl} 的“准”线性区域，在该区域它接近常数 T_{min}，如图 3 所示。因此，粘滑现象可能在开始时发生，但不会持续很长时间，如图 7b 所示，这是在零初始条件下对非线性模型的数值仿真。

真正的挑战是低期望角速度 Ω_0 的情况。图 7c 显示了对非线性模型的仿真结果，$\Omega_0 = 5$ rad.s^{-1} ($k_p = 10^{-3}$，$k_i = 10$)。首先，注意到振荡频率为 0.2Hz，振幅约为 15 rad.s^{-1}。这与使用图 2 估计的结果非常接近。因此，

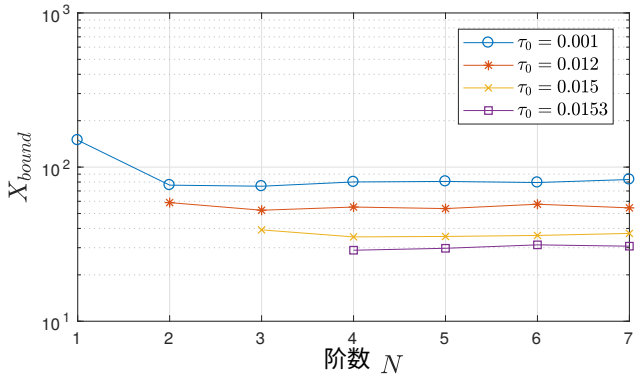

图 8: BMI (27) 的解 X_{bound}，参数为 $k_p = 10^{-3}$，$k_i = 10$ 和 $\Omega_0 = 5$ 以及一些 τ_0 值。界限为 $X_{bound} = 28$

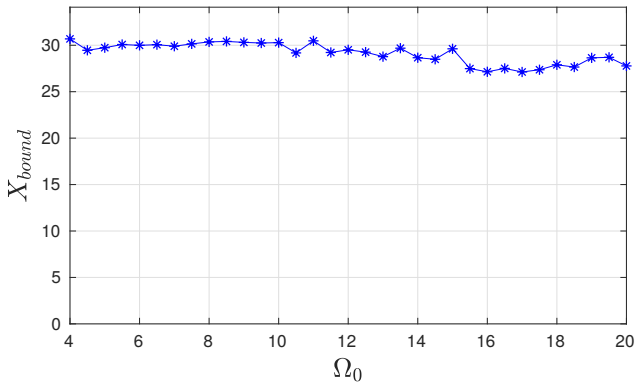

图 9: BMI (27) 的解 X_{bound}，参数为 $k_p = 10^{-3}$，$k_i = 10$，$\tau_0 = 0.0153$ 和 $N = 5$

II 中提出的模型似乎是实际行为的有效近似，至少在粘滑现象方面。

C. 实际稳定性分析

现在，可以使用定理 2 评估振荡的幅度，参数为 $k_p = 10^{-3}$ 和 $k_i = 10$。图 8 显示了对于不同的 τ_0 值和阶数在 0 到 7 之间的结果。注意，阶数超过 8 后，优化过程中会出现数值误差，结果不准确。最大 τ_0 为 $2\mu_{max} = 0.0155$，τ_0 越高，优化效果越好。对于 $k_i = 10$，$k_p = 10^{-3}$ 和 $\Omega_0 = 5$，最优 X_{bound} 约为 28。

图 10 显示了系统能量随时间的变化。可以看到，X_{bound} 的界限相当准确，因为自振荡的最大值与 X_{bound} 之间的误差约为 53%。此外，注意到 $\max|z_1 - \Omega_0| = 11.7 = 0.4X_{bound}$，换句话说，几乎一半的振荡集中在变量 z_1 上，这意味着粘滑主要作用于变量 z_1，对系统的其余部分影响不大。特别是，似乎很难仅通过 $\phi_t(0,t)$ 估计 z_1 的变化。

最后一个观察是关于不同 Ω_0 的 X_{bound} 的变化。这在图 9 中有所描述。尽管在数值优化中存在误差，但似乎当 Ω_0 增加时，X_{bound} 没有显著变化。这是违反直觉的，并且与图 7 中的观察结果不一致。一个解释是我们没有声明 T_{nl} 是正 θ 的严格递减函数。

D. PI 控制器的设计

最后，本文开头提出的问题是找到最佳 PI 控制器，即最小化 X_{bound}。图 11a 显示了积分增益 k_i 的值确实影响了由于粘滑引起的振荡，因为 X_{bound} 在 $k_i \in [0.5, 16]$ 时从 25 增加到 43，并且在此点之后 LMI 变得不可行（这些值是使用 $\Omega_0 = 5$，$k_p = 10^{-3}$ 和 $N = 5$ 获得的）。

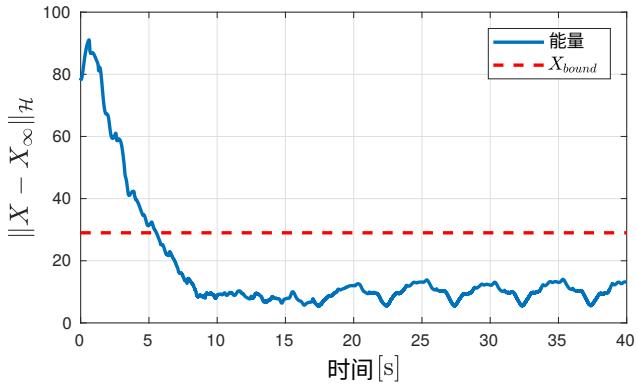

图 10: 非线性系统的 X 能量，参数为 $k_p = 10^{-3}$，$k_i = 10$ 和 $\Omega_0 = 5$。初始条件与图 5 相同

为了在环路中对小延迟保持鲁棒稳定，如第 IV-C 节所述，我们应考虑 $0 \le k_p \le 2.1 \cdot 10^{-3}$，这并没有提供很多选择。对于 $k_i = 10$，我们得到图 11b。似乎 X_{bound} 的最小值在 k_p 接近 0 时获得。因此，增加增益 k_p 似乎并不能减少粘滑效应。因此，即使 PI 控制器不能减弱粘滑效应，受控系统的平衡点也是实际稳定的。此外，它确实允许围绕期望平衡点的振荡和局部收敛到该点。

VII. 结论

本文重点分析了钻柱的 PI 控制器性能。首先，通过讨论文献中现有的模型，我们得出结论：无限维模型更接近真实的钻柱，因此应用于仿真和分析。基于这一模型，使用依赖于无限维状态在多项式基上投影的 Lyapunov 泛函，确保了闭环系统的指数稳定性。这种方法使得可以估计线性系统的衰减率并获得其指数稳定性。然后将这一结果扩展到非线性情况，考虑实际稳定性。示例部分表明，可以估计最小的吸引和不变集，并且该估计接近最小值。进一步的研究将集中在使用不同控制器进行类似分析，例如 [13], [30], [41] 中开发的控制器或 [38] 第 10 章中的控制器。

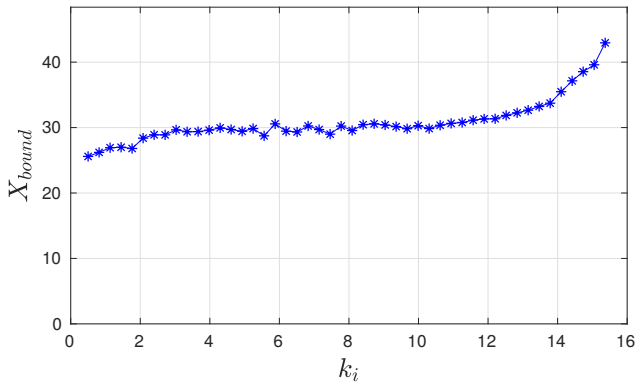

(a) $k_p = 10^{-3}$ 但不同 k_i 值的 X_{bound}

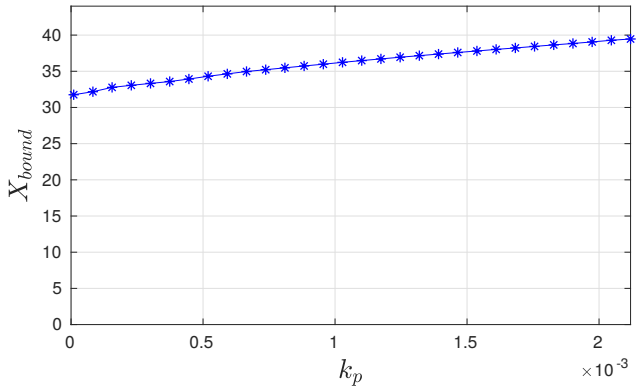

(b) $k_i = 10$ 但不同 k_p 值的 X_{bound}

图 11: 使用定理 2 获得的最小 X_{bound}，参数为 $\Omega_0 = 5$ 和 $N = 5$

附录

A. 勒让德多项式和贝塞尔不等式

Lyapunov 泛函 (16) 的性能高度依赖于 [42] 中开发的投影方法。为了帮助读者更好地理解定理 1 的证明，回顾了勒让德多项式的定义和一些性质。更多信息可以在 [17] 中找到。

定义 4: 勒让德多项式的正交归一族 $\{\mathcal{L}_k\}_{k\in\mathbb{N}}$ 在 $L^2([0,1])$ 上嵌入了标准内积，定义如下：

$$\mathcal{L}_k(x) = (-1)^k \sum_{l=0}^{k} (-1)^l \binom{k}{l} \binom{k+l}{l} x^l,$$

其中 $\binom{k}{l} = \frac{k!}{l!(k-l)!}$。

它们的展开形式在本文中并不实用，但以下两个引理非常重要。

引理 4: 对于任何函数 $\chi \in L^2$ 和对称正定矩阵 $R \in \mathbb{S}^2_+$，以下贝塞尔类积分不等式对所有 $N \in \mathbb{N}$ 成立：

$$\int_0^1 \chi^\top(x) R \chi(x) dx \geq \sum_{k=0}^{N} (2k+1) \mathfrak{x}_k^\top R \mathfrak{x}_k \qquad (31)$$

其中 $\mathfrak{x}_k$ 是 χ 相对于勒让德多项式 $\mathcal{L}_k$ 的投影系数，如 (15) 中定义。

引理 5: 对于满足 (15) 的任何函数 $\chi \in L^2$，以下表达式对任何 $N \in \mathbb{N}$ 成立：

$$\begin{bmatrix} \dot{\mathfrak{x}}_0 \\ \vdots \\ \dot{\mathfrak{x}}_N \end{bmatrix} = \mathbb{1}_N \chi(1) - \bar{\mathbb{1}}_N \chi(0) - L_N \begin{bmatrix} \mathfrak{x}_0 \\ \vdots \\ \mathfrak{x}_N \end{bmatrix}, \qquad (32)$$

其中 $L_N, \mathbb{1}_N$ 和 $\bar{\mathbb{1}}_N$ 定义在 (13) 中。

证明. 这个证明主要参考了 [8]。由于 $\chi \in L^2$ 满足 (15)，可以对方程 (18) 求导，得到以下结果：

$$\dot{\mathfrak{x}}_k = \Lambda \left[\chi(x)\mathcal{L}_k(x)\right]_0^1 - \Lambda \int_0^1 \chi(x)\mathcal{L}'(x)dx - \frac{\gamma_t}{2} \begin{bmatrix} 1 & 1 \\ 1 & 1 \end{bmatrix} \mathfrak{x}_k.$$

如 [17] 所述，勒让德多项式的有趣性质如下：

1) 勒让德多项式的边界条件确保 $\mathcal{L}_k(0) = (-1)^k$ 和 $\mathcal{L}_k(1) = 1$；
2) 勒让德多项式的导数规则为 $\frac{d}{dx}\mathcal{L}_k(x) = \sum_{j=0}^{k} \ell_{j,k}\mathcal{L}_j(x)$。

这两个性质导致了方程 (32) 中提出的结果。 ■

参考文献

[1] U. J. F. Aarsnes and O. M. Aamo. Linear stability analysis of self-excited vibrations in drilling using an infinite dimensional model. *Journal of Sound and Vibration*, 360:239 – 259, 2016.

[2] U.J.F. Aarsnes and J.S. Roman. Torsional vibrations with bit off bottom: Modeling, characterization and field data validation. *Journal of Petroleum Science and Engineering*, 163:712 – 721, 2018.

[3] B. Armstrong-Helouvry. Stick-slip arising from stribeck friction. In *Proceedings., IEEE International Conference on Robotics and Automation*, pages 1377–1382. IEEE, 1990.

[4] B. Armstrong-Hélouvry, P. Dupont, and C. Canudas De Wit. A survey of models, analysis tools and compensation methods for the control of machines with friction. *Automatica*, 30(7):1083–1138, 1994.

[5] M. Barreau. *Stability analysis of coupled ordinary differential systems with a string equation - Application to a Drilling Mechanism.* Université Fédérale Toulouse Midi-Pyrénées, 2019.

[6] M. Barreau, F. Gouaisbaut, A. Seuret, and R. Sipahi. Input/output stability of a damped string equation coupled with ordinary differential system. *International Journal of Robust and Nonlinear Control*, 28(18):6053–6069, 2018.

[7] M. Barreau, A. Seuret, and F. Gouaisbaut. Exponential Lyapunov stability analysis of a drilling mechanism. In *57st Annual Conference on Decision and Control (CDC)*, pages 2952–2957, 2018.

[8] M. Barreau, A. Seuret, F. Gouaisbaut, and L. Baudouin. Lyapunov stability analysis of a string equation coupled with an ordinary differential system. *IEEE Transactions on Automatic Control*, 63(11):3850–3857, Nov 2018.

[9] G. Bastin and J.-M. Coron. *Stability and boundary stabilization of 1-d hyperbolic systems*, volume 88. Springer, 2016.

[10] H.I. Basturk. Observer-based boundary control design for the suppression of stick–slip oscillations in drilling systems with only surface measurements. *Journal of Dynamic Systems, Measurement, and Control*, 139(10):104501, 2017.

[11] A. Bisoffi, M. Da Lio, A. R. Teel, and L. Zaccarian. Global asymptotic stability of a PID control system with coulomb friction. *IEEE Transactions on Automatic Control*, 63(8):2654–2661, 2017.

[12] D. Bresch-Pietri and M. Krstic. Output-feedback adaptive control of a wave PDE with boundary anti-damping. *Automatica*, 50(5):1407–1415, 2014.

[13] C. Canudas de Wit, F. Rubio, and M. Corchero. DOSKIL: A New Mechanism for Controlling Stick-Slip Oscillations in Oil Well Drillstrings. *IEEE Transactions on Control Systems Technology*, 16(6):1177–1191, November 2008.

[14] N. Challamel. Rock destruction effect on the stability of a drilling structure. *Journal of Sound and Vibration*, 233(2):235–254, 2000.

[15] A. P. Christoforou and A. S. Yigit. Fully coupled vibrations of actively controlled drillstrings. *Journal of sound and vibration*, 267(5):1029–1045, 2003.

[16] J. M. Coron. *Control and nonlinearity*. Number 136 in Mathematical Surveys and Monographs. American Mathematical Soc., 2007.

[17] R. Courant and D. Hilbert. *Methods of mathematical physics*. John Wiley & Sons, Inc., 1989.

[18] Y. Ebihara, D. Peaucelle, and D. Arzelier. *S-Variable Approach to LMI-Based Robust Control*, volume 17 of *Communications and Control Engineering*. Springer, 2015.

[19] A. F. Filippov. Classical solutions of differential equations with multi-valued right-hand side. *SIAM Journal on Control*, 5(4):609–621, 1967.

[20] E. Fridman, S. Mondié, and B. Saldivar. Bounds on the response of a drilling pipe model. *IMA Journal of Mathematical Control and Information*, 27(4):513–526, 2010.

[21] J. K. Hale and S. M. V. Lunel. Effects of small delays on stability and control. In *Operator theory and analysis*, pages 275–301. Springer, 2001.

[22] A. Helmicki, C. A. Jacobson, and C. N. Nett. Ill-posed distributed parameter systems: A control viewpoint. *IEEE Trans. on Automatic Control*, 36(9):1053–1057, 1991.

[23] D. Karnopp. Computer simulation of stick-slip friction in mechanical dynamic systems. *Journal of dynamic systems, measurement, and control*, 107(1):100–103, 1985.

[24] H.K. Khalil. *Nonlinear Systems*. Pearson Education. Prentice Hall, 1996.

[25] M. Krstic. *Delay compensation for nonlinear, adaptive, and PDE systems*. Springer, 2009.

[26] N. Levinson. Transformation theory of non-linear differential equations of the second order. *Annals of Mathematics*, pages 723–737, 1944.

[27] X. Liu, N. Vlajic, X. Long, G. Meng, and B. Balachandran. Coupled axial-torsional dynamics in rotary drilling with state-dependent delay: stability and control. *Nonlinear Dynamics*, 78(3):1891–1906, Nov 2014.

[28] J. Löfberg. YALMIP: A toolbox for modeling and optimization in MATLAB. In *IEEE International Symposium on Computer Aided Control Systems Design*, pages 284–289, 2005.

[29] Ö. Morgül. On the stabilization and stability robustness against small delays of some damped wave equations. *IEEE Trans. on Automatic Control*, 40(9):1626–1630, 1995.

[30] E. Navarro-López. An alternative characterization of bit-sticking phenomena in a multi-degree-of-freedom controlled drillstring. *Nonlinear Analysis: Real World Applications*, 10:3162–3174, 2009.

[31] E. Navarro-López and D. Cortes. Sliding-mode control of a multi-dof oilwell drillstring with stick-slip oscillations. In *Proceedings of the American Control Conference*, pages 3837 – 3842, 2007.

[32] E. Navarro-López and R. Suarez. Practical approach to modelling and controlling stick-slip oscillations in oilwell drillstrings. In *Proceedings of the 2004 IEEE International Conference on Control Applications, 2004.*, volume 2, pages 1454–1460 Vol.2, 2004.

[33] C. Prieur, S. Tarbouriech, and J. M. G. da Silva. Wave equation with cone-bounded control laws. *IEEE Trans. on Automatic Control*, 61(11):3452–3463, 2016.

[34] T. Richard, C. Germay, and E. Detournay. A simplified model to explore the root cause of stick-slip vibrations in drilling systems with drag bits. *Journal of Sound and Vibration*, 305(3):432–456, 8 2007.

[35] C. Roman, D. Bresch-Pietri, E. Cerpa, C. Prieur, and O. Sename. Backstepping observer based-control for an anti-damped boundary wave PDE in presence of in-domain viscous damping. In *55th IEEE Conference on Decision and Control (CDC)*, 2016.

[36] M. Safi, L. Baudouin, and A. Seuret. Tractable sufficient stability conditions for a system coupling linear transport and differential equations. *Systems and Control Letters*, 110:1–8, December 2017.

[37] C. Sagert, F. Di Meglio, M. Krstic, and P. Rouchon. Backstepping and flatness approaches for stabilization of the stick-slip phenomenon for drilling. *IFAC Proceedings Volumes*, 46(2):779–784, 2013.

[38] B. Saldivar, I. Boussaada, H. Mounier, and S.-I. Niculescu. *Analysis and Control of Oilwell Drilling Vibrations: A Time-Delay Systems Approach*. Springer, 2015.

[39] B. Saldivar, S. Mondié, and J. C. Ávila Vilchis. The control of drilling vibrations: A coupled PDE-ODE modeling approach. *International Journal of Applied Mathematics and Computer Science*, 2016.

[40] B. Saldivar, S. Mondie, S.-I. Niculescu, H. Mounier, and I. Boussaada. A control oriented guided tour in oilwell drilling vibration modeling. *Annual Reviews in Control*, 42:100–113, September 2016.

[41] A. Serrarens, M.J.G. Molengraft, J.J. Kok, and L. van den Steen. H_∞ control for suppressing stick-slip in oil well drillstrings. *IEEE Control Systems*, 18:19 – 30, 05 1998.

[42] A. Seuret and F. Gouaisbaut. Hierarchy of LMI conditions for the stability analysis of time-delay systems. *Systems & Control Letters*, 81:1–7, 2015.

[43] S. Tarbouriech, G. Garcia, J. M. G. da Silva Jr, and I. Queinnec. *Stability and stabilization of linear systems with saturating actuators*. Springer Science & Business Media, 2011.

[44] A. Terrand-Jeanne, V. Andrieu, M. Tayakout-Fayolle, and V. Dos Santos Martins. Regulation of inhomogeneous drilling model with a P-I controller. *IEEE Transactions on Automatic Control*, pages 1–1, 2020.

[45] A. Terrand-Jeanne, V. Dos Santo Martins, and V. Andrieu. Regulation of the downside angular velocity of a drilling string with a P-I controller. *ECC 2018, Cyprus*, pages 2647–2652, 2018.

[46] K.-C. Toh, M. J. Todd, and R. H. Tütüncü. SDPT3 - a MATLAB software package for semidefinite programming. *Optimization methods and software*, 11(1-4):545–581, 1999.

[47] W. R. Tucker and C. Wang. On the effective control of torsional vibrations in drilling systems. *Journal of Sound and Vibration*, 224(1):101–122, 1999.

[48] M. Tucsnak and G. Weiss. *Observation and control for operator semigroups*. Springer, 2009.

[49] W. Jr. Weaver, S. P. Timoshenko, and D. H. Young. *Vibration problems in engineering*. John Wiley & Sons, 1990.

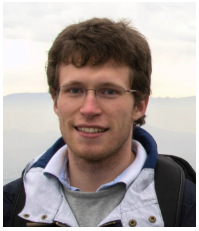

M. Barreau M. Barreau 于 2015 年获得法国图卢兹 ISAE-ENSICA 航空工程学工程师学位和瑞典皇家理工学院 (KTH) 空间工程专业学位。随后，他在法国图卢兹的 LAAS-CNRS（“Laboratoire d’Analyse et d’Architecture des Systèmes”）进行博士研究，师从 A. Seuret 和 F. Gouaisbaut。2019 年，他获得法国保罗 • 萨巴捷大学（Université Paul Sabatier）系统理论博士学位。他的研究兴趣主要集中在无限维系统的稳定性分析，尤其是钻井系统的研究。

F. Gouaisbaut 于 1973 年 4 月 26 日出生于法国雷恩。他于 1997 年 9 月获得法国里尔中央理工学院（Ecole Centrale de Lille）自动控制专业的“工程师学位”（Diplôme d’Ingénieur），并于同年 9 月获得法国里尔科技大学（University of Science and Technology of Lille）同一专业的“深造学位”（Diplôme d’Etudes Approfondies，硕士学位）。从 1998 年 10 月至 2001 年 10 月，他在法国里尔的自动化、计算机工程与信号实验室（LAGIS）攻读博士学位，并于 2001 年 10 月获得法国里尔中央理工学院和里尔科技大学的“博士学位”（Diplôme de Doctorat）。自 2003 年 10 月以来，他一直在保罗 • 萨巴捷大学（图卢兹）担任副教授。他的研究兴趣包括时延系统、量化系统和鲁棒控制。

A. Seuret 于 1980 年出生于法国。他于 2003 年获得法国里尔中央理工学院（Ecole Centrale de Lille）的工程师学位，并获得法国里尔科技大学（University of Science and Technology of Lille）系统理论硕士学位。2006 年，他获得了法国里尔中央理工学院和里尔科技大学的自动化控制博士学位。2006 至 2008 年，他分别在英国莱斯特大学（University of Leicester）和瑞典皇家理工学院（KTH，斯德哥尔摩）担任为期一年的博士后研究员。2008 至 2012 年，他在法国格勒诺布尔的 GIPSA-Lab 担任初级 CNRS 研究员（Chargé de Recherche）。自 2012 年以来，他一直在法国图卢兹的“系统架构与分析实验室”（LAAS）担任初级 CNRS 研究员。他的研究兴趣包括时延系统、网络控制系统和多智能体系统。

Practical Stability Analysis of a Drilling Pipe Under Friction With a PI-Controller

Matthieu Barreau, Frédéric Gouaisbaut, and Alexandre Seuret

***Abstract*— This article deals with the stability analysis of a drilling pipe controlled by a PI controller. The model is a coupled ordinary differential equation/partial differential equation (PDE) and is consequently of infinite dimension. Using recent advances in time-delay systems, we derive a new Lyapunov functional based on a state extension made up of projections of the Riemann coordinates. First, we will provide an exponential stability result expressed using the linear matrix inequality (LMI) framework. This result is dedicated to a linear version of the torsional dynamic. On the other hand, the influence of the nonlinear friction force, which may generate the well-known stick-slip phenomenon, is analyzed through a new stability theorem. Numerical simulations show the effectiveness of the method and that the stick-slip oscillations cannot be weakened using a PI controller.**

***Index Terms*— Friction, linear matrix inequality (LMI), Lyapunov methods, oil drilling, partial differential equations (PDEs), PI control, stability analysis.**

I. Introduction

STUDYING the behavior of complex machineries is a real challenge since they usually present nonlinear and coupled behaviors [49]. A drilling mechanism is a very good example of this. Many nonlinear effects can occur on the drilling pipe, such as bit bouncing, stick-slip, or whirling [14]. These phenomena induce generally some vibrations, increasing the drill pipe fatigue and affecting, therefore, the life expectancy of the well. The first challenge is then to provide a dynamical model which reflects such behaviors.

Looking at the literature, many models exist from the simplest finite-dimensional ones presented in, for instance [13], [41], to the more complex but more realistic infinite-dimensional systems. Finite-dimensional systems were an important first step since they showed which characteristics are responsible for vibrations in the well. Nevertheless, they are too far from the physical laws which are expressed in terms of partial differential equation (PDE). Then, a coupled finite-/infinite-dimensional model seems more natural in the context of a drilling pipe, and it was proposed in [14], [20], and [38] for instance.

Manuscript received April 3, 2019; revised July 31, 2019; accepted September 16, 2019. Date of publication December 20, 2019; date of current version February 9, 2021. Manuscript received in final form September 19, 2019. This work was supported by the ANR project SCIDiS under Contract 15-CE23-0014. Recommended by Associate Editor Y. Orlov. *(Corresponding author: Matthieu Barreau.)*

The authors are with the Laboratory for Analysis and Architecture of Systems, Centre national de la recherche scientifique, Paul Sabatier University, 31062 Toulouse, France (e-mail: mbarreau@laas.fr; aseuret@laas.fr; fgouaisb@laas.fr).

Color versions of one or more of the figures in this article are available online at https://ieeexplore.ieee.org.

Digital Object Identifier 10.1109/TCST.2019.2943458

The second challenge was then to design a controller to remove, or at least weaken, these undesirable effects. Many control techniques were applied on the finite-dimensional model from the simple PI controller investigated in [13] and [15], to more advance controllers as sliding mode control [30] or H_∞ [41]. Nevertheless, extending these controllers on the coupled finite-/infinite-dimensional system is not straightforward.

The last decade has seen many developments regarding the analysis of infinite-dimensional systems. The semigroup theory, investigated in [48] for instance, was a great tool to simplify the proof of existence and uniqueness of a solution to this kind of problems. This leads to an extension of the Lyapunov theory to some classes of PDEs [9], [16], [33]. These advances have given rise to the stability analysis of the linearized infinite-dimensional drilling pipe with a PI controller [44], [45]. Since this kind of controller provides only two degrees of freedom, to better enhance the performances, slightly different controllers arose. One of the most famous is the modified PI controller in [47], but there is also a delayed PI or a flatness-based control in [38]. More complex controllers, coming from the backstepping technique for PDE, originally developed in [25], were also applied in [10], [12], and [35] for instance.

Nevertheless, these techniques almost always use a Lyapunov argument to conclude, and they consequently suffer from the lack of an efficient Lyapunov functional for coupled systems. Recent advances in the domain of time-delay systems [42] have lead to a hierarchy of Lyapunov functionals which are very efficient for coupled ordinary differential equation (ODE)/string equation [8]. Since it relies on a state extension, the stability analysis cannot be assessed manually, but it translates into an optimization problem expressed using linear matrix inequalities (LMIs) and consequently easily solvable.

This article takes advantage of this enriched Lyapunov functional to revisit the stability analysis of a PI-controlled infinite-dimensional model of a drilling pipe for the torsion only. The first contribution of this article results in Theorem 1, which provides an LMI to ensure the asymptotic stability of the linear closed-loop system. The second theorem deals with the practical stability of the controlled nonlinear plant. It shows, for example, that if the linear system is stable, the nonlinear system is also stable. Moreover, it provides an accurate bound on the oscillations during the stick-slip.

This article is organized as follows. Section II discusses the different models presented in the literature and enlighten the importance of treating the infinite-dimensional problem.

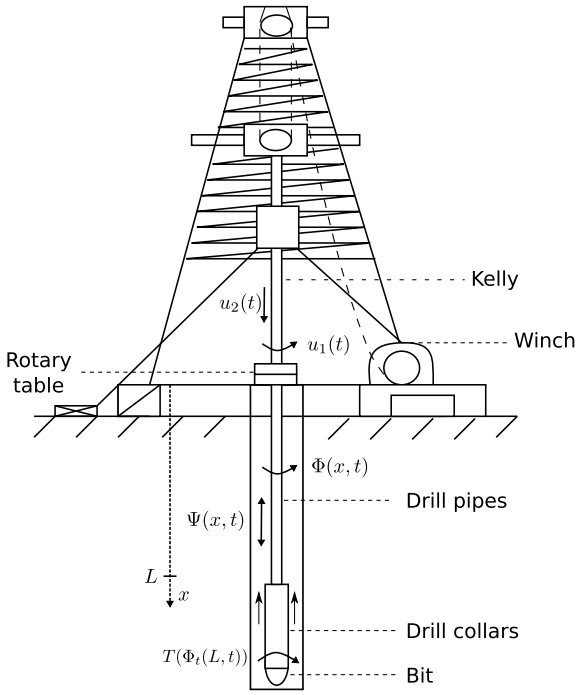

Fig. 1. Schematic of a drilling mechanism originally taken from [39]. Data corresponding to physical values are given in Table II.

Section III is the problem statement. Section IV is dedicated to the study of the linear system. This is a first step before dealing with the nonlinear system, which is the purpose of Section V. Finally, Section VI proposes simulations to demonstrate the effectiveness of this approach and conclude about the design of a PI controller.

Notations: For a multivariable function $(x,t) \mapsto u(x,t)$, the notation u_t stands for $(\partial u/\partial t)$ and $u_x = (\partial u/\partial x)$. We also use the notations $L^2 = L^2((0,1);\mathbb{R})$ and for the Sobolov spaces, $H^n = \{z \in L^2; \forall m \leqslant n, (\partial^m z/\partial x^m) \in L^2\}$. The norm in L^2 is $\|z\|^2 = \int_\Omega |z(x)|^2 dx =< z,z >$. For any square matrices A and B, the following operations are defined: $\mathrm{He}(A) = A + A^\top$ and $\mathrm{diag}(A,B) = \left[\begin{smallmatrix} A & 0 \\ 0 & B \end{smallmatrix}\right]$. The set of positive definite matrices of size n is denoted by $\mathbb{S}^n_+$ and, for simplicity, a matrix P belongs to this set if $P \succ 0$.

II. Model Description

A drilling pipe is a mechanism used to pump oil deep under the surface thanks to a drilling pipe, as shown in Fig. 1. Throughout the article, $\Phi(\cdot,t)$ is the twisting angle along the pipe, and then, $\Phi(0,t)$ and $\Phi(L,t)$ are the angles at the top and at the bottom of the well, respectively. The well is a long-metal rod of around one kilometer and consequently, the rotational velocity applied at the top using the torque $u_1(t)$ is different from the one at the bottom. Moreover, the interaction of the bit with the rock at the bottom is modeled by torque T, which depends on $\Phi_t(L,t)$.

As the bit drills the rock, axial compression of the rod occurs and is denoted Ψ. This compression arises because of the propagation along the rod of the vertical force u_2 applied at the top to push up and down the well.

This description leads naturally to two control objectives to prevent the mechanism from breaking. The first one is to maintain the rotational speed at the end of the pipe $\Phi(L,t)$ at a constant value, denoted here Ω_0, preventing any twisting of the pipe. The other one is to keep the penetration rate constant such that there is no compression along the rod.

Several models have been proposed in the literature to achieve these control objectives. They are of very different natures and lead to a large variety of analysis and control techniques. The book [38, Ch. 2] and the survey [40] provide overviews of these techniques, which are, basically, of four kinds. To better motivate the model used in the sequel, a brief overview of the existing modeling tools is proposed; but the reader can refer to [40] and the original articles to get a better understanding of how the models are constructed.

A. Lumped Parameter Models

These models are the first obtained in the literature [13], [27], [41] and the full mechanism is described by a sequence of harmonic oscillators. They can be classified into two main categories as follows.

1) The first kind assumes that the dynamics of the twisting angles $\Phi(0,t) = \Phi_r(t)$ (at the top) and $\Phi(L,t) = \Phi_b(t)$ (at the bottom) are described by two coupled harmonic oscillators. The torque u_1 driving the system is applied on the dynamic of Φ_r and the controlled angle is Φ_b. The axial dynamic is not taken into account in this model. This model can be found in [13], [32], and [41], for instance.
2) The other two degrees of freedom model is described in [27] and [34] for example. There also are two coupled harmonic oscillators for $\Psi(L,t)$ and $\Phi(L,t)$ representing the axial and torsional dynamics, respectively. This model only considers the motions at the end of the pipe and forget about the physics occurring along the rod.

The first class of models can be described by the following set of equations:

$$\begin{cases} I_r\ddot{\Phi}_r + \lambda_r(\dot{\Phi}_r - \dot{\Phi}_b) + k(\Phi_r - \Phi_b) + d_r\dot{\Phi}_r = u_1 \\ I_b\ddot{\Phi}_b + \lambda_b(\dot{\Phi}_b - \dot{\Phi}_r) + k(\Phi_b - \Phi_r) + d_b\dot{\Phi}_b = -T(\dot{\Phi}_b) \end{cases} \tag{1}$$

where the parameters are given in Table I. T is a torque modeled by a nonlinear function of $\dot{\Phi}_b$, and it describes the bit-rock interaction[1]. A second-order LPM can be derived by only taking into account the two dominant poles of the previous model.

An example of on-field measurements, shown in Fig. 2, shows the effect of this torque T on the angular speed. The periodic scheme which arises is called *stick-slip*. It emerges because of the difference between the static and Coulomb friction coefficients making an antidamping on the torque function T. Even though the surface angular velocity seems not to vary much, there is a cycle for the downhole one, and the angular speed is periodically close to zero, meaning that the bit is stuck to the rock.

The stick-slip effect appears mostly when dealing with a low-desired angular velocity Ω_0 on a controlled drilling mechanism. Indeed, if the angular speed $\Phi_t(L,t)$ is small,

[1] See [38, Ch. 3] for a detailed description about various models for T.

TABLE I
PARAMETERS VALUES AND THEIR MEANINGS FOR THE LPM TAKEN FROM [13], [32], AND [41]

Parameter meaning		Value
I_r	Rotary table and drive inertia	2122 kg.m^2
I_b	Bit and drillstring inertia	374 kg.m^2
k	Drillstring stiffness	1111 N.m.rad^{-1}
λ_r	Coupled damping at top	425 N.m.s.rad^{-1}
λ_b	Coupled damping at bottom	23.2 N.m.s.rad^{-1}
d_r	Rotary table damping	425 N.m.s.rad^{-1}
d_b	Bit damping	50 N.m.s.rad^{-1}
γ_b	Velocity decrease rate	0.9 s.rad^{-1}
μ_{cb}	Coulomb friction coefficient	0.5
μ_{sb}	Static friction coefficient	0.8
c_b	Bottom damping constant	0.03 N.m.s.rad^{-1}
T_{sb}	Static / Friction torque	15 145 N.m

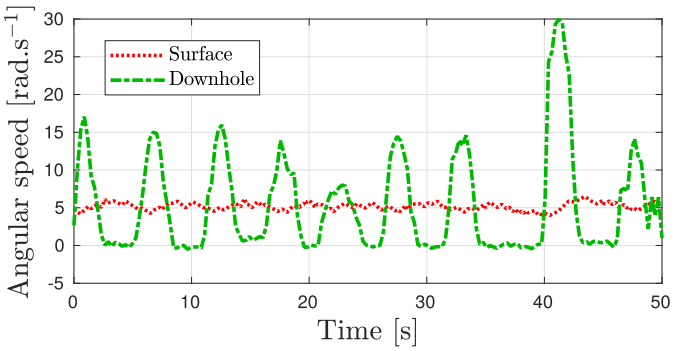

Fig. 2. Nonlinear effect on the drilling mechanism due to the friction torque at the bottom of the pipe. These measurements are done on the field [41].

the torque provided by the rotary table at $x = 0$ increases the torsion along the pipe. This increase leads to a higher $\Phi_t(L,t)$ but the negative damping on the torque function implies a smaller T. Consequently, $\Phi_t(L,t)$ increases, and this phenomenon is called the *slipping* phase. Then, the control law reduces the torque in order to match $\Phi_t(L,t)$ to Ω_0. Since the torque increases as well, that leads to a *sticking* phase where $\Phi(L,t)$ remains close to 0. A stick-slip cycle then emerges. Notice that this is not the case for high values of Ω_0 since torque T does not vary much with respect to $\Phi_t(L,t)$ making the system easier to control. In Fig. 2, one can see that the frequency of the oscillations is 0.17 Hz and its amplitude is between 10 and 25 rad.s^{-1}.

Modeling this phenomenon is of great importance as friction effects are quite common when studying mechanical machinery. Saldivar *et al.* [40] compare some models for T and conclude that they produce very similar results. The main characteristic is a decrease of T as $\Phi_t(L,t)$ increases. One standard model refers to the preliminary work of Karnopp [23]

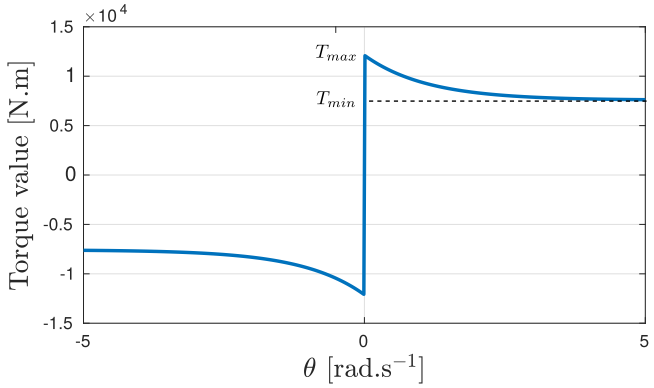

Fig. 3. Nonlinear part of the torque. T_{nl} is an approximation of the real friction torque coming from Karnopp [23].

and Armstrong-Helouvry *et al.* [3], [4] with an exponential decaying friction term, described in [31] for instance. This law (depicted in Fig. 3) is written thereafter where $\theta = \Phi_t(L,\cdot)$ is expressed in rad.s^{-1}

$$\begin{aligned} T(\theta) &= T_l(\theta) + T_{nl}(\theta) \\ T_l(\theta) &= c_b\theta \\ T_{nl}(\theta) &= T_{sb}(\mu_{cb} + (\mu_{sb} - \mu_{cb})e^{-\gamma_b|\theta|})\,\mathrm{sign}(\theta). \end{aligned} \tag{2}$$

This model has been used in [32] and [38], for instance.

Notice that an on-field description of this mechanism applied in the particular context of drilling systems is provided in [2] and concludes that these models are fair approximations of the nonlinear phenomena visible in similar structures.

At this stage, a lumped parameter model (LPM) is interesting for its simplicity but does not take into account the infinite-dimensional nature of the problem and, as a consequence, is a good approximation in the case of small vibrations only [39]. A deeper modeling can be done considering continuum mechanics and leading to a distributed parameter system.

B. Distributed Parameter Models (DPM)

To tackle the finite-dimensional approximation of the previous model, another one derived from mechanical equations leads to a set of PDEs as described in the works [14] and [49]. This model has been enriched in [1] and [2], where the system is presented from a control viewpoint and compared with on-field measurements. In the first articles, the model focuses on the propagation of the torsion only along the pipe. The axial propagation was introduced in the model by [1] and [40]. The new model is made up of two 1D wave equations representing each deformation for $x \in (0, L)$ and $t > 0$

$$\Phi_{tt}(x,t) = c_t^2\Phi_{xx}(x,t) - \gamma_t\Phi_t(x,t) \tag{3a}$$
$$\Psi_{tt}(x,t) = c_a^2\Psi_{xx}(x,t) - \gamma_a\Psi_t(x,t) \tag{3b}$$

where again Φ is the twist angle, Ψ is the axial movement, $c_t = (G/\rho)^{1/2}$ is the propagation speed of the angle, γ_t is the internal damping, $c_a = (E/\rho)^{1/2}$ is the axial velocity, and γ_a is the axial distributed damping. A list of physical parameters and their values is given in Table II, and Fig. 1

TABLE II
PHYSICAL PARAMETERS, MEANINGS, AND THEIR VALUES [1], [40]

Parameter meaning		Value
L	Pipe length	2000m
G	Shear modulus	79.3×10^9 N.m^{-2}
E	Young modulus	200×10^9 N.m^{-2}
Γ	Drillstring's cross-section	35×10^{-4} m^4
J	Second moment of inertia	1.19×10^{-5} m^4
I_B	Bottom hole lumped inertia	89 kg.m^2
M_B	Bottom hole mass	40 000 kg
ρ	Density	8000 kg.m^{-3}
g	Angular momentum	2000 N.m.s.rad^{-1}
h	Viscous friction coefficient	200 kg.s^{-1}
γ_a	Distributed axial damping	0.69 s^{-1}
γ_t	Distributed angle damping	0.27 s^{-1}
δ	Weight on bit coefficient	1 m^{-1}

helps giving a better understanding of the physical system. In other words, if $\Psi(\cdot, t) = 0$, then there is no compression in the pipe, meaning that the bit is not bouncing; if $\Phi_{tt}(\cdot, t) = 0$, then the angular speed along the pipe is the same, meaning that there is no increase or decrease of the torsion.

For the previous model to be well-posed, top and bottom boundary conditions (at $x = 0$ and $x = L$) must be incorporated in (3). In this part, only the topside boundary condition is derived. There is viscous damping at $x = 0$, and consequently a mismatch between the applied torque at the top and the angular speed. The topside boundary condition for the axial part is built on the same scheme, and the following conditions are obtained for $t > 0$:

$$GJ\Phi_x(0,t) = g\Phi_t(0,t) - u_1(t) \tag{4a}$$
$$E\Gamma\Psi_x(0,t) = h\Psi_t(0,t) - u_2(t). \tag{4b}$$

The downside boundary condition ($x = L$) is more difficult to grasp and is consequently derived later when dealing with a more complex model.

C. Neutral-Type Time-Delay Model

Studying an infinite-dimensional problem stated in terms of PDEs represents a relevant challenge. The equations obtained previously are damped wave equations, but for the special case where $\gamma_a = \gamma_t = 0$, the system can be converted into a neutral time-delay system as done in [38]. This new formulation enables to use other tools to analyze its stability as the Lyapunov–Krasovskii Theorem or a frequency-domain approach making its stability analysis slightly easier.

Nevertheless, the main drawback of this formulation is the assumption that the damping occurs at the boundary and not all along the pipe. This useful simplification, even if it encountered in many articles [12], [38], [39], is known to change in a significant manner the behavior of the system [1]. Indeed, it appears that without internal damping, the wave equation rephrases easily as a system of transport equations. It is then directly possible to observe with a delay of c^{-1} at the top of the pipe what happened at the bottom of the pipe. This makes control easier.

D. Coupled ODE/PDE Model

To overcome the issue mentioned earlier, a simpler model than the one derived in (3a) is proposed in [39], where a harmonic oscillator is used to describe axial vibrations and the model results in a coupled ODE/PDE.

A second possibility, reported in [14] and [38] for example, is to propose a second-order ODE as the bottom boundary condition ($x = L$) for $t > 0$

$$GJ\Phi_x(L,t) = -I_B\Phi_{tt}(L,t) - T(\Phi_t(L,t)) \tag{5a}$$
$$E\Gamma\Psi_x(L,t) = -M_B\Psi_{tt}(L,t) - \delta T(\Phi_t(L,t)) \tag{5b}$$

where T represents the torque applied on the drilling bit by the rocks, described in (2). Notice that (5a) is coming from the conservation of angular momentum, where $GJ\Phi_x(L,t)$ is the torque coming from the top of the pipe. Equation (5b) is the direct application of Newton's second law of motion, where $E\Gamma\Psi_x(L,t)$ is the force transmitted from the top to the bit and $\delta T(\Phi_t(L,t))$ is the weight on bit due to the rock interaction. Since (5a) is a second order in time differential equation, note that (3a) together with (5a) indeed leads to a coupled ODE/PDE.

There exist other bottom boundary conditions leading to more complex coupling between axial and torsional dynamics. They, nevertheless, introduce delays which require to have a better knowledge of the drilling bit. To keep the content general, the boundary conditions (5a) used throughout this article is proposed accordingly with [14], [39], and [45].

As a final remark, using some transformations based on (3a)–(5a), it is possible to derive a system for which backstepping controllers can be used [12], [37]. This is the main reason why this model is widely used today.

E. Models Comparison

We propose in this section to compare the coupled ODE/PDE model and the LPMs for the torsion only. We consider here a linearization of the system for large Ω_0, and consequently, we neglect the stick-slip effect by setting $T = 0$.

First, denote by $\mathcal{H}_{DPM}$ the transfer function from u_1 to $\Phi(L, \cdot)$ for the distributed parameter model (DPM) and $\mathcal{H}_{LPM}$ from u_1 to Φ_b for the LPM. We also define by $\mathcal{H}_{LPM2}$ a truncation of $\mathcal{H}_{LPM}$ considering only the two dominant poles. The Bode diagrams of $\mathcal{H}_{DPM}$, $\mathcal{H}_{LPM}$, and $\mathcal{H}_{LPM2}$ are drawn in Fig. 4.

Clearly, the LPMs catch the behavior of the DPM at steady states and low frequencies until the resonance occurring around $(k/I_b)^{1/2}$ rad.s^{-1}. From a control viewpoint, the DPM has infinitely many harmonics as it can be seen on the plots but

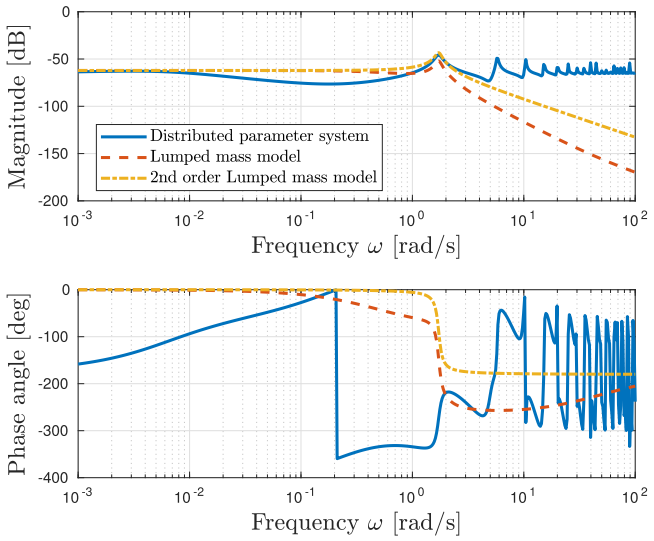

Fig. 4. Bode diagram of $\mathcal{H}_{DPM}$, $\mathcal{H}_{LPM}$, and $\mathcal{H}_{LPM2}$.

of lower magnitudes and damped as the frequency increases (around -10 dB at each decade). The magnitude plots are not sufficient to make a huge difference between the three models. Nevertheless, considering the phase, we see a clear difference. It appears that the DPM crosses the frequency -180 many times, making the control margins quite difficult to assess. Moreover, it shows that the DPM is harder to control because of the huge difference of behavior after the resonance. They may consequently have very different behavior when controlled. That is why we focus in this article on the DPM, even if it is far more challenging to control than the LPMs.

III. Problem Statement

The coupled nonlinear ODE/PDE model derived in Section II-B can be written as follows for $t > 0$ and $x \in [0, 1]$:

$$\begin{cases} \phi_{tt}(x,t) = \tilde{c}_t^2 \phi_{xx}(x,t) - \gamma_t \phi_t(x,t) \\ \phi_x(0,t) = \tilde{g}\phi_t(0,t) - \tilde{u}_1(t) \\ \phi_t(1,t) = z_1(t) \\ \dot{z}_1(t) = -\alpha_1 \phi_x(1,t) - \alpha_2 T(z_1(t)) \end{cases} \tag{6}$$

$$\begin{cases} \psi_{tt}(x,t) = \tilde{c}_a^2 \psi_{xx}(x,t) - \gamma_a \psi_t(x,t) \\ \psi_x(0,t) = \tilde{h}\psi_t(0,t) - \tilde{u}_2(t) \\ \psi_t(1,t) = y_1(t) \\ \dot{y}_1(t) = -\beta_1 \psi_x(1,t) - \beta_2 T(z_1(t)) \end{cases} \tag{7}$$

where the normalized parameters are given in Table III. Note that the range for the spacial variable is now $x \in [0, 1]$ to ease the calculations. The initial conditions are as follows:

$$\begin{cases} \phi(x,0) = \phi^0(x), & \phi_t(x,0) = \phi^1(x) \\ \psi(x,0) = \psi^0(x), & \psi_t(x,0) = \psi^1(x) \\ z_1(0) = \phi^1(1), & y_1(0) = \psi^1(1). \end{cases}$$

Since the existence and uniqueness of a solution to the previous problem is not the main contribution of this article, it is assumed in the sequel. This problem has been widely studied

TABLE III
Normalized Parameters

Parameter	Expression	Value
$\phi(x,t)$	$\Phi(xL,t)$	-
$\psi(x,t)$	$\Psi(xL,t)$	-
$\tilde{c}_t$	$c_t L^{-1}$	1.57
$\tilde{c}_a$	$c_a L^{-1}$	2.5
α_1	$\frac{GJ}{LI_B}$	5.3
β_1	$\frac{E\Gamma}{LM_B}$	8.75
α_2	I_B^{-1}	$1.12 \cdot 10^{-2}$
β_2	$\frac{\delta}{M_B}$	$2.5 \cdot 10^{-5}$
$\tilde{g}$	$\frac{g}{GJ}$	$2.1 \cdot 10^{-3}$
$\tilde{h}$	$\frac{h}{E\Gamma}$	$2.86 \cdot 10^{-7}$
$\tilde{u}_1(t)$	$\frac{1}{GJ}u_1(t)$	-
$\tilde{u}_2(t)$	$\frac{1}{E\Gamma}u_2(t)$	-

(see [10], [12], [37], [39], [44] among many others), and the solution belongs to the following space if the initial conditions (ϕ^0, ϕ^1, ψ^0, and ψ^1) satisfy the boundary conditions (see [9] for more details):

$$\mathbb{X} = H^1 \times L^2, \quad \mathbb{X}_1 = H^2 \times H^1$$
$$(\phi, \phi_t, \psi, \psi_t, z_1, y_1) \in C^0\big(\mathbb{X}_1^2 \times \mathbb{R}^2\big).$$

Remark 1: One may note that $\theta \mapsto T_{nl}(\theta)$ is not well defined for $\theta = 0$ because of the sign function. Nevertheless, since the nonlinearity acts directly on the variable z, it follows that there exists a unique solution to the ODE system in the sense of Filipov [19]. A more detailed discussion on this point is provided in [11]. □

Systems (6) and (7) is a cascade of two subsystems.

1) System (6) is a coupled nonlinear ODE/string equation describing the torsion angle ϕ.
2) System (7) is a coupled linear ODE/string equation subject to the external perturbation $T(z_1)$ for Ψ.

It appears clearly that the perturbation on the second subsystem depends on the first subsystem in ϕ. Since they are very similar, the same analysis than the one conducted in this article applies for the second subproblem. That is why we only study the evolution of the torsion.

IV. Exponential Stability of the Linear System

System (6) is a nonlinear system because of the friction term T_{nl} introduced in (2). Nevertheless, for a high-desired angular speed Ω_0, T_{nl} can be assumed constant, as seen in Fig. 3. Moreover, studying this linear system can be seen as a first

step before studying the nonlinear system, which relies mostly on the stability theorem derived in this section.

The proposed linear model of T around $\Omega_0 \gg 1$ is

$$T(\theta) = c_b\theta + T_{nl}(\Omega_0) = c_b\theta + T_0. \tag{8}$$

For high values of Ω_0, $T_0 = T_{nl}(\Omega_0)$ is close to $T_{smooth}(\Omega_0)$, and at the limit when Ω_0 tends to infinity, they are equal. Hence, the nonlinear friction term for relatively large angular velocity does not influence much the system.

In our case, the proposed controller for this problem has been studied in a different setting in [13], [15], and [45] and is a simple proportional/integral controller based on the single measurement of the angular velocity at the top of the drill (i.e., $\phi_t(0,t)$). The following variables are, therefore, introduced:

$$\begin{aligned} \tilde{u}_1(t) &= -k_p(\phi_t(0,t) - \Omega_0) - k_i z_2(t) \\ \dot{z}_2(t) &= \phi_t(0,t) - \Omega_0 \end{aligned} \tag{9}$$

where k_p and k_i are the gains of the PI controller. Combining (6), (8), and (9) leads to

$$\begin{cases} \phi_{tt}(x,t) = c^2\phi_{xx}(x,t) - \gamma_t\phi_t(x,t) \\ \phi_x(0,t) = (\tilde{g} + k_p)\phi_t(0,t) - k_p\Omega_0 + k_i C_2\ Z(t) \\ \phi_t(1,t) = C_1 Z(t) \\ \dot{Z}(t) = AZ(t) + B\begin{bmatrix} \phi_t(0,t) \\ \phi_x(1,t) \end{bmatrix} + B_2\begin{bmatrix} \Omega_0 \\ T_0 \end{bmatrix} \end{cases} \tag{10}$$

where

$$A = \begin{bmatrix} -\dfrac{c_b}{I_B} & 0 \\ 0 & 0 \end{bmatrix},\quad B = \begin{bmatrix} 0 & -\alpha_1 \\ 1 & 0 \end{bmatrix},\ B_2 = \begin{bmatrix} 0 & -\alpha_2 \\ -1 & 0 \end{bmatrix}$$

$$Z = \begin{bmatrix} z_1 & z_2 \end{bmatrix}^\top,\quad C_1 = \begin{bmatrix} 1 & 0 \end{bmatrix},\ C_2 = \begin{bmatrix} 0 & 1 \end{bmatrix}.$$

To ease the notations, $c = \tilde{c}_t$. We denote by

$$X = (\phi_x, \phi_t, z_1, z_2) \in C^1([0,\infty), \mathcal{H})$$

with $\mathcal{H} = L^2 \times L^2 \times \mathbb{R}^2$ the infinite-dimensional state of system (10). The control objective in the linear case is to achieve the exponential stabilization of an equilibrium point of (10) in angular speed, i.e., $\phi_t(1)$ is going exponentially to a given constant reference value Ω_0. To this extent, the following norm on $\mathcal{H}$ is introduced:

$$\|X\|_{\mathcal{H}}^2 = z_1^2 + z_2^2 + c^2\|\phi_x(\cdot)\|^2 + \|\phi_t(\cdot)\|^2.$$

The definition of an equilibrium point of (10) and its exponential stability follows from the earlier definitions.

Definition 1: $X_\infty \in \mathcal{H}$ is an **equilibrium point** of (10) if for the trajectory $X \in C^1([0,\infty), \mathcal{H})$ of (10) with initial condition X_∞, the following holds:

$$\forall t > 0,\quad \|\dot{X}(t)\|_{\mathcal{H}} = 0.$$

Definition 2: Let X_∞ be an equilibrium point of (10). X_∞ is said to be μ **exponentially stable** if

$$\forall t > 0,\quad \|X(t) - X_\infty\|_{\mathcal{H}} \le \gamma\ \|X_0 - X_\infty\|_{\mathcal{H}}\ e^{-\mu t}$$

holds for $\gamma \geqslant 1$, $\mu > 0$ and for any initial conditions $X_0 \in \mathcal{H}$ satisfying the boundary conditions. Here, X is the trajectory of (10) whose initial condition is X_0.

Hence, X_∞ is said to be **exponentially stable** if there exists $\mu > 0$ such that X_∞ is μ exponentially stable.

Before stating the main result of this part, a lemma about the equilibrium point is proposed.

Lemma 1: Assume $k_i \neq 0$, then there exists a unique equilibrium point $X_\infty = (\phi_x^\infty, \phi_t^\infty, z_1^\infty, z_2^\infty) \in \mathcal{H}$ of (10) and it satisfies $\phi_t^\infty = \Omega_0$.

Proof: An equilibrium point X_∞ of (10) is such that: $(\phi_{xt}^\infty, \phi_{tt}^\infty, (d/dt)z_1^\infty, (d/dt)z_2^\infty) = 0$.

Since $(d/dt)z_2^\infty = \phi_t^\infty(0,t) - \Omega_0 = 0$ and $\partial_x\phi_t^\infty = 0$ and $\partial_t\phi_t^\infty = 0$, $\phi_t^\infty = \Omega_0$ holds.

We also get from $\phi_{xx}^\infty = 0$ and $\partial_t\phi_x^\infty = 0$ that ϕ_x^∞ is a first order polynomial in x. Together with the boundary conditions, this system has a unique solution if $k_i \neq 0$ such as:

$$X_\infty = \left(\phi_x^\infty, \Omega_0, \Omega_0, \frac{\phi_x^\infty(0) - \tilde{g}\Omega_0}{k_i}\right)$$

where $\phi_x^\infty(x) = (\gamma_t\Omega_0/c^2)(x-1) - (c_b/\alpha_1\ I_B)\Omega_0 - (\alpha_2/\alpha_1)T_0$ for $x \in [0,1]$. ■

A. Exponential Stability of the Closed-Loop System (10)

The main result of this part is then stated as follows.

Theorem 1: Let $N \in \mathbb{N}$. Assume there exists $P_N \in \mathbb{S}^{2+2(N+1)}$, $R = \operatorname{diag}(R_1, R_2) \succeq 0$, $S = \operatorname{diag}(S_1, S_2) \succ 0$, $Q \in \mathbb{S}_+^2$ such that the following LMIs hold:

$$\begin{aligned} \Theta_N &= c\ \Theta_{1,N} + \Theta_{2,N} - Q_N \prec 0 \\ P_N + S_N &\succ 0 \end{aligned} \tag{11}$$

and

$$\begin{aligned} \Gamma_0 &= cR + \frac{\gamma_t}{2}U_0 - Q \succeq 0 \\ \Gamma_1 &= cR + \frac{\gamma_t}{2}U_1 - Q \succeq 0 \end{aligned} \tag{12}$$

where

$$\begin{aligned} \Theta_{1,N} &= H_N^\top \begin{bmatrix} S_1 + R_1 & 0 \\ 0 & -S_2 \end{bmatrix} H_N - G_N^\top \begin{bmatrix} S_1 & 0 \\ 0 & -S_2 - R_2 \end{bmatrix} G_N \\ \Theta_{2,N} &= \operatorname{He}\left(D_N^\top P_N F_N\right) \\ F_N &= [I_{2+2(N+1)} \quad 0_{2+2(N+1),2}] \\ D_N &= \begin{bmatrix} J_N^\top & cM_N^\top \end{bmatrix}^\top,\quad J_N = [A \quad 0_{2,2(N+1)} \quad B] \\ M_N &= \mathbb{1}_N H_N - \bar{\mathbb{1}}_N G_N - \begin{bmatrix} 0_{2(N+1),2} & L_N & 0_{2(N+1),2} \end{bmatrix} \\ U_0 &= \begin{bmatrix} 2\ S_1 & S_1 + S_2 + R_2 \\ S_1 + S_2 + R_2 & 2(S_2 + R_2) \end{bmatrix} \\ U_1 &= \begin{bmatrix} 2(S_1 + R_1) & S_1 + S_2 + R_1 \\ S_1 + S_2 + R_1 & 2\ S_2 \end{bmatrix} \\ G_N &= \begin{bmatrix} ck_iC_2 & 0_{2,2(N+1)} & G \end{bmatrix},\quad G = \begin{bmatrix} 1 + c(\tilde{g} + k_p) & 0 \\ 1 - c(\tilde{g} + k_p) & 0 \end{bmatrix} \\ H_N &= \begin{bmatrix} C_1 & 0_{2,2(N+1)} & H \end{bmatrix},\quad H = \begin{bmatrix} 0 & c \\ 0 & -c \end{bmatrix} \\ Q_N &= \operatorname{diag}(0_2, Q, 3\ Q, \ldots, (2N+1)Q, 0_2) \\ S_N &= \operatorname{diag}(0_2, S, 3S, \ldots, (2N+1)S) \\ L_N &= \left[\ell_{j,k}\Lambda\right]_{j,k\in[0,N]} - \frac{\gamma_t}{2}\operatorname{diag}\left(\begin{bmatrix} 1 & 1 \\ 1 & 1 \end{bmatrix}, \ldots, \begin{bmatrix} 1 & 1 \\ 1 & 1 \end{bmatrix}\right) \end{aligned}$$

$$\mathbb{1}_N = \begin{bmatrix} \Lambda \\ \vdots \\ \Lambda \end{bmatrix}, \quad \bar{\mathbb{1}}_N = \begin{bmatrix} \Lambda \\ \vdots \\ (-1)^N \Lambda \end{bmatrix}, \quad \Lambda = \begin{bmatrix} c & 0 \\ 0 & -c \end{bmatrix} \tag{13}$$

and

$$\ell_{k,j} = \begin{cases} (2j+1)(1-(-1)^{j+k}), & \text{if } j \leqslant k \\ 0, & \text{otherwise} \end{cases}$$

then the equilibrium point of system (10) is exponentially stable. As a consequence, $\lim_{t\to+\infty} |\phi_t(1,t) - \Omega_0| = 0$.

The proof is given thereafter, but some practical consequences and preliminary results are derived first.

Remark 2: The methodology used to derive the previous result has been introduced first in [42] to deal with time-delay systems. It has been proven in the former article that this theorem provides a hierarchy of LMI conditions. That means if the conditions of Theorem 1 are met for $N = N_1 \geqslant 0$, and then the conditions are also satisfied for all $N > N_1$. Then, the LMIs provide a sharper analysis as the order N of the theorem increases. Nevertheless, the price to pay for a more precise analysis is the increase in the number of decision variables and consequently a higher computational burden. It has been noted in [42] for a time-delay system and in [8] for a coupled ODE/string equation system that very sharp results are obtained even for low orders N. □

As we aim at showing that X_∞ is an exponentially stable equilibrium point of system (10) in the sense of Definition 2, the following variable is consequently defined for $t \geq 0$:

$$\tilde{X}(t) = X(t) - X_\infty = (\tilde{\phi}_x(t), \tilde{\phi}_t(t), \tilde{z}_1(t), \tilde{z}_2(t))$$

where X is a trajectory of system (10).

The following lemma, given in [7], provides a way for estimating the exponential decay rate of system (10) as soon as a Lyapunov functional V is known.

Lemma 2: Let V be a Lyapunov functional for system (10) and $\mu \geq 0$. Assume there exist $\varepsilon_1, \varepsilon_2, \varepsilon_3 > 0$ such that the following holds:

$$\begin{cases} \varepsilon_1 \|\tilde{X}\|^2_{\mathcal{H}} \leqslant V(\tilde{X}) \leqslant \varepsilon_2 \|\tilde{X}\|^2_{\mathcal{H}} \\ \dot{V}(\tilde{X}) + 2\mu V(\tilde{X}) \leqslant -\varepsilon_3 \|\tilde{X}\|^2_{\mathcal{H}} \end{cases} \tag{14}$$

then the equilibrium point of system (10) is μ exponentially stable. If $\mu = 0$, then it is exponentially stable.

Proof of Theorem 1: For simplicity, the following notations are used throughout this article for $k \in \mathbb{N}$:

$$\tilde{\chi}(x) = \begin{bmatrix} \tilde{\phi}_t(x) + c\tilde{\phi}_x(x) \\ \tilde{\phi}_t(x) - c\tilde{\phi}_x(x) \end{bmatrix}, \quad \tilde{\mathfrak{X}}_k(t) = \int_0^1 \tilde{\chi}(x,t)\mathcal{L}_k(x)dx \tag{15}$$

where $\{\mathcal{L}_k\}_{k\in\mathbb{N}}$ is the orthogonal family of Legendre polynomials as defined in Appendix. $\tilde{\mathfrak{X}}_k$ is then the projection coefficient of $\tilde{\chi}$ along the Legendre polynomial of degree k. $\tilde{\chi}$ refers to the Riemann coordinates and presents useful properties as discussed in [8] for instance.

1) Choice of a Lyapunov Functional Candidate: The proposed Lyapunov functional is inspired from [7], [8], and [36] and is divided into two parts as follows:

$$V_N(\tilde{X}) = \tilde{Z}_N^\top P_N \tilde{Z}_N + \mathcal{V}(\tilde{\chi}) \tag{16}$$

where $\tilde{Z}_N = [\tilde{z}_1 \ \tilde{z}_2 \ \tilde{\mathfrak{X}}_0^\top \ \cdots \ \tilde{\mathfrak{X}}_N^\top]^\top$ and

$$\mathcal{V}(\tilde{\chi}) = \int_0^1 \tilde{\chi}^\top(x) \begin{bmatrix} S_1 + xR_1 & 0 \\ 0 & S_2 + (1-x)R_2 \end{bmatrix} \tilde{\chi}(x)dx.$$

$\mathcal{V}$ is a traditional Lyapunov functional candidate for a transport system, as shown in [16].

2) Exponential Stability: Existence of ε_1: This part is inspired by [7]. The inequalities $P_N + S_N \succ 0$, $R \succeq 0$ imply the existence of $\varepsilon_1 > 0$ such that

$$P_N + S_N \succeq \varepsilon_1 \text{diag}\left(I_2, \frac{1}{2}\mathcal{I}_N\right)$$
$$S \succeq \frac{\varepsilon_1}{2} I_2 \tag{17}$$

with $\mathcal{I}_N = \text{diag}\{(2k+1)I_2\}_{k\in[0,N]}$. This statement implies the following on V_N:

$$\begin{aligned} V_N(\tilde{X}) &\geq \tilde{Z}_N^\top (P_N + S_N)\tilde{Z}_N - \sum_{k=0}^{N}(2k+1)\tilde{\mathfrak{X}}_k^\top S \tilde{\mathfrak{X}}_k \\ &\quad + \int_0^1 \tilde{\chi}(x)^\top \left(S - \frac{\varepsilon_1}{2} I_2\right)\tilde{\chi}(x)dx + \frac{\varepsilon_1}{2}\|\tilde{\chi}\|^2 \\ &\geq \varepsilon_1 \left(\tilde{z}_1^2 + \tilde{z}_2^2 + \frac{1}{2}\|\tilde{\chi}\|^2\right) \\ &\quad - \sum_{k=0}^{N}(2k+1)\tilde{\mathfrak{X}}_k^\top \tilde{S}\tilde{\mathfrak{X}}_k + \int_0^1 \tilde{\chi}^\top(x)\tilde{S}\tilde{\chi}(x)dx \\ &\geq \varepsilon_1 \|\tilde{X}\|^2_{\mathcal{H}} \end{aligned}$$

where $\tilde{S} = S - (\varepsilon_1/2)I_2$ which ends the proof of existence of ε_1.

Existence of ε_2: Following the same line as earlier, the following holds for a sufficiently large $\varepsilon_2 > 0$:

$$P_N \preceq \varepsilon_2 \text{diag}\left(I_2, \frac{1}{4}\mathcal{I}_N\right)$$
$$\frac{\varepsilon_2}{4} I_2 \succeq \begin{bmatrix} S_1 + xR_1 & 0 \\ 0 & S_2 + (1-x)R_2 \end{bmatrix}.$$

Using these inequalities in (16) leads to

$$\begin{aligned} V_N(\tilde{X}) &\leq \varepsilon_2 \left(\tilde{z}_1^2 + \tilde{z}_2^2 + \sum_{k=0}^{N}\frac{2k+1}{4}\tilde{\mathfrak{X}}_k^\top \tilde{\mathfrak{X}}_k + \frac{1}{4}\|\tilde{\chi}\|^2\right) \\ &\leq \varepsilon_2 \left(\tilde{z}_1^2 + \tilde{z}_2^2 + \frac{1}{2}\|\tilde{\chi}\|^2\right) = \varepsilon_2 \|\tilde{X}\|^2_{\mathcal{H}}. \end{aligned}$$

The last inequality is a direct application of Lemma 4.

Existence of ε_3: The time derivation of $\tilde{\chi}$ leads to

$$\tilde{\chi}_t(x) = \Lambda \tilde{\chi}_x(x) - \gamma_t \begin{bmatrix} 1 \\ 1 \end{bmatrix} \tilde{\phi}_t(x).$$

Noting that $\tilde{\phi}_t(x) = (1/2)[1 \ 1]\tilde{\chi}(x)$, we get

$$\tilde{\chi}_t(x) = \Lambda \tilde{\chi}_x(x) - \frac{\gamma_t}{2}\begin{bmatrix} 1 & 1 \\ 1 & 1 \end{bmatrix}\tilde{\chi}(x). \tag{18}$$

The derivative of $\mathcal{V}$ along the trajectories of (6) leads to

$$\dot{\mathcal{V}}(\tilde{\chi}) = 2c\mathcal{V}_1(\tilde{\chi}) - \frac{\gamma_t}{2}\mathcal{V}_2(\tilde{\chi})$$

with

$$\mathcal{V}_1(\tilde{\chi}) = \int_0^1 \tilde{\chi}_x^\top(x) \begin{bmatrix} S_1 + xR_1 & 0 \\ 0 & -S_2 - (1-x)R_2 \end{bmatrix} \tilde{\chi}(x)dx$$

$$\mathcal{V}_2(\tilde{\chi}) = \int_0^1 \tilde{\chi}^\top(x) U(x) \tilde{\chi}(x) dx$$
$$U(x) = \begin{bmatrix} 2(S_1 + xR_1) & S_1 + S_2 + xR_1 + (1-x)R_2 \\ S_1 + S_2 + xR_1 + (1-x)R_2 & 2(S_2 + (1-x)R_2) \end{bmatrix}.$$

An integration by part on $\mathcal{V}_1$ shows that

$$\begin{aligned} 2\mathcal{V}_1(\tilde{\chi}) = {} & \tilde{\chi}^\top(1) \begin{bmatrix} S_1 + R_1 & 0 \\ 0 & -S_2 \end{bmatrix} \tilde{\chi}(1) \\ & - \tilde{\chi}^\top(0) \begin{bmatrix} S_1 & 0 \\ 0 & -S_2 - R_2 \end{bmatrix} \tilde{\chi}(0) \\ & - \int_0^1 \tilde{\chi}^\top(x) \begin{bmatrix} R_1 & 0 \\ 0 & R_2 \end{bmatrix} \tilde{\chi}(x) dx. \end{aligned}$$

The previous calculations lead to the following derivative:

$$\begin{aligned} \dot{\mathcal{V}}(\tilde{\chi}) = {} & c \left(\tilde{\chi}^\top(1) \begin{bmatrix} S_1 + R_1 & 0 \\ 0 & -S_2 \end{bmatrix} \tilde{\chi}(1) \right. \\ & \left. - \tilde{\chi}^\top(0) \begin{bmatrix} S_1 & 0 \\ 0 & -S_2 - R_2 \end{bmatrix} \tilde{\chi}(0) \right) \\ & - \int_0^1 \tilde{\chi}^\top(x) \left(cR + \frac{\gamma_t}{2} U(x) \right) \tilde{\chi}(x) dx. \end{aligned} \quad (19)$$

By a convexity argument, if (12) is verified, then $cR + U(x) \geq Q \succ 0$ holds for $x \in [0, 1]$. Consequently, noticing that $\tilde{\chi}(0) = G_N \tilde{\xi}_N$, $\tilde{\chi}(1) = H_N \tilde{\xi}_N$, we get

$$\dot{\mathcal{V}}(\tilde{\chi}) \leq c \tilde{\xi}_N^\top \Theta_{1,N} \tilde{\xi}_N - \int_0^1 \tilde{\chi}^\top(x) Q \tilde{\chi}(x) dx$$

with

$$\tilde{\xi}_N = \begin{bmatrix} \tilde{Z}_N^\top & \tilde{\phi}_t(0) & \tilde{\phi}_x(1) \end{bmatrix}^\top.$$

Using Lemma 5 and the fact that $\dot{\tilde{Z}}_N = D_N \tilde{\xi}_N$ and $\tilde{Z}_N = F_N \tilde{\xi}_N$, we get the following:

$$\begin{aligned} \dot{V}_N(\tilde{X}) = {} & \mathrm{He}\left(\dot{\tilde{Z}}_N^\top P_N \tilde{Z}_N \right) + \dot{\mathcal{V}}(\tilde{\chi}) \\ \leq {} & \tilde{\xi}_N^\top \Theta_N \tilde{\xi}_N + \sum_{k=0}^{N} (2k+1) \tilde{\mathfrak{X}}_k Q \tilde{\mathfrak{X}}_k \\ & - \int_0^1 \tilde{\chi}^\top(x) Q \tilde{\chi}(x) dx \end{aligned} \quad (20)$$

with Θ_N defined in (11). Since $\Theta_N \prec 0$ and $Q \succ 0$, we get

$$\begin{aligned} \Theta_N \preceq {} & -\varepsilon_3 \mathrm{diag}\left(I_2, \frac{1}{2} I_2, \frac{3}{2} I_2, \ldots, \frac{2N+1}{2} I_2, 0_2 \right) \\ Q \succeq {} & \frac{\varepsilon_3}{2} I_2. \end{aligned}$$

Then, $\dot{V}_N$ is upper bounded by

$$\begin{aligned} \dot{V}_N(\tilde{X}) \leq {} & -\varepsilon_3 \left(\tilde{z}_1^2 + \tilde{z}_2^2 + \frac{1}{2} \|\tilde{\chi}\|^2 \right) \\ & + \sum_{k=0}^{N} (2k+1) \tilde{\mathfrak{X}}_k^\top \left(Q - \frac{\varepsilon_3}{2} I_2 \right) \tilde{\mathfrak{X}}_k \\ & - \int_0^1 \tilde{\chi}^\top(x) \left(Q - \frac{\varepsilon_3}{2} I_2 \right) \tilde{\chi}(x) dx \\ \leq {} & -\varepsilon_3 \|\tilde{X}\|_{\mathcal{H}}^2. \end{aligned}$$

The last inequality comes from a direct application of Bessel's inequality (31).

Conclusion: Using Lemma 2, we indeed get the exponential convergence of all trajectories of (10) to the desired equilibrium point.

B. Exponential Stability With a Guaranteed Decay Rate

It is possible to estimate the decay rate μ of the exponential convergence with a slight modification of the LMIs as it is proposed in the following corollary.

Corollary 1: Let $N \in \mathbb{N}$, $\mu > 0$ and $\gamma_t \geq 0$. If there exist $P_N \in \mathbb{S}^{2+2(N+1)}$, $R = \mathrm{diag}(R_1, R_2) \succeq 0$, $S = \mathrm{diag}(S_1, S_2) \succ 0$, *and* $Q \in \mathbb{S}_+^2$ such that (12) and the following LMIs hold:

$$\begin{aligned} \Theta_{N,\mu} = {} & \Theta_N + 2\mu F_N^\top (P_N + S_N) F_N \prec 0 \\ & 0 \prec P_N + S_N \end{aligned} \quad (21)$$

with the parameters defined as in Theorem 1, then the equilibrium point of system (10) is μ exponentially stable.

Proof: To prove the exponential stability with a decay rate of at least $\mu > 0$, we use Lemma 2. Similar to the previous proof, we have the existence of ε_1 and $\varepsilon_2 > 0$. The existence of ε_3 is slightly different. First, note that for the Lyapunov functional candidate (16), we get

$$\begin{aligned} V_N(\tilde{X}_\phi) \geq {} & \tilde{Z}_N^\top P_N \tilde{Z}_N + \int_0^1 \tilde{\chi}^\top(x) S \tilde{\chi}(x) dx \\ \geq {} & \tilde{Z}_N^\top P_N \tilde{Z}_N + \sum_{k=0}^{N} (2k+1) \tilde{\mathfrak{X}}_k^\top S \tilde{\mathfrak{X}}_k. \end{aligned}$$

This inequality was obtained using (31). Using the notations of the previous theorem yields

$$V_N(\tilde{X}_\phi) \geq \tilde{\xi}_N^\top F_N^\top (P_N + S_N) F_N \tilde{\xi}_N. \quad (22)$$

Coming back to (20) and using (21) leads to:

$$\begin{aligned} \dot{V}_N(\tilde{X}_\phi) \leq {} & \tilde{\xi}_N^\top \Theta_{N,\mu} \tilde{\xi}_N - 2\mu \tilde{\xi}_N^\top \left(F_N^\top P_N F_N + S_N \right) \tilde{\xi}_N \\ & + \sum_{k=0}^{N} (2k+1) \tilde{\mathfrak{X}}_k^\top Q \tilde{\mathfrak{X}}_k - \int_0^1 \tilde{\chi}^\top(x) Q \tilde{\chi}(x) dx. \end{aligned}$$

Injecting inequality (22) into the previous inequality leads to

$$\begin{aligned} \dot{V}_N(\tilde{X}_\phi) + 2\mu V_N(\tilde{X}_\phi) \leq {} & \tilde{\xi}_N^\top \Theta_{N,\mu} \tilde{\xi}_N + \sum_{k=0}^{N} (2k+1) \tilde{\mathfrak{X}}_k^\top Q \tilde{\mathfrak{X}}_k \\ & - \int_0^1 \tilde{\chi}^\top(x) Q \tilde{\chi}(x) dx. \end{aligned}$$

Using the same techniques than for the previous proof leads to the existence of $\varepsilon_3 > 0$ such that

$$\dot{V}_N(\tilde{X}_\phi) + 2\mu V_N(\tilde{X}_\phi) \leq -\varepsilon_3 \|\tilde{X}_\phi\|_{\mathcal{H}}^2.$$

Lemma 2 concludes then on the μ-exponential stability. ■

Remark 3: Wave equations can sometimes be modeled as neutral time-delay systems [6], [38]. This kind of system is known to possess some necessary stability conditions as noted in [6] and [9]. In [9], the following criterion is derived:

$$\mu \leq \frac{c}{2} \log \left| \frac{1 + c(\tilde{g} + k_p)}{1 - c(\tilde{g} + k_p)} \right| = \mu_{\max}. \quad (23)$$

This result implies that there exists a maximum decay rate, and if this maximum is negative, then the system is unstable. The LMI $\Theta_N^\mu \prec 0$ contains the same necessary condition, meaning that the neutral aspect of the system is well captured. □

C. Strong Stability Against Small Delay in the Control

A practical consequence of the neutral aspect of system (10) is that it is very sensitive to delay in the control (9). Indeed, if the control is slightly delayed, a new necessary stability condition [equivalent to (23)] coming from frequency analysis can be derived [21, Corollary 3.3]

$$\left|\frac{1-c\tilde{g}}{1+c\tilde{g}}\right| + 2\left|\frac{ck_p}{1+c\tilde{g}}\right| < 1.$$

It is more restrictive and taking $k_p \neq 0$ practically leads to a decrease of the robustness (even if some other performances might be enhanced). This phenomenon has been studied in many articles [22], [29], [44]. Hence, to be robust to delays in the loop, one then needs to ensure the following:

$$0 \leq k_p \leq \frac{1}{2c}\left(|1+c\tilde{g}| - |1-c\tilde{g}|\right) = \tilde{g} = 2.1 \cdot 10^{-3}.$$

This inequality on k_p comes when considering the infinite-dimensional problem and does not arise when dealing with any finite-dimensional model. That point enlightens that it is more realistic to consider the infinite-dimensional problem. For more information on that point, the interested reader can refer to [5].

V. Practical Stability of System (6)–(9)

The experiments conducted previously show for Ω_0 large, the trajectory of the nonlinear system (6)–(9) goes exponentially to X_∞, so does the linear system. In other words, the previous result is a local stability test for the nonlinear system in case of large-desired angular velocity Ω_0 and does not extend straightforwardly to a global analysis.

In general, for a nonlinear system, ensuring the global exponential stability of an equilibrium point could be complicated. In many engineering situations, global exponential stability is not the requirement. Indeed, considering uncertainties in the system or nonlinearities, it is far more reasonable and acceptable for engineers to ensure that the trajectory remains close to the equilibrium point. This property is called dissipativeness in the sense of Levinson [26] or practical stability (also called globally uniformly ultimately bounded in [24]).

Definition 3: System (6) is **practically stable** if there exists $X_{\text{bound}} \geq 0$ such that for X the solution of (6) with initial condition $X_0 \in \mathcal{H}$

$$\forall \eta > 0, \quad \exists T_\eta > 0 \ \forall t \geq T_\eta, \ \ \|X(t) - X_\infty\|_{\mathcal{H}} \leq X_{\text{bound}} + \eta. \quad (24)$$

Saying that system (6)–(9) is practically stable means that there exists $T_\eta > 0$ such that for any $x \in [0,1]$, $\phi_t(x,t)$ stays close to Ω_0 for $t \geq T_\eta$. This property has already been applied to a drilling system in [39] for instance. In the nonlinear case, the aim is then to design a control law reducing the amplitude of the stick-slip when it occurs.

The objective of this section is to derive an LMI test ensuring the practical stability of nonlinear system (6) together with the control defined in (9)

$$\begin{cases} \phi_{tt}(x,t) = c^2\phi_{xx}(x,t) - \gamma_t\phi_t(x,t) \\ \phi_x(0,t) = (\tilde{g}+k_p)\phi_t(0,t) - k_p\Omega_0 + k_iC_2\ Z(t) \\ \phi_t(1,t) = C_1Z(t) \\ \dot{Z}(t) = AZ(t) + B\begin{bmatrix}\phi_t(0,t)\\ \phi_x(1,t)\end{bmatrix} + B_2\begin{bmatrix}\Omega_0\\ T_{nl}(z_1(t))\end{bmatrix}. \end{cases} \quad (25)$$

Remark 4: To simplify the writing, ϕ can both means the solution of the linear or nonlinear system depending on the context. In this part, it refers to a solution of nonlinear system (25). □

A. Practical Stability of System (25)

The idea behind practical stability is to embed the static nonlinearities by the use of suitable sector conditions, as it has been done for the saturation, for instance [43]. Then, the use of robust tools will lead to some LMI tests ensuring the practical stability.

Lemma 3: For almost all $\tilde{z}_1 \in \mathbb{R}$, the following holds:

$$\begin{aligned} T_{nl}(\tilde{z}_1+\Omega_0)^2 \leq T_{\max}^2, \quad T_{\min}^2 \leq T_{nl}(\tilde{z}_1+\Omega_0)^2 \\ -2(\tilde{z}_1+\Omega_0)T_{nl}(\tilde{z}_1+\Omega_0) \leq 0. \end{aligned} \quad (26)$$

Proof: These inequalities can be easily verified using (2). ■

This new information is the basis of the following theorem.

Theorem 2: Let $N \in \mathbb{N}$ and $V_{\max} > 0$. If there exist $P_N \in \mathbb{S}^{2+2(N+1)}$, $R = \text{diag}(R_1, R_2) \succeq 0$, $S = \text{diag}(S_1, S_2) \succ 0$, *and* $Q \in \mathbb{S}_+^2$, $\tau_0, \tau_1, \tau_2, \tau_3 \geq 0$ such that (12) holds together with:

$$\begin{aligned} \Xi_N &= \bar{\Theta}_N - \tau_0\Pi_0 - \tau_1\Pi_1 - \tau_2\Pi_2 - \tau_3\Pi_3 \prec 0 \\ 0 &\prec P_N + S_N \end{aligned} \quad (27)$$

where

$$\begin{aligned} \bar{\Theta}_N &= \text{diag}(\Theta_N, 0_2) - \alpha_2\text{He}\big((F_{m1} - T_0\ F_{m2})^\top e_1^\top P_N\tilde{F}_N\big) \\ \tilde{F}_N &= [F_N \quad 0_{2(N+1)+2,2}], \quad e_1 = [1 \quad 0_{1,2(N+1)+1}]^\top, \\ F_{m1} &= [0_{1,2(N+1)+4} \quad 1 \quad 0], \quad F_{m2} = [0_{1,2(N+1)+4} \quad 0 \quad 1] \\ \Pi_0 &= V_{\max}F_{m2}^\top F_{m2} - \tilde{F}_N^\top(P_N+S_N)\tilde{F}_N \\ \Pi_1 &= \pi_2^\top\pi_2 - T_{\max}^2\pi_3^\top\pi_3, \quad \Pi_2 = T_{\min}^2\pi_3^\top\pi_3 - \pi_2^\top\pi_2 \\ \Pi_3 &= -\text{He}((\pi_1+\Omega_0\pi_3)^\top\pi_2) \\ \pi_1 &= [1, 0_{1,2(N+1)+3}, 0, 0], \quad \pi_2 = [0_{1,2(N+1)+4}, 1, 0] \\ \pi_3 &= [0_{1,2(N+1)+4}, 0, 1] \end{aligned}$$

and all the parameters defined as in Theorem 1, then the equilibrium point X_∞ of system (25) is practically stable. More precisely, (24) holds for $X_{\text{bound}} = (V_{\max}\varepsilon_1^{-1})^{1/2}$ where ε_1 is defined in (17).

Proof: First, let us do the same change of variable as before

$$\tilde{X} = X - X_\infty.$$

Since the nonlinearity affects only the ODE part of system (25), the difference with the previous part lies in the dynamic of $\tilde{Z}$:

$$\dot{\tilde{Z}}(t) = \frac{d}{dt}\left(Z(t) - \begin{bmatrix} z_1^\infty \\ z_2^\infty \end{bmatrix}\right) = A\tilde{Z}(t) + B\begin{bmatrix}\tilde{\phi}_t(0,t) \\ \tilde{\phi}_x(1,t)\end{bmatrix} + B_2\begin{bmatrix} 0 \\ T_{nl}(\tilde{z}_1(t)+\Omega_0) - T_0\end{bmatrix}.$$

Using the same Lyapunov functional as in (16), the positivity is ensured in exactly the same way. For the bound on the time derivative, following the same strategy as before, we easily get:

$$\dot{V}_N(\tilde{X}) \leq \tilde{\xi}_N^\top \Theta_N \tilde{\xi}_N - 2\alpha_2(T_{nl}(\tilde{z}_1+\Omega_0)-T_0)e_1^\top P_N \tilde{Z}_N + \sum_{k=0}^{N}(2k+1)\tilde{\mathfrak{X}}_k^\top Q\tilde{\mathfrak{X}}_k - \int_0^1 \tilde{\chi}^\top(x)Q\tilde{\chi}(x)dx. \quad (28)$$

We introduce a new extended state variable $\bar{\xi}_N = [\tilde{\xi}_N^\top \; T_{nl}(\tilde{z}_1+\Omega_0)\; 1]^\top$. Using the notation of Theorem 2, (28) rewrites as:

$$\dot{V}_N(\tilde{X}) \leq \bar{\xi}_N^\top \bar{\Theta}_N \bar{\xi}_N^\top + \sum_{k=0}^{N}(2k+1)\tilde{\mathfrak{X}}_k^\top Q\tilde{\mathfrak{X}}_k - \int_0^1 \tilde{\chi}^\top(x)Q\tilde{\chi}(x)dx.$$

It is impossible to ensure $\bar{\Theta}_N \prec 0$ since its last 2×2 diagonal block is 0_2.

We then use the definition of practical stability. We want to show that if there exists $\varepsilon_3 > 0$ such that $\dot{V}_N(\tilde{X}) \leq -\varepsilon_3\|\tilde{X}\|_{\mathcal{H}}^2$ when $V_N(\tilde{X}) \geq V_{\max}$ then the system is practically stable. Let $\mathcal{S} = \{\tilde{X} \in \mathcal{H} \mid V_N(\tilde{X}) \leq V_{\max}\}$, the previous assertion implies that this set is invariant and attractive. Using (17), we get that $\{\tilde{X} \in \mathcal{H} \mid \|\tilde{X}\|_{\mathcal{H}} \leq X_{\text{bound}} = V_{\max}^{1/2}\varepsilon_1^{-1/2}\} \supseteq \mathcal{S}$, meaning that the system is practically stable.

A sufficient condition to be practically stable is that V_N should be strictly decreasing when outside the ball of radius $V_{\max}$. This condition rewrites as $V_N(\tilde{X}) \geq V_{\max}$ and the following holds:

$$V_N(\tilde{X}) - V_{\max} \geq \tilde{Z}_N^\top P_N \tilde{Z}_N + \int_0^1 \tilde{\chi}^\top(x)S\tilde{\chi}(x)dx - V_{\max} \geq -\bar{\xi}_N^\top \Pi_0 \bar{\xi}_N \geq 0.$$

The previous inequality is obtained using Bessel inequality (31) on $\int_0^1 \tilde{\chi}^\top(x)S\tilde{\chi}(x)dx$. Hence, $V_N(\tilde{X}) \geq V_{\max}$ if $\bar{\xi}_N^\top \Pi_0 \bar{\xi}_N \leq 0$.

Noting that $\tilde{z}_1 = \pi_1\bar{\xi}_N$, $T_{nl}(\tilde{z}_1+\Omega_0) = \pi_2\bar{\xi}_N$ and $1 = \pi_3\bar{\xi}_N$, Lemma 3 rewrites as:

$$\forall i \in \{1,2,3\}, \quad \bar{\xi}_N \; \Pi_i \; \bar{\xi}_N \leq 0.$$

Consequently, a sufficient condition to be practically stable is:

$$\forall \bar{\xi}_N \neq 0 \text{ s. t. } \forall i \in [0,3], \quad \bar{\xi}_N^\top \Pi_i \bar{\xi}_N \leq 0, \; \bar{\xi}_N^\top \bar{\Theta}_N \bar{\xi}_N < 0. \quad (29)$$

The technique called *S-variable*, explained in [18] for instance, translates the previous inequalities into an LMI condition. Indeed, [18, Th. 1.1] shows that condition (29) is verified if there exists $\tau_0, \tau_1, \tau_2, \tau_3 > 0$ such that

$$\bar{\Theta}_N - \sum_{k=0}^{3}\tau_i\Pi_i \prec 0.$$

Consequently, in a similar way for Theorem 1, condition (27) implies that $\mathcal{S}$ is an invariant and attractive set for system (25). Then, the equilibrium point X_∞ of system (25) is practically stable with $X_{\text{bound}} = (V_{\max}\varepsilon_1^{-1})^{1/2}$. ■

Note that if the torque function is not perfectly known, one can change the lower and upper bounds $T_{\min}$ and $T_{\max}$ to get a more conservative result but robust to uncertainties on T_{nl}. For (27) to be feasible, the constraint $\bar{\xi}_N^\top \Pi_1 \bar{\xi}_N \leq 0$ must hold, meaning that an upper bound of T_{nl} needs to be proposed.

B. On the Optimization of X_{bound}

The condition (27) is a bilinear matrix inequality (BMI) since τ_0, τ_1, τ_2, and τ_3 are decision variables and it is, therefore, difficult to get its global optimum. Nevertheless, the following lemma gives a sufficient condition for the existence of a solution to this problem.

Corollary 2: There exists $V_{\max}$ and $\tau_0 > 0$ such that Theorem 2 holds if and only if there exists $N > 0$ such that LMIs (11) and (12) are satisfied.

In other words, the equilibrium point of system (25) is practically stable if and only if the linear system (10) is exponentially stable.

Proof: Note first that expending (27) with $\tau_3 = 0$ leads to

$$\Xi_N = \left[\begin{array}{c|cc} \Theta_{N,\tau_0/2} & \multicolumn{2}{c}{\kappa_{P_N}} \\ \hline & \tau_2-\tau_1 & 0 \\ \kappa_{P_N}^\top & \hline 0 & \tau_1 T_{\max}^2 - \tau_2 T_{\min}^2 \\ & & -\tau_0 V_{\max} \end{array}\right] \quad (30)$$

where $\kappa_{P_N} \in \mathbb{R}^{(4+2(N+1))\times 2}$ depends only on P_N.

Proof of Sufficiency: Assume there exists $N > 0$ such that LMIs (11) and (12) are satisfied. Considering $\tau_2 = 0$ and using Schur complement on Ξ_N, $\Xi_N \prec 0$ is equivalent to

$$\Theta_{N,\tau_0/2} - \kappa_{P_N}\begin{bmatrix} -\dfrac{1}{\tau_1} & 0 \\ 0 & \dfrac{1}{\tau_1 T_{\max}^2 - \tau_0 V_{\max}}\end{bmatrix}\kappa_{P_N}^\top \prec 0$$

with $\tau_0 V_{\max} > \tau_1 \; T_{\max}^2$. Since $\Theta_N \prec 0$, considering τ_0 small enough, τ_1 large and $V_{\max} > \tau_1\tau_0^{-1}T_{\max}^2$ the previous condition is always satisfied and Theorem 2 applies.

Proof of Necessity: Assume $\Xi_N \prec 0$ and (12) holds. Then, its first diagonal block must be definite negative. Consequently, $\Theta_N \prec 0$ and, according to Theorem 1, system (10) is exponentially stable. ■

Remark 5: Note that (30) provides a necessary condition for Theorem 2 which is $\Theta_{N,\tau_0/2} \prec 0$. In other words, τ_0 is related to the decay rate of the linear system, and we get the following condition: $\tau_0 < 2\mu_{\max}$. □

Thanks to Corollary 2, the following method should help solving the BMI if Theorem 1 is verified; assuming that (11) and (12) are verified for a given $N \in \mathbb{N}$.

1) Fix $\tau_0 = 2\mu_{\max}$ as defined in (23).
2) Check that (11), (12), and (27) are satisfied for $V_{\max}$ a strictly positive decision variable. If this is not the case, then decrease τ_0 and do this step again.
3) Thanks to Corollary 2, there exists a τ_0 small enough for which (11), (12), and (27) hold. Freeze this value.
4) Since the problem is unbounded, it is possible to fix a variable without loss of generality, let $V_{\max} = 10^4$ for instance and solve the following optimization problem:

$$\begin{aligned} \min_{P_N,S,R,Q,\tau_1,\tau_2,\tau_3,\varepsilon_P} \quad & -\varepsilon_P \\ & (11), (12) \text{ and } (27) \\ \text{s.t.} \quad & P_N + S_N - \operatorname{diag}(\varepsilon_P, 0_{2N+3}) \succ 0 \\ & R \succeq 0, \quad S \succ 0, \quad Q \succ 0. \end{aligned}$$

5) Then, compute $X_{\text{bound}} = (V_{\max}\varepsilon_1^{-1})^{1/2}$, where ε_1 is defined in (17).

VI. Examples and Simulations

This section is devoted to numerical simulations[2] and draw some conclusions about the PI regulation. In Section VI-A, we focus on the linear system and Section VI-B is dedicated to the nonlinear case.

A. On the Linear Model

This section recaps the result of the linear model.

1) Estimation of the Decay Rate: The main result is a direct application of Corollary 1 for $k_p = 10^{-3}$ and $k_i = 10$. Indeed, using a dichotomy-kind algorithm, Table IV is obtained. It shows the estimated decay rate μ at a given order between 0 and 6.

The first thing to note in Table IV is the hierarchy property, and the decay rate is an increasing function of the degree, as noted in Remark 2. Note also that the gap between order 0 and order 1 is significant, showing that using projections indeed improves the results.

For orders higher than 2, the estimated decay rate increases slightly, and, up to a four digits precision, it reaches its maximum value at $N = 6$. Since it is then the maximum allowable decay rate obtained using (23), it tends to show that the Lyapunov functional used in this article together with condition (21) are sharp and provide a good analysis. Fig. 5 represents a simulation on the linear system, and it confirms the same observation. Indeed, one can see that the energy of the system is well-bounded by an exponential curve and the bound becomes more and more accurate as N increases.

2) Stability of the Closed-Loop System: We are interested now in estimating the stability area in terms of the gains k_p and k_i such that the decay rate of the coupled system is $\mu_{\max}$ for an order $N = 5$. That leads to Fig. 6, where it is easy to see that increasing the gain k_p decreases the range of possible k_i while it increases its speed (see (23)). It is quite natural to note that the larger k_i is, the slower the system is, while increasing the proportional gain leads to a faster system. As a conclusion, for small values of k_p and k_i, the system is stable, and that was the conclusion of the two articles [44], [45] using a different Lyapunov functional. Note that with the earlier articles, it was not possible to quantify the notion of "small enough gains k_p and k_i" while it is possible to give an estimation with the method of this article.

[2]Numerical simulations are done using a first-order approximation with at least 80 space-discretization points and 9949 time-discretization points. Simulations are done using Yalmip [28] together with the SDP solver SDPT-3 [46]. The code is available at *https://homepages.laas.fr/mbarreau*.

TABLE IV

Estimated Decay Rate as a Function of the Order N Used. Note That $\mu_{\max} = 7.73 \cdot 10^{-3}$ is Calculated Using (23) for $k_p = 10^{-3}, k_i = 10$

Order	$N = 0$	$N = 1$	$N = 2$	$N = 3$	$N = 6$
μ $(\times 10^{-3})$	0.87	4.24	7.31	7.59	7.73

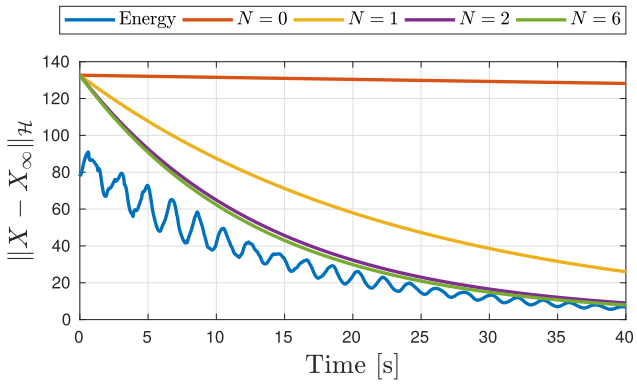

Fig. 5. Energy of X with the linear system for $k_p = 10^{-3}$, $k_i = 10$, and $\Omega_0 = 5$. The initial condition is $\phi^0(x) = 4(\int_0^x \phi_x^\infty(s)ds + 0.1\cos(2x))$, $\phi^1 = 2\Omega_0$, and $Z(0) = 2[z_1^\infty \; z_2^\infty]^\top$.

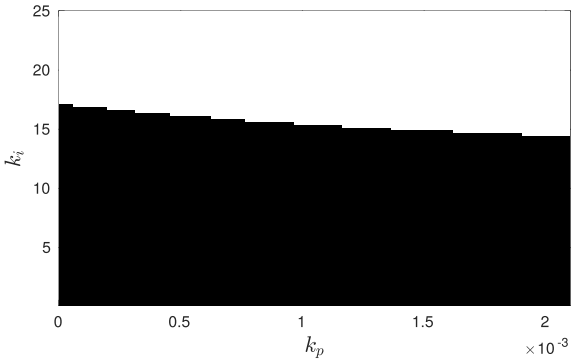

Fig. 6. Values of gains k_p and k_i leading to a stable system with the maximum decay rate for $N = 5$ using Theorem 1. The black area is stable, and the white area is said unstable up to an order 5.

B. Stick-Slip Effect on the Nonlinear Model

Section VI-A shows that the linear model is globally asymptotically stable for some values of gains k_p and k_i, and therefore, the nonlinear system (25) is locally asymptotically stable for a large-desired angular velocity Ω_0. This can been verified in Fig. 7(a) for $k_p = 10^{-3}$, $k_i = 10$, and $\Omega_0 = 10$. We can see that the linear and the nonlinear systems behave similarly if their initial condition is close to the equilibrium.

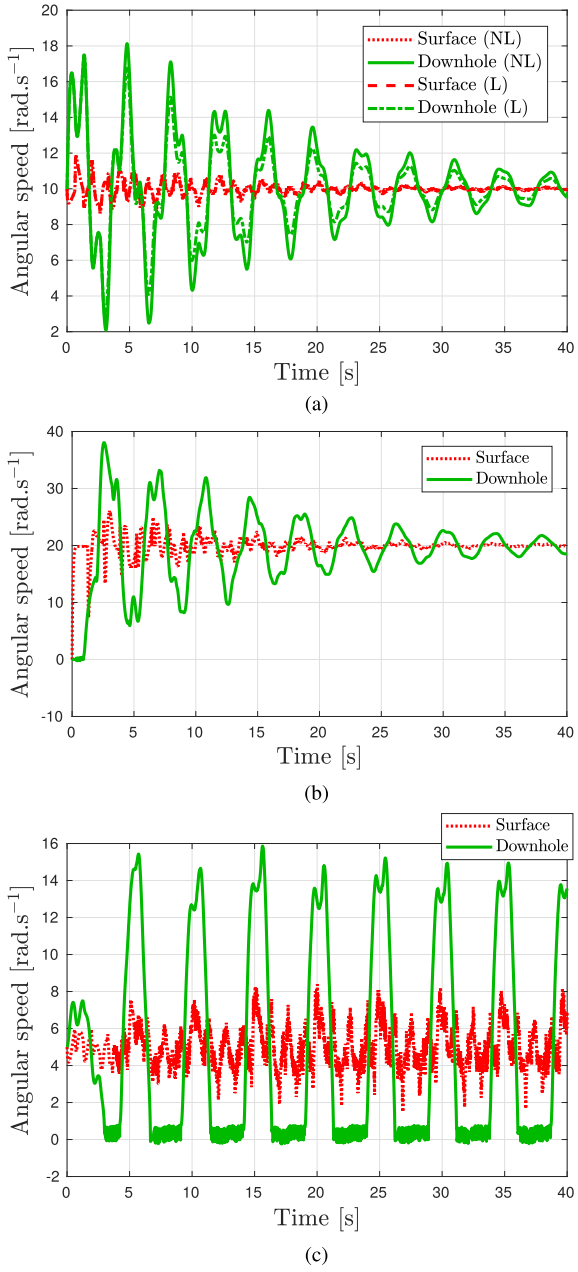

Fig. 7. Numerical simulations for systems (10) and (25) with $k_p = 10^{-3}$ and $k_i = 10$. (a) Systems (10) and (25)—$\Omega_0 = \phi^1 = 10$, $\phi^0(x) = (1 + 0.32\sin(x))\int_0^x \phi_x^\infty(s)ds$, and $Z(0) = (z_1^\infty\ z_2^\infty)^\top$. (b) System (25)—$\Omega_0 = 20$, $\phi^0 = 0$, $\phi^1 = 0$, and $Z(0) = 0_{2,1}$. (c) System (25)—$\Omega_0 = \phi^1 = 5$, $\phi^0(x) = (1 + 0.1\sin(x))\int_0^x \phi_x^\infty(s)ds$, and $Z(0) = (z_1^\infty\ z_2^\infty)^\top$.

The higher Ω_0 is, the larger the basin of attraction is. Indeed, the regulation tries to bring the system into the "quasi-linear" zone of T_{nl}, where it is close to a constant $T_{\min}$, as seen in Fig. 3, and consequently, the stick-slip phenomenon may occur at the beginning, but it is not effective for a long time as shown in Fig. 7(b) which is a numerical simulation on the nonlinear model with a zero initial condition.

The real challenge is then the case of low-desired angular velocities Ω_0. The result of a simulation on the nonlinear model for $\Omega_0 = 5$ rad.s^{-1} ($k_p = 10^{-3}$, $k_i = 10$) is shown in Fig. 7(c). First of all, note that the oscillations are with

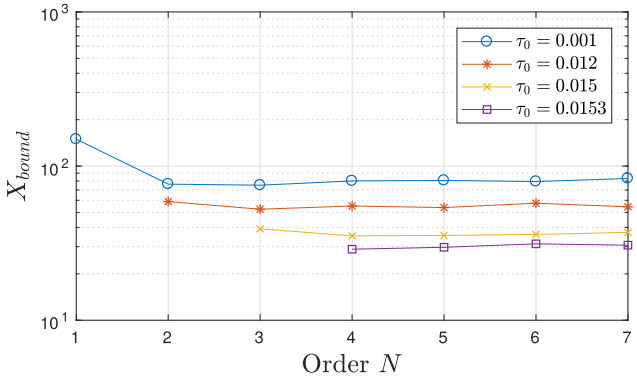

Fig. 8. Solution X_{bound} of BMI (27) for $k_p = 10^{-3}$, $k_i = 10$, and $\Omega_0 = 5$ and some values of τ_0. The limit is $X_{\text{bound}} = 28$.

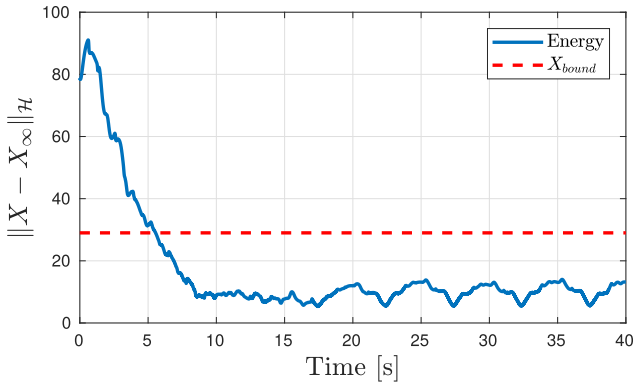

Fig. 9. Energy of X with the nonlinear system for $k_p = 10^{-3}$, $k_i = 10$, and $\Omega_0 = 5$. The initial condition is the same as in Fig. 5.

a frequency of 0.2 Hz and with an amplitude of roughly 15 rad.s^{-1}. This is very close to what has been estimated using Fig. 2. Then, the model presented in Section II seems to be a valid approximation of the real behavior, at least concerning the stick-slip phenomenon.

C. Practical Stability Analysis

Now, one can evaluate the amplitude of the oscillations using Theorem 2 with $k_p = 10^{-3}$ and $k_i = 10$. The result for several values of τ_0 and for an order between 0 and 7 is shown in Fig. 8. Note that after order 8, there are numerical errors in the optimization process, and the result is not accurate. The maximum τ_0 is $2\mu_{\max} = 0.0155$ and the higher τ_0 is, the better is the optimization. It appears that for $k_i = 10$, $k_p = 10^{-3}$, and $\Omega_0 = 5$, the optimal X_{bound} is around 28.

Fig. 9 shows the energy of the system as a function of time. One can see that the bound X_{bound} is quite accurate since the error between the maximum of the auto-oscillations and X_{bound} is around 53%. Moreover, note that $\max|z_1 - \Omega_0| = 11.7 = 0.4\ X_{\text{bound}}$, in other words, nearly half of the oscillations are concentrated in the variable z_1, which means the stick-slip mostly acts on the variable z_1 and does not affect much the rest of the system. In particular, it seems very difficult to estimate the variation of z_1 knowing only $\phi_t(0, t)$.

The final observation is about the variation of X_{bound} for different Ω_0. This is shown in Fig. 10. Up to errors in

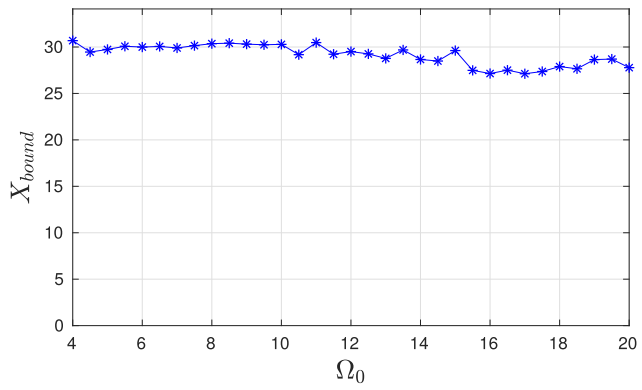

Fig. 10. Solution X_{bound} of BMI (27) for $k_p = 10^{-3}$, $k_i = 10$, $\tau_0 = 0.0153$, and $N = 5$.

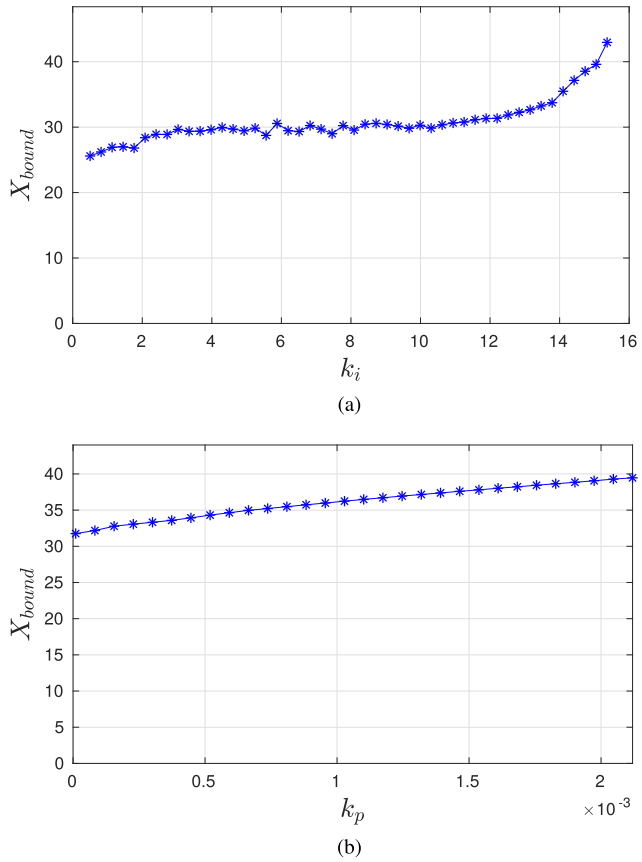

Fig. 11. Minimal X_{bound} obtained using Theorem 2 with $\Omega_0 = 5$ and $N = 5$. (a) X_{bound} for $k_p = 10^{-3}$ but with different values of k_i. (b) X_{bound} for $k_i = 10$ but with different values of k_p.

the numerical optimization, it seems that there is not an important variation of X_{bound} when Ω_0 increases. This is counter-intuitive and does not reflect the observations made with Fig. 7. One explanation is that we did not state that T_{nl} is a strictly decreasing function for positive θ.

D. Design of a PI Controller

Finally, the problem stated at the beginning of this article was to find the best PI controller, meaning that it minimizes X_{bound}. The plot in Fig. 11(a) shows that the value of the integral gain k_i does impact the oscillations due to stick-slip since X_{bound} increases from 25 to 43 for $k_i \in [0.5, 16]$, and the LMIs become infeasible after this point (these values have been obtained with $\Omega_0 = 5$, $k_p = 10^{-3}$, and $N = 5$).

To stay robustly stable against small delay in the loop, as noted in Section IV-C, we should consider $0 \leq k_p \leq 2.1 \cdot 10^{-3}$ which does not offer a large set of choices. For $k_i = 10$, we get Fig. 11(b). It appears that the minimum of X_{bound} is obtained for k_p close to 0. Consequently, increasing the gain k_p seems not to reduce the stick-slip effect. Consequently, even if a PI controller does not weaken the stick-slip effect, the equilibrium point of the controlled system is practically stable. Moreover, it does enable an oscillation around the desired equilibrium point and a local convergence to that point.

VII. Conclusion

This article focused on the analysis of the performance of a PI controller for a drilling pipe. First, a discussion between the existing models in the literature allows us to conclude that the infinite-dimensional model is closer to the real drilling pipe and should then be used for simulations and analysis. Based on this last model, the exponential stability of the closed-loop system was ensured using a Lyapunov functional depending on projections of the infinite-dimensional state on a polynomials basis. This approach enables getting exponential stability of the linear system with an estimation of the decay rate. This result was then extended to the nonlinear case considering practical stability. The example section shows that it is possible to get an estimate of the smallest attractive and invariant set and that this estimate is close to the minimal one. Further research would focus on similar analysis but using different controllers as the ones developed in [13], [30], [41], or [38, Ch. 10].

Appendix
Legendre Polynomials and Bessel Inequality

The performance of the Lyapunov functional (16) highly depends on the projection methodology developed in [42]. To help the reader to better understand the proof of Theorem 1, a definition and some properties of Legendre polynomials are reminded. More information can be found in [17].

Definition 4: The orthonormal family of Legendre polynomials $\{\mathcal{L}_k\}_{k\in\mathbb{N}}$ on $L^2([0,1])$ embedded with the canonical inner product is defined as follows:

$$\mathcal{L}_k(x) = (-1)^k \sum_{l=0}^{k} (-1)^l \binom{k}{l} \binom{k+l}{l} x^l$$

where $\binom{k}{l} = (k!/l!(k-l)!)$.

Their expended formulation is not useful in this article, but the two following lemmas are of main interest.

Lemma 4: For any function $\chi \in L^2$ and symmetric positive matrix $R \in \mathbb{S}_+^2$, the following Bessel-like integral inequality holds for all $N \in \mathbb{N}$:

$$\int_0^1 \chi^\top(x) R \chi(x) dx \geqslant \sum_{k=0}^{N} (2k+1) \mathfrak{X}_k^\top R \mathfrak{X}_k \qquad (31)$$

where $\mathfrak{X}_k$ is the projection coefficient of χ with respect to the Legendre polynomial $\mathcal{L}_k$ as defined in (15).

Lemma 5: For any function $\chi \in L^2$ satisfying (15), the following expression holds for any N in $\mathbb{N}$:

$$\begin{bmatrix} \dot{\mathfrak{X}}_0 \\ \vdots \\ \dot{\mathfrak{X}}_N \end{bmatrix} = \mathbb{1}_N \chi(1) - \bar{\mathbb{1}}_N \chi(0) - L_N \begin{bmatrix} \mathfrak{X}_0 \\ \vdots \\ \mathfrak{X}_N \end{bmatrix} \tag{32}$$

where $L_N, \mathbb{1}_N$ and $\bar{\mathbb{1}}_N$ are defined in (13).

Proof: This proof is highly inspired from [8]. Since $\chi \in L^2$ satisfies (15), (18) can be derived and the following holds:

$$\dot{\mathfrak{X}}_k = \Lambda[\chi(x)\mathcal{L}_k(x)]_0^1 - \Lambda \int_0^1 \chi(x)\mathcal{L}'(x)dx - \frac{\gamma_t}{2}\begin{bmatrix} 1 & 1 \\ 1 & 1 \end{bmatrix}\mathfrak{X}_k.$$

As noted in [17], the interesting properties of Legendre polynomials are stated as follows.

1) The boundary conditions on $\mathcal{L}_k$ ensures $\mathcal{L}_k(0) = (-1)^k$ and $\mathcal{L}_k(1) = 1$;
2) The derivation rule for Legendre polynomials is $(d/dx)\mathcal{L}_k(x) = \sum_{j=0}^{k} \ell_{j,k}\mathcal{L}_j(x)$.

These two properties lead to the proposed result in (32). ■

REFERENCES

[1] U. J. F. Aarsnes and O. M. Aamo, "Linear stability analysis of self-excited vibrations in drilling using an infinite dimensional model," *J. Sound Vib.*, vol. 360, pp. 239–259, Jan. 2016.

[2] U. J. F. Aarsnes and J. S. Roman, "Torsional vibrations with bit off bottom: Modeling, characterization and field data validation," *J. Petroleum Sci. Eng.*, vol. 163, pp. 712–721, Apr. 2018.

[3] B. Armstrong-Helouvry, "Stick-slip arising from stribeck friction," in *Proc. IEEE Int. Conf. Robot. Automat.*, May 1990, pp. 1377–1382.

[4] B. Armstrong-Hélouvry, P. Dupont, and C. C. De Wit, "A survey of models, analysis tools and compensation methods for the control of machines with friction," *Automatica*, vol. 30, pp. 1083–1138, Jul. 1994.

[5] M. Barreau, *Stability analysis of coupled ordinary differential systems with a string equation—Application to a Drilling Mechanism*. Toulouse, France: Université Fédérale Toulouse Midi-Pyrénées, 2019.

[6] M. Barreau, F. Gouaisbaut, A. Seuret, and R. Sipahi, "Input/output stability of a damped string equation coupled with ordinary differential system," *Int. J. Robust Nonlinear Control*, vol. 28, no. 18, pp. 6053–6069, Dec. 2018.

[7] M. Barreau, A. Seuret, and F. Gouaisbaut, "Exponential Lyapunov stability analysis of a drilling mechanism," in *Proc. 57st IEEE Conf. Decis. Control (CDC)*, Dec. 2018, pp. 6579–6584.

[8] M. Barreau, A. Seuret, F. Gouaisbaut, and L. Baudouin, "Lyapunov stability analysis of a string equation coupled with an ordinary differential system," *IEEE Trans. Autom. Control*, vol. 63, no. 11, pp. 3850–3857, Nov. 2018.

[9] G. Bastin and J.-M. Coron, *Stability and Boundary Stabilization of 1-D Hyperbolic Systems*, vol. 88. Basel, Switzerland: Birkhäuser, 2016.

[10] H. I. Basturk, "Observer-based boundary control design for the suppression of stick–slip oscillations in drilling systems with only surface measurements," *J. Dyn. Syst., Meas., Control*, vol. 139, no. 10, Oct. 2017, Art. no. 104501.

[11] A. Bisoffi, M. Da Lio, A. R. Teel, and L. Zaccarian, "Global asymptotic stability of a PID control system with Coulomb friction," *IEEE Trans. Autom. Control*, vol. 63, no. 8, pp. 2654–2661, Aug. 2017.

[12] D. Bresch-Pietri and M. Krstic, "Output-feedback adaptive control of a wave PDE with boundary anti-damping," *Automatica*, vol. 50, no. 6, pp. 1407–1415, 2014.

[13] C. Canudas-de-Wit, F. Rubio, and M. Corchero, "D-OSKIL: A new mechanism for controlling stick-slip oscillations in oil well drillstrings," *IEEE Trans. Control Syst. Technol.*, vol. 16, no. 6, pp. 1177–1191, Nov. 2008.

[14] N. Challamel, "Rock destruction effect on the stability of a drilling structure," *J. Sound Vibrat.*, vol. 233, no. 2, pp. 235–254, 2000.

[15] A. P. Christoforou and A. S. Yigit, "Fully coupled vibrations of actively controlled drillstrings," *J. Sound Vibrat.*, vol. 267, no. 5, pp. 1029–1045, 2003.

[16] J.-M. Coron, "Control and nonlinearity," in *Mathematical Surveys and Monographs*. Providence, RI, USA: AMS, 2007, no. 136.

[17] R. Courant and D. Hilbert, *Methods of Mathematical Physics*. Hoboken, NJ, USA: Wiley, 1989.

[18] Y. Ebihara, D. Peaucelle, and D. Arzelier, *S-Variable Approach to LMI-Based Robust Control, Communications and Control Engineering*, vol. 17. London, U.K.: Springer, 2015.

[19] A. F. Filippov, "Classical solutions of differential equations with multi-valued right-hand side," *SIAM J. Control*, vol. 5, no. 4, pp. 609–621, 1967.

[20] E. Fridman, S. Mondié, and B. Saldivar, "Bounds on the response of a drilling pipe model," *IMA J. Math. Control Inf.*, vol. 27, no. 4, pp. 513–526, 2010.

[21] J. K. Hale and S. M. V. Lunel, "Effects of small delays on stability and control," in *Operator Theory and Analysis*. Basel, Switzerland: Birkhäuser, 2001, pp. 275–301.

[22] A. J. Helmicki, C. A. Jacobson, and C. N. Nett, "Ill-posed distributed parameter systems: A control viewpoint," *IEEE Trans. Autom. Control*, vol. 36, no. 9, pp. 1053–1057, Sep. 1991.

[23] D. Karnopp, "Computer simulation of stick-slip friction in mechanical dynamic systems," *J. Dyn. Syst., Meas., Control*, vol. 107, no. 1, pp. 100–103, Mar. 1985.

[24] H. K. Khalil, *Nonlinear Systems*. London, U.K.: Pearson Education, 1996.

[25] M. Krstic, *Delay Compensation for Nonlinear, Adaptive, and PDE Systems*. Cambridge, MA, USA: Birkhäuser, 2009.

[26] N. Levinson, "Transformation theory of non-linear differential equations of the second order," *Ann. Math.*, vol. 45, no. 4, pp. 723–737, 1944.

[27] X. Liu, N. Vlajic, X. Long, G. Meng, and B. Balachandran, "Coupled axial-torsional dynamics in rotary drilling with state-dependent delay: Stability and control," *Nonlinear Dyn.*, vol. 78, no. 3, pp. 1891–1906, Nov. 2014.

[28] J. Löfberg, "YALMIP: A toolbox for modeling and optimization in MATLAB," in *Proc. IEEE Int. Conf. Robot. Automat.*, Sep. 2004, pp. 284–289.

[29] O. Morgul, "On the stabilization and stability robustness against small delays of some damped wave equations," *IEEE Trans. Autom. Control*, vol. 40, no. 9, pp. 1626–1630, Sep. 1995.

[30] E. Navarro-López, "An alternative characterization of bit-sticking phenomena in a multi-degree-of-freedom controlled drillstring," *Nonlinear Anal., Real World Appl.*, vol. 10, no. 5, pp. 3162–3174, 2009.

[31] E. Navarro-López and D. A. Cortes, "Sliding-mode control of a multi-DOF oilwell drillstring with stick-slip oscillations," in *Proc. Amer. Control Conf.*, Jul. 2007, pp. 3837–3842.

[32] E. Navarro-López and R. Suarez, "Practical approach to modelling and controlling stick-slip oscillations in oilwell drillstrings," in *Proc. IEEE Int. Conf. Control Appl.*, vol. 2, Sep. 2004, pp. 1454–1460.

[33] C. Prieur, S. Tarbouriech, and J. M. G. da Silva, "Wave equation with cone-bounded control laws," *IEEE Trans. Autom. Control*, vol. 61, no. 11, pp. 3452–3463, Nov. 2016.

[34] T. Richard, C. Germay, and E. Detournay, "A simplified model to explore the root cause of stick–slip vibrations in drilling systems with drag bits," *J. Sound Vib.*, vol. 305, no. 3, pp. 432–456, 2007.

[35] C. Roman, D. Bresch-Pietri, E. Cerpa, C. Prieur, and O. Sename, "Backstepping observer based-control for an anti-damped boundary wave PDE in presence of in-domain viscous damping," in *Proc. IEEE 55th Conf. Decis. Control (CDC)*, Dec. 2016, pp. 549–554.

[36] M. Safi, L. Baudouin, and A. Seuret, "Tractable sufficient stability conditions for a system coupling linear transport and differential equations," *Syst. Control Lett.*, vol. 110, pp. 1–8, Dec. 2017.

[37] C. Sagert, F. Di Meglio, M. Krstic, and P. Rouchon, "Backstepping and flatness approaches for stabilization of the stick-slip phenomenon for drilling," *IFAC Proc. Volumes*, vol. 46, no. 2, pp. 779–784, 2013.

[38] B. Saldivar, I. Boussaada, H. Mounier, and S.-I. Niculescu, *Analysis and Control of Oilwell Drilling Vibrations: A Time-Delay Systems Approach*. Cham, Switzerland: Springer, 2015.

[39] B. Saldivar, S. Mondié, and J. C. Ávila Vilchis, "The control of drilling vibrations: A coupled PDE-ODE modeling approach," *Int. J. Appl. Math. Comput. Sci.*, vol. 26, no. 2, pp. 335–349, 2016.

[40] B. Saldivar, S. Mondié, S.-I. Niculescu, H. Mounier, and I. Boussaada, "A control oriented guided tour in oilwell drilling vibration modeling," *Annu. Rev. Control*, vol. 42, pp. 100–113, Sep. 2016.

[41] A. Sevrarens, M. J. G. Molengraft, J. J. Kok, and L. van den Steen, "H∞ control for suppressing stick-slip in oil well drillstring," *IEEE Trans. Control Syst.*, vol. 18, no. 4, pp. 19–30, May 1998.
[42] A. Seuret and F. Gouaisbaut, "Hierarchy of LMI conditions for the stability analysis of time-delay systems," *Syst. Control Lett.*, vol. 81, pp. 1–7, Jal. 2015.
[43] S. Tarbouriech, G. Garcia, J. M. G. da Silva, Jr, and I. Queinnec, *Stability and Stabilization of Linear Systems with Saturating Actuators*. London, U.K.: Springer-Verlag, 2011.
[44] A. Terrand-Jeanne, V. Andrieu, M. Tayakout-Fayolle, and V. Dos Santos Martins, "Regulation of inhomogeneous drilling model with a P-I controller," *IEEE Trans. Autom. Control*, to be published.
[45] A. Terrand-Jeanne, V. Dos Santo Martins, and V. Andrieu, "Regulation of the downside angular velocity of a drilling string with a P-I controller," in *Proc. Eur. Control Conf. (ECC)*, Jun. 2018, pp. 2647–2652.
[46] K.-C. Toh, M. J. Todd, and R. H. Tütüncü, "SDPT3—A MATLAB software package for semidefinite programming," *Optim. Methods Softw.*, vol. 11, nos. 1–4, pp. 545–581, 1999.
[47] W. R. Tucker and C. Wang, "On the effective control of torsional vibrations in drilling systems," *J. Sound Vibrat.*, vol. 224, no. 1, pp. 101–122, 1999.
[48] M. Tucsnak and G. Weiss, *Observation and Control for Operator Semigroups*. Basel, Switzerland: Birkhäuser, 2009.
[49] W., Jr., Weaver, S. P. Timoshenko, and D. H. Young, *Vibration Problems in Engineering*. Hoboken, NJ, USA: Wiley, 1990.

Matthieu Barreau received the Engineering Degree in aeronautical engineering from the Institut Supérieur de l'Aéronautique et de l'Espace, Toulouse, France, in 2016, the Diplôme d'Ingénieur and Civilingenjörsexamen degree in space engineering, with specialization in system engineering, from the KTH Royal Institute of Technology, Stockholm, Sweden, in 2015, in 2016, the Ph.D. degree from the Laboratory for Analysis and Architecture of Systems, Centre national de la recherche scientifique, Toulouse, and the Diplôme de Doctorate degree in system theory from Paul Sabatier University, Toulouse, in 2019.

His Ph.D. study was carried out under the supervision of A. Seuret and F. Gouaisbaut. His current research interests include stability analysis of infinite-dimensional systems with a particular focus on drilling systems.

Frédéric Gouaisbaut was born in Rennes, France, in April 1973. He received the Dipl.-Ing. degree (Engineer) in automatic control from the Ecole Centrale de Lille, Villeneuve-d'Ascq, France, in September 1997, and the D.E.A. degree (master) in automatic control from Lille 1 University, Villeneuve-d'Ascq, in September 1997, and the Ph.D. degrees from the Laboratoire d'Automatique, Génie Informatique et Signal (LAGIS), Ecole Centrale de Lille, Lille, France, and Lille 1 University, in October 2001.

Since October 2003, he has been an Associate Professor with Paul Sabatier University, Toulouse, France. His current research interests include time-delay systems, quantized systems, and robust control.

Alexandre Seuret was born in France in 1980. He received the Engineering Degree from the Ecole Centrale de Lille, Lille, France, the master's degree in system theory from Lille 1 University, Villeneuve-d'Ascq, France, in 2003, and the Ph.D. degree in automatic control from the Ecole Centrale de Lille and Lille 1 University in 2006.

From 2006 to 2008, he held 1-year postdoctoral positions with the University of Leicester, Leicester, U.K., and the KTH Royal Institute of Technology, Stockholm, Sweden. From 2008 to 2012, he was a Junior CNRS Researcher (Chargé de Recherche) with the Grenoble Images Parole Signal Automatique Laboratory, Grenoble, France. Since 2012, he has been a Junior CNRS Researcher with the Laboratory for Analysis and Architecture of Systems, Toulouse, France. His current research interests include time-delay systems, networked control systems, and multiagent systems.